Protein Nanopore Membranes Prepared by a Simple Langmuir-Schaefer Approach

vorgelegt von

M. Sc.

Magnus Stefan Schwieters

an der Fakultät III – Prozesswissenschaften

der Technischen Universität Berlin

zur Erlangung des akademischen Grades

Doktor der Ingenieurwissenschaften
- Dr.-Ing. -

genehmigte Dissertation

Promotionsausschuss:

Vorsitzender: Prof. Dr. Peter Neubauer

Gutachter: Prof. Dr. Dietmar Werner Auhl

Gutachter: Prof. Dr. Alexander Böker

Tag der wissenschaftlichen Aussprache: 30. November 2021

Berlin 2021

Erklärung

Hiermit erkläre ich, dass die vorliegende Arbeit selbstständig und nur unter Zuhilfenahme der im Literaturverzeichnis genannten Quellen und Hilfsmittel angefertigt wurde. Alle Stellen der Arbeit, die anderen Werken dem Wortlaut oder dem Sinn nach entnommen wurden, sind kenntlich gemacht. Ich versichere, dass die Dissertation in der vorgelegten oder einer ähnlichen Fassung noch nicht zu einem früheren Zeitpunkt an einer anderen in- oder ausländischen Hochschule als Dissertation eingereicht worden ist.

Magnus Stefan Schwieters

Declaration

I hereby declare that the present work was prepared independently and only with the aid of the sources and aids mentioned in the bibliography. All parts of the work that have been taken from other works in terms of their wording or meaning are marked. I affirm that the dissertation in the version presented or a similar version has not been submitted as a dissertation to another domestic or foreign university at an earlier point in time.

Magnus Stefan Schwieters

Acknowledgements

It is my pleasure to thank everyone who supported me throughout the years of my dissertation. First, I thank Prof. Dr. Alexander Böker for giving me the opportunity to research such an exciting topic at Fraunhofer IAP and for being a reliable supervisor, airing serenity at all times. Likewise, I thank Prof. Dr. Dietmar Auhl and Dr. Konstanze Schäfer for valuable discussions and supervision on the part of TU Berlin.

I especially thank Dr. Ulrich Glebe for truly extra-ordinary scientific and personal mentoring that will shape me for a lifetime. Many thanks also to Maria, her passion for our project and her readiness to help and cooperate were inspiring. Having Maria and Uli by my side throughout this doctoral journey of meetings, trips, and scientific highs and lows was an honor.

Due to the interdisciplinarity of our project, I was able to meet and collaborate with a lot of enthusiastic research partners. My thanks go to Daniel and Marco from the group of Prof. Dr. Ulrich Schwaneberg, Yang, Raphael, Michael and André from the group of Prof. Dr. Armin Gölzhäuser, Thomas and Prof. Dr. Petra Wendler, Max and Prof. Dr. Thomas Hellweg, Daizong, Hao and Konrad from the group of Prof. Dr. Mischa Bonn, and Stephanie from Synchrotron SOLEIL.

Furthermore, I do thank all colleagues at Fraunhofer IAP contributing to a creative and collaborative working environment. Special thanks to Sany and Chris with whom I was allowed to share an office and who helped to balance research and life.

Thanks to my friends and my wonderful family for always reminding me what really matters.

Publications and posters

Parts of this thesis have already been published, as shown below:

Publication:

Protein Nanopore Membranes Prepared by a Simple Langmuir-Schaefer Approach, M. S. Schwieters, M. Mathieu-Gaedke, M. Westphal, R. Dalpke, M. Dirksen, D. Qi, M. Grull, T. Bick, S. Taßler, D. F. Sauer, M. Bonn, P. Wendler, T. Hellweg, A. Beyer, A. Gölzhäuser, U. Schwaneberg, U. Glebe, A. Böker
Small, **2021**, DOI: 10.1002/smll.2021102975

Conference posters:

Annual Congress Biotechnologie 2020+, Berlin, October 4, 2018.
Chiral Membranes, M. Schwieters, M. Mathieu, L. Al-Shok, H. Charan, M. Tutuş, U. Glebe, A. Böker

Scandinavian Society for Biomaterials (ScSB) 2019 Conference, Helsinki, Finland, June 12-14, 2019
Integration of functional proteins into a membrane for nanofiltration, M. Schwieters, M. Mathieu, U. Glebe, A. Böker

Polydays Conference 2019, Berlin, September 11-13, 2019
Integration of functional proteins into a membrane for nanofiltration, M. Schwieters, M. Mathieu, M. Tutus, U. Glebe, A. Böker

International Conference & Exhibition for Filtration and Separation Technology (FILTECH), Köln, October 22-24, 2019
Integration of functional transmembrane proteins into a membrane for nanofiltration, M. Schwieters, M. Mathieu, U. Glebe, A. Böker

Bayreuth Polymer Symposium, Bayreuth, September 20, 2021 (online)
Ultrathin Protein Nanopore Membranes, M. Schwieters, A. Böker, U. Glebe

This doctoral thesis was conducted in the framework of the
BMBF project “Chiral Membranes II” (FKZ: 0331B0559B).

Table of content

List of abbreviations

Materials and bioparticles

BSA	Bovine serum albumin
CP	Coat protein
DNA	Deoxyribonucleic acid
E. Coli	*Escherichia Coli*
FhuA	Ferric hydroxamate uptake protein component A
MPD	2-Methyl-2,4-pentanediol
RNA	Ribonucleic acid
SDS	Sodium dodecyl sulfate
TMV	Tobacco mosaic virus
TP	Transmembrane protein
UA	Uranyl acetate
VLP	Virus-like particle

Technical terms

AFM	Atomic force microscopy
CD	Circular dichroism
DLS	Dynamic light scattering
GISAXS	Grazing-incidence small-angle X-ray scattering
HIM	Helium ion microscopy
PeakForce QNM	PeakForce quantitative nanomechanical property mapping
SDS-PAGE	Sodium dodecyl sulfate polyacrylamide gel electrophoresis
SEM	Scanning electron microscopy

SFG	Sum-frequency generation
TEM	Transmission electron microscopy
XRR	X-ray reflectivity

Formular signs

A	m^2	Membrane area
F	N	Force acting on Wilhelmy plate
$F_{buoyancy}$	N	Buoyancy force acting on Wilhelmy plate
$F_{gravity}$	N	Gravitational force acting on Wilhelmy plate
F_{point}	N	Point force applied to the center of the freestanding membrane covering a circular hole
h	m	Membrane thickness
L	m	Contact line of Wilhelmy plate and subphase
M	kg mol^{-1}	Molecular mass
Δm	kg	Mass change of the container in water permeation measurements
P	mol Pa^{-1} m^{-2} s^{-1}	Water permeance
Δp	Pa	Vapor pressure difference
R	m	Radius of a hole covered by a membrane
t	s	Time interval of water permeation measurement
σ	N m^{-1}	Surface tension
δ	m	Membrane deformation in the hole center
Π	N m^{-1}	Surface pressure

1 Abstract

Filtration through membranes with nanopores is typically associated with high transmembrane pressures and high energy consumption. This problem can be addressed by reducing the respective membrane thickness, and the present thesis describes a simple procedure to prepare ultrathin membranes based on protein nanopores. To form such membranes, the transmembrane protein ferric hydroxamate uptake protein component A (FhuA) or its open-pore variant are assembled at the air-water interface of a Langmuir trough, compressed to a dense film, crosslinked by glutaraldehyde, and transferred to various support materials. This approach allows to prepare monolayer or multilayer membranes with a very high density of protein nanopores aligned vertically to the membrane plane, as demonstrated by sum-frequency generation (SFG) spectroscopy. Freestanding membranes covering holes up to 7 µm in diameter are visualized by atomic force microscopy (AFM), helium ion microscopy (HIM), and transmission electron microscopy (TEM). AFM PeakForce quantitative nanomechanical property mapping (PeakForce QNM) demonstrates remarkable mechanical stability and elastic properties of freestanding monolayer membranes with a thickness of only 5 nm. Multilayer membranes significantly reject bovine serum albumin (BSA) molecules with a molecular size below 10 nm, and exhibit excellent water permeance, two orders of magnitude superior to comparable, industrially applied membranes. Furthermore, incorporation of either closed or open protein nanopores allows tailoring the membrane's ion permeability. In addition, first attempts to similar membrane formation with nanopores based on tobacco mosaic virus (TMV) discs could be demonstrated. The new protein membrane could pave the way to energy-efficient nanofiltration.

2 Introduction

Applications of membranes are as versatile as their structures, sizes, shapes, and the materials and methods used to fabricate them. Dense, polymeric membranes conduct protons in fuel cells generating electric energy from hydrogen.[1] Porous, ceramic membranes absorb CO_2 in post-combustion capture reducing emissions of the green-house gas to the environment.[2] Porous, polymeric membranes separate oil from water purifying industrial wastewater.[3] In most cases though, membranes are used to separate solid particles from a liquid. Examples range from simple coffee filtration to more advanced membrane processes such as water desalination[4,5] or biomedical hemodialysis[6]. Moreover, from an industrial point of view, membrane processes are seen as cost-efficient because they enable continuous workflows and good scalability.[7] Hence, membrane processes have great technical, economic and societal value.

Generally, a *good* membrane process enables sufficient membrane selectivity or functionality at the lowest energy consumption possible. The energy consumption of a membrane process is typically measured with the parameter permeance, relating the membrane flux to the operational transmembrane pressure. The flux through a membrane with a certain selectivity/functionality, e.g., determined by the membrane's pore size (distribution), may be increased by increasing the transmembrane pressure. However, increasing the transmembrane pressure requires higher energy consumption in return. Keeping the transmembrane pressure constant, on the other hand, the simplest way to increase the membrane flux is to enlarge the membrane's pore size. The latter is usually not an appropriate measure as it limits the membrane's functionality in the desired application, e.g., rejecting particles with a certain size. The parameters selectivity/functionality, flux and transmembrane pressure thus interdependently frame a membrane process (**Figure 2.1**), which in literature is often referred to as permeability-selectivity trade-off.[8]

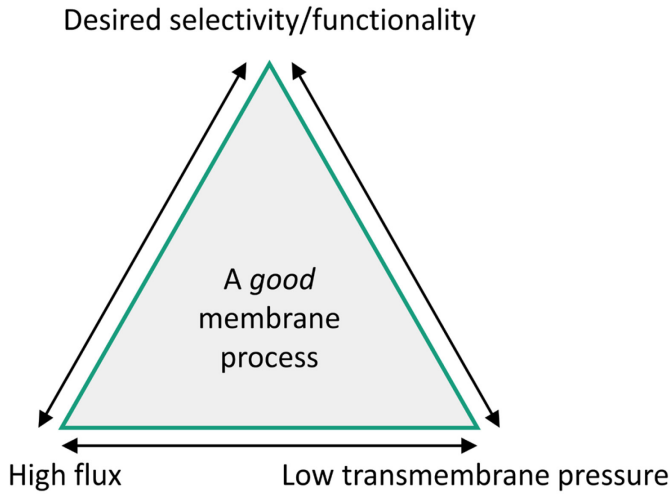

Figure 2.1: Triangle of a good membrane process illustrating the interdependence and desired optimization route of the basic process parameters.

To understand how the trade-off between high membrane permeance and high membrane selectivity may still be reduced, one has to consider the internal membrane structure.[8] Nowadays, most membranes are made of polymers by phase inversion, interfacial polymerization, or a combination of both.[9] By phase inversion, integral asymmetric membranes with pores of rather random size and orientation are formed, limiting both selectivity and permeability.[10] By interfacial polymerization, composite membranes with a thin and dense top layer are prepared. The transport across this selective layer requires high transmembrane pressures and high energy consumption. Easy, large-scale manufacturing of such membranes and excellent stability in many applications explain their great commercial success. However, as their technical optimization is well-advanced, significant improvements of membrane processes regarding energy-efficiency and separation precision require fundamentally new concepts of membranes with a defined internal structure. This particularly holds true for membranes with rejection properties in the challenging sub-nanometer to few nanometer size-range.[11]

Ideally, such membranes would be ultrathin, yet stable in a pressure-driven filtration process, and have densely packed, monodisperse pores aligned vertically to the membrane plane.[10] Promising approaches toward such membranes include graphene-[12] and carbon-nanotube-based[13] membranes, as well as ultrathin carbon nanomembranes prepared by crosslinking of self-assembled monolayers, e.g., from terphenylthiol molecules.[14,15] Furthermore, self-assembled block copolymer membranes with nearly monodisperse nanometer-sized pores in a thin selective layer and strategies for tailoring the pore size and functionality have been

introduced.[16] Another group of promising approaches may be found in bio-inspired membranes.

Biological membranes, on a cellular scale, fulfill many of the aforementioned criteria. Biological membranes separate cells or cell components and mainly consist of a dense phospholipid bilayer that is less than 10 nm thick. The phospholipid bilayer incorporates membrane proteins, which enable signal transmission and selective transport of molecules across the membrane. Membrane proteins connecting both sides of the membrane are referred to as transmembrane proteins (TP) and some TPs form a nanopore.[17] As such TPs are truly monodisperse pores and their large-scale biotechnological production and modification has made significant progress, TPs can be considered as functional building blocks for the engineering of new biohybrid membranes.[17–19]

In the past, TPs have been incorporated and studied in amphiphilic lipid or block copolymer membranes mimicking the natural phospholipid bilayer of biological membranes.[20,21] Those TP-loaded biomimetic membranes were either vesicles,[22–25] then referred to as lipo- or polymersomes, or planar nanosheets.[24,26] Vesicle-spreading or layering of nanosheets on top of membrane supports allowed to prepare highly permeable, planar membranes with TPs acting as monodisperse nanopores.[11,23,27] However, incorporation of TPs into lipid or block copolymer bilayers solely relies on non-covalent interactions, which limits the membrane stability. Furthermore, homogeneous defect-free vesicle spreading is highly challenging.[28,29] Alternatively, the incorporation of whole liposomes with inserted TPs in a membrane was investigated.[30] Such membranes were thicker and more stable, but less energy-efficient as compared to ultrathin approaches. It should also be mentioned that membrane preparation based on lipid or block copolymer bilayers is solely suited for TPs and, so far, the incorporation of other interesting biological nanopores, such as virus-like particles (VLPs) derived from tobacco mosaic virus (TMV),[31] into stable membranes required rather cumbersome procedures.[32,33]

To bypass these limitations, different strategies of membrane fabrication that provide covalent stabilization and dense arrangement of protein nanopores have been the research focus of Prof. Alexander Böker, who also supervises the present work. Previously, ferritin-polymer conjugates were crosslinked to ultrathin membranes and nanopores were formed by denaturation of the protein.[34–38] Using naturally pore-forming TPs instead of ferritin, TP-polymer conjugates were synthesized,[39] which were then transformed into stable membranes by assembly at Pickering emulsion interfaces and subsequent UV-crosslinking of the polymer chains.[40] Inspired by the previous work, a straightforward strategy for the integration of

functional TPs into planar, ultrathin membranes was investigated within the scope of the present doctoral thesis. This strategy is based on the Langmuir technique and a simple homobifunctional protein crosslinker. For demonstration, variants of the largest monomeric β-barrel TP ferric hydroxamate uptake protein component A (FhuA) with a central pore of 2.5 nm and TMV-derived virus-like particles with a central pore of 4 nm were used. The work covers membrane fabrication and a detailed characterization of the membranes regarding thickness, mechanical stability, water permeance, ion permeability and rejection properties for nano-sized molecules. The research establishes a powerful route to new, energy-efficient, protein-based nanofiltration membranes that could be tailored to various applications in future.

3 Fundamentals

The doctoral project described in this thesis aimed to develop a straightforward method to incorporate protein pores into an ultrathin membrane for nanofiltration, as emphazised in the Introduction (Chapter 2). First, fundamentals relevant to enable the reader an optimal understanding of such elaborations are summarized hereinafter. This is followed by a detailed overview of concepts previously investigated to realize membranes with biological nanopores as given in Chapter 4. Then, results of the corresponding experimental investigation are presented in Chapter 5, and complemented by a summary in Chapter 6.

3.1 Nanopores of biological origin

Preparation of protein nanopore membranes as covered in this thesis may be referred to as bottom-up approach, in a sense that the membranes are built from the pore.[31] By contrast, in a top-down approach, pores would be created retrospectively as done, e.g., when track-etching pores into an initially densely casted polymer membrane.[31] The motivation behind designing a membrane bottom-up is that special thought can be put into choosing pores with either superior uniformity or even imprinted functionality, later resulting in a membrane with advanced performance. As pointed out in the Introduction (Chapter 2), in biology, many nanoscale building blocks forming uniform pores are known, e.g., single molecules or supramolecular arrangements such as some TPs or VLPs, respectively. Such nanopores of biological origin[31] may be biotechnologically engineered and isolated to be used as uniform building blocks in bioinspired membranes. Exemplarily, this section introduces the TP FhuA and VLPs derived from TMV, both nanopores of biological origin used for membrane preparation in the experimental part of the present work.

3.1.1 FhuA

Naturally, the TP FhuA can be found in the outer membrane of *Escherichia Coli* (*E. Coli*) bacteria (**Figure 3.1**a) and functions as iron transporter, ensuring sufficient uptake of this in biological systems usually rare but essential/vital element.[41] FhuA is a large, monomeric TP with a hollow, barrel-shaped structure featuring a height of 6.9 nm and an elliptical cross section of 3.9-4.6 nm, the barrel mostly being clogged with a so-called cork domain (Figure 3.1b).[42] Furthermore, its amphiphilic nature characterized by a hydrophilic loop region and a hydrophobic transmembrane region allows FhuA to anchor in the bacteria's phospholipid bilayer membrane, solely based on hydrophobic interactions.[43]

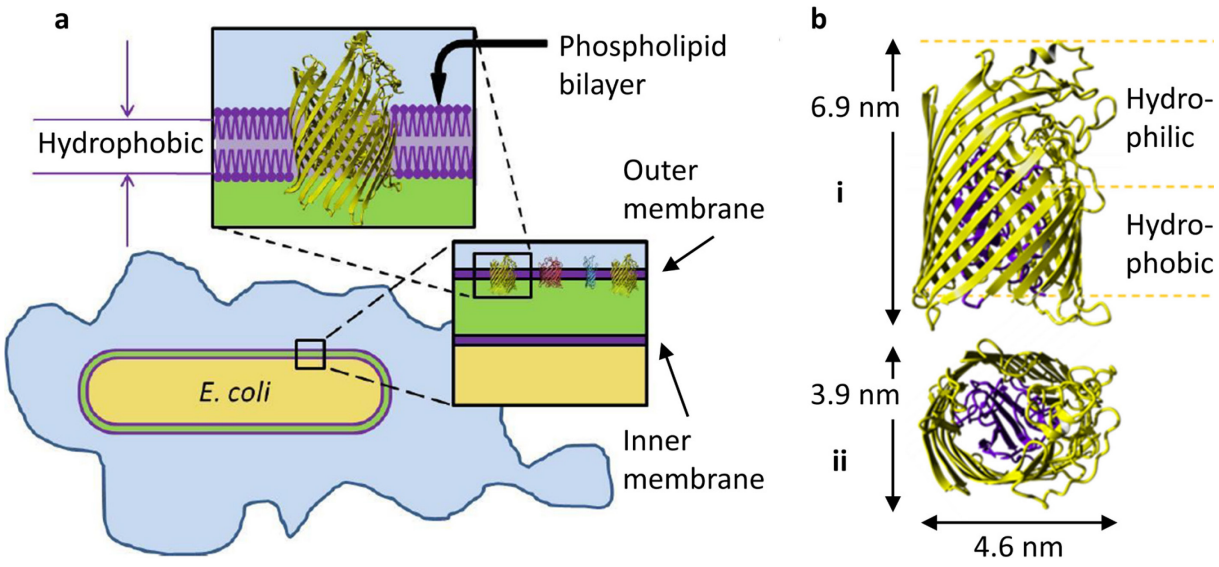

Figure 3.1: Transmembrane protein FhuA. a, Illustration of FhuA in the outer phospholipid bilayer membrane of *E. Coli* bacteria. Image adapted with permission from the reference.[44] b, Schematic illustration of FhuA in (i) side and (ii) top view indicating its dimensions and hydrophilic/hydrophobic regions; FhuA's cork domain blocking most of its central pore is colored purple. Image adapted with permission from the reference.[40]

Like all monomeric proteins, FhuA consists of a single chain of covalently bond amino acids. All proteins in nature are build up from just 20 different amino acids, and the covalent bond between two amino acids is referred to as peptide bond. A chain of several amino acids is consequently referred to as polypeptide chain and the protein-specific order and lengths of the polypeptide chain is commonly denoted as primary protein structure.[45]

However, most proteins show a very well ordered three-dimensional arrangement of its linear polypeptide chain, which enables the protein to function physiologically and is denoted as tertiary protein structure. Following this logic, repeating substructure motifs in the tertiary protein structure are denoted as secondary protein structure.[45] The secondary structure of FhuA is dominated by a motif called antiparallel ß-sheet (yellow strands winding up and down in Figure 3.1b), which - in FhuA - forms a characteristic three-dimensional barrel. The latter defines the tertiary structure of FhuA that is thus referred to as ß-barrel and occurs in other transmembrane proteins as well.[46]

Both arrangements of secondary and tertiary protein structure predominantly rely on polar or hydrophobic interactions between side chains of amino acids.[45] However, certain pairs of amino acid residues even bind covalently, e.g., in FhuA, two cysteine residues form a so-called disulfide bridge.[45] All these interactions cause folding and stabilization of a protein structure, which is a barrel in case of FhuA.

Proteins in general and FhuA in particular are thus functional biomolecules with well-defined shape and as such interesting to be used in various, including technical, applications. In fact, protein engineering and extraction/isolation have become highly dynamic research areas in biotechnology aiming to provide pure and functionally tailored protein samples.[47,48] Briefly, to engineer a protein, the gene that encodes the sequence of amino acids forming the polypeptide chain is modified. Typically, single amino acids or sequences of amino acids are deleted from/ added to the gene or are replaced by other amino acids. Various bacteria like *E. Coli* can be exploited to express proteins in large amount from (modified) genes, hence featuring the desired changes in the protein. However, even small changes in the polypeptide chain may compromise adequate folding of engineered proteins, which is why protein engineering requires detailed knowledge on intramolecular interactions and typically goes along with computational simulations.[48] For details on protein engineering, the reader is referred to other sources.[47–49]

In this thesis, FhuA is intended to act as a membrane pore, and FhuA membranes with open and closed pores are compared (Chapter 5). For this purpose, FhuA wild type (FhuA WT) with an almost closed pore and two engineered FhuA variants with open pores were used. Engineering and extraction of such FhuA variants was performed in the group of Prof. Schwaneberg at the Department of Biotechnology at RWTH Aachen University. The three FhuA variants are shown in **Figure 3.2** with lysine residues highlighted magenta and two β-sheets with so-called cleavage sites for protease from Tobacco Etch Virus (TEV) highlighted blue. The latter can be used to cleave two β-sheets for easier analysis, e.g., using matrix-assisted laser desorption-ionization time-of-flight (MALDI-ToF) mass spectrometry (MS);[50] this is not important for the work presented here though. The lysine residues, on the other hand, contain amino groups which are often used for protein modification and, here, relevant for FhuA membrane stabilization using the protein crosslinker glutaraldehyde (Chapter 3.3).

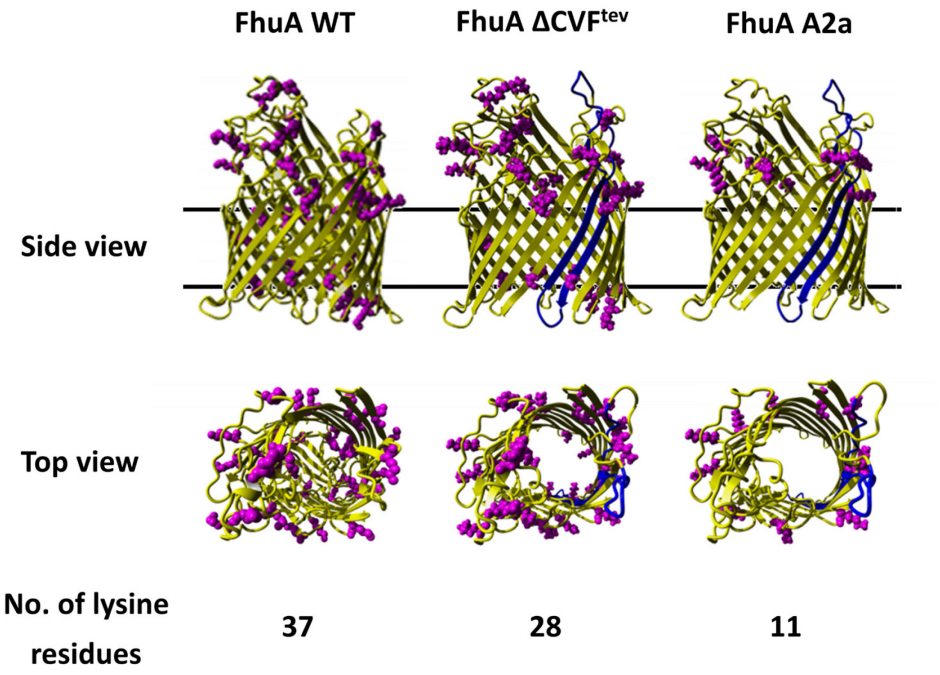

Figure 3.2: FhuA WT and engineered FhuA variants. Schematic illustration of FhuA WT as compared to the two engineered, open pore variants FhuA ΔCVF^{tev} and FhuA ΔCVF^{tev} amino 2a (short FhuA A2a) used in this study. Lysine residues are colored magenta. Image adapted with permission from the reference.[39]

To economically produce larger amounts of FhuA as, e.g., needed for the investigations in this thesis, *E. Coli* bacteria are cultured in a fermentation process and triggered to overexpress FhuA.[50,51] This means that the bacteria produce a large amount of the protein that is defined by the gene added to the bacteria. In a second step, the bacteria culture is harvested by centrifugation and the resulting cell pellet is solubilized using the detergent sodium dodecyl sulfate (SDS)[50] that destroys the bacteria's phospholipid bilayer membrane and denatures all proteins. This includes FhuA, which is then present in linear form and covered with SDS. Next, FhuA is extracted from the bacteria slurry in several purification steps finally resulting in a pure, SDS-denatured FhuA sample. To use FhuA as a functional nanopore, the denatured FhuA sample has to be refolded to its native β-barrel structure, as elaborated in the next section.

In nature, FhuA folds into the phospholipid bilayer membrane so that its hydrophobic transmembrane region is effectively stabilized (Figure 3.1).[43] Without this stabilization, FhuA does not fold and precipitates in aqueous media. That is why simply removing the SDS from SDS-denatured FhuA samples is not expedient. Instead, following a dialysis protocol developed at the Department of Biotechnology at RWTH Aachen University, SDS is successively replaced by many non-denaturing, amphiphilic 2-methyl-2,4-pentanediol (MPD) molecules. MPD is typically used as a stabilizing agent for proteins, including TPs,[52,53] and has been demonstrated

to also refold FhuA variants.[54] MPD does not form micelles in water but preferentially attaches to hydrophobic parts of FhuA and thus enables refolding and subsequent stabilization of FhuA, even in aqueous media. In fact, a simulation of FhuA exposed to a mixture of water and MPD nicely visualizes that MPD molecules densely occupy FhuA's hydrophobic transmembrane region (**Figure 3.3**a), which is thus kept free from contact to water (Figure 3.3b). According to this simulation, about 200 MPD molecules are needed to stabilize one FhuA molecule. Furthermore, a constant exchange of MPD from the transmembrane region and MPD in the surrounding water phase is predicted, overall indicating dynamic interactions between FhuA and MPD.

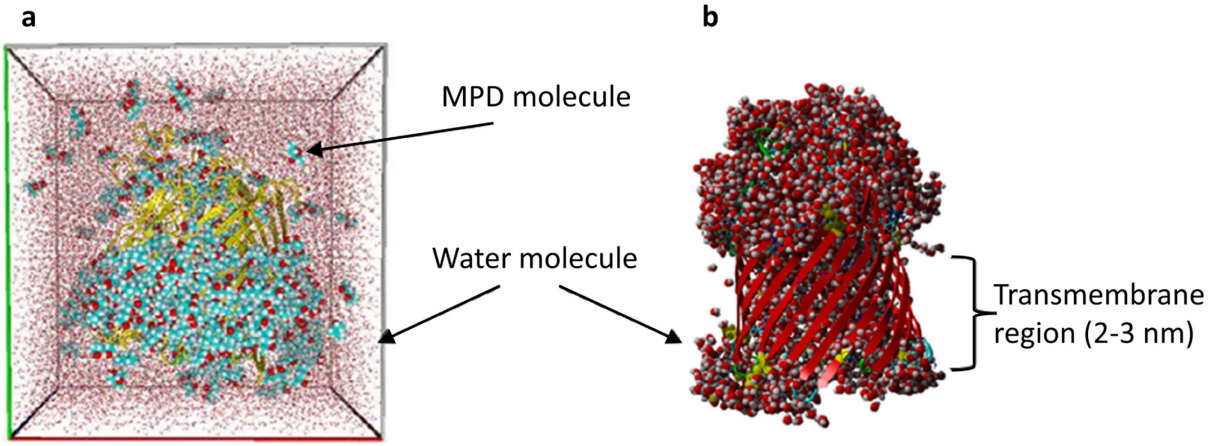

Figure 3.3: FhuA stabilization using MPD. Simulations by Kinzel et al. showing that a, MPD molecules preferentially attach to and thus stabilize the hydrophobic transmembrane region of FhuA, which in that case is b, completely water free. Image adapted with permission from the reference.[54]

In summary, FhuA is a monomeric protein that naturally forms a defined nanopore. While the nanopore is naturally clogged with a so-called cork domain, engineered variants with open pores are available. Furthermore, FhuA features lysine residues that allow for chemical modification and crosslinking, and can be placed at positions optimal for the envisioned application. During extraction, FhuA is denatured but may be refolded by dialysis against a buffer containing the stabilizing agent MPD. MPD-stabilized FhuA can be handled in aqueous media. All these features reason why FhuA was selected as demonstrator protein to investigate the new approach for preparation of protein nanopore membranes.

3.1.2 TMV virus-like particles

In the previous section, the TP FhuA was described as a representative of monomeric nanopores of biological origin. In this section, the plant virus tobacco mosaic virus (TMV) and virus-like-particles (VLPs) derived from TMV are introduced, representing nanopores of biological origin

assembled from multiple biomolecules. Here, the focus lies on the structure of TMV as a supramolecular building block forming a nanopore. For more information on the biological meaning of TMV as a plant virus, the reader is kindly referred to other sources.[55]

In total, native TMV consists of 2130 identical coat proteins (CP) and a single-stranded ribonucleic acid (RNA) that is build up from 6395 nucleotides.[31,56] Nucleotides are the basic building blocks of nucleic acids used to encode genetic information in all organisms on planet earth in form of RNA and deoxyribonucleic acid (DNA).[57] In a process described in detail elsewhere,[56] RNA and CPs assemble into a tube-shaped TMV complex with a height of 300 nm, a diameter of 18 nm and a central pore with a diameter of 4 nm. In this TMV complex, the RNA functions as helical scaffold entrapped between superimposed CPs, each CP non-covalently interacting with three nucleotides of the RNA scaffold.[56] Additionally, the viral structure is stabilized by hydrophobic interactions between neighboring CPs.[56] The principal arrangement of RNA scaffold and CPs is schematically illustrated in **Figure 3.4**, not showing a native TMV though, but a modified, shorter VLP derived from TMV. Because of its shape and appearance when investigated using TEM, this particular VLP is referred to as TMV disc.

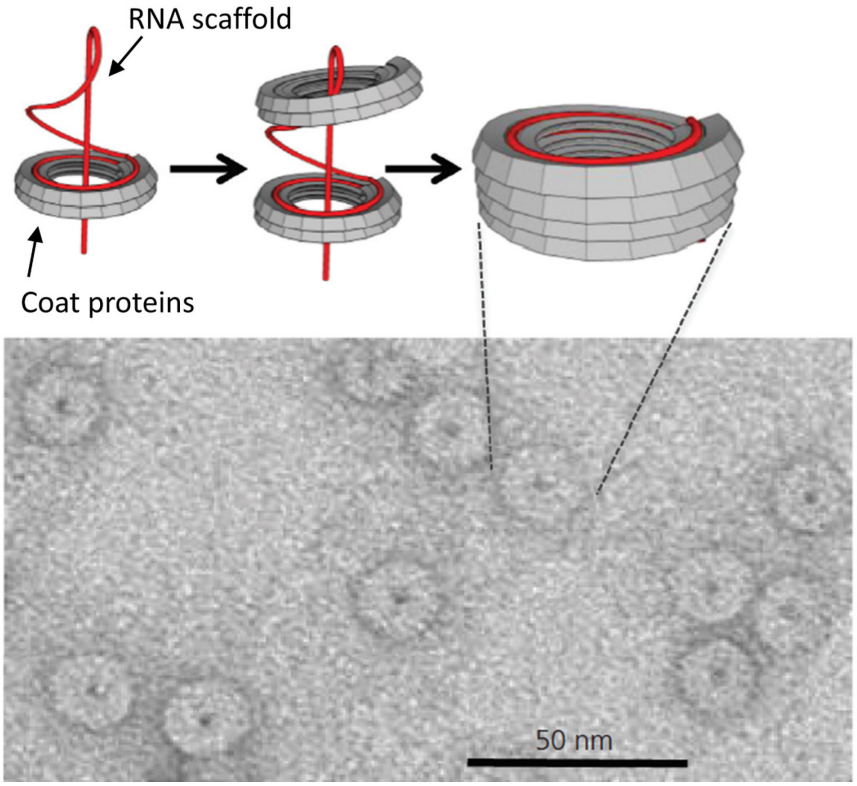

Figure 3.4: VLPs derived from TMV. Schematic illustration of assembly of the engineered TMV disc mutant from a single RNA and 68 CPs. TEM shows the TMV discs to be well dispersed and almost uniform in shape. Image adapted with permission from the reference.[31]

Similar to the protein engineering described for FhuA, VLPs from TMV may be tailored for use in technical applications by biotechnological modification of both, the RNA scaffold and the CPs.[58] In case of the TMV disc shown in Figure 3.4, for example, the RNA strand was shortened and certain amino acids of the CPs were exchanged so that – when assembled as TMV disc - each CP laterally presents a lysine residue allowing for chemical modification,[31] e.g., with glutaraldehyde (Chapter 3.3). This TMV disc-lysine mutant has a diameter of 18 nm, a height of 9.2 nm, a central pore with a diameter of 4 nm,[31] and is investigated for the preparation of TMV membranes in the experimental part of this thesis (Chapter 5.8).

Because of its well-known robustness over broad temperature (50 °C for 30 min) and pH ranges (5-8), and its stability even in organic solvent–water mixtures,[58] TMV has been investigated as building block in many applications. This includes nanowires, biomimetic surfaces, novel sensors, high performance microbatteries, solid-state electronics, and engineered biosystems, as nicely reviewed by Fan et al.[58]

3.2 Film balance and Langmuir technique

The previous section introduced nanopores of biological origin as suitable building blocks for the design of new, biohybrid devices and materials. In this thesis, such nanopores of biological origin (Chapter 3.1) are used to prepare planar monolayer membranes employing a film balance known as Langmuir trough. The name goes back to Irving Langmuir[a] who first introduced a prototype film balance in 1935 to study monomolecular oil films on water.[60] To facilitate the reader's understanding of the experimental part of this work, the principles of monolayer preparation using a Langmuir trough are summarized hereinafter.

The set-up of a Langmuir trough[b] shown in **Figure 3.5**a allows for the preparation and investigation of planar films of amphiphiles assembled at the liquid-gas interface. For this purpose, the Langmuir trough consists of a trough fully filled with a liquid that is referred to as subphase. In most experiments the subphase is an aqueous solution and the Langmuir trough is surrounded by air; the Langmuir interface is thus an air-water interface. Furthermore, the Langmuir trough features two software-controlled barriers, which symmetrically frame the air-water interface and can be moved laterally. A rectangular platinum-iridium plate, termed Wilhelmy plate, that vertically touches the air-water interface and is connected to a force gauge,

[a] Langmuir (1881-1957) was awarded the Noble Prize in Chemistry in 1932 for 'his discoveries and investigations in surface chemistry.[59]

[b] The Langmuir trough set-up presented in this section corresponds to the set-up which is available at Fraunhofer IAP and was used for the experiments described in this thesis. Other Langmuir troughs, e.g., featuring one instead of two barriers are available and follow the same principles.

allows to constantly measure the surface pressure. The meaning of the parameter surface pressure and how it is measured using a Wilhelmy plate are explained in the following. Afterwards, the course of a typical Langmuir experiment is outlined.

If an amphiphilic substance is spread to the air-water interface (Figure 3.5b), the interfacial tension drops. The closer the molecules of the amphiphilic substance pack at the air-water interface, the more the interfacial tension drops. This difference in interfacial tension before (σ_0) and after (σ) spreading an amphiphilic substance is defined as the parameter surface pressure Π (Equation 1).[61]

$$\Pi = \sigma_0 - \sigma \quad (1)$$

The surface pressure can be measured using the Wilhelmy plate connected to a force gauge. To do so, the Wilhelmy plate is positioned to intersect the air-water interface, typically in a way that one third of the plate is immersed into the subphase while two third of the plate reach out of the subphase. Due to the high surface energy of platinum-iridium (platinum: 2195 mJ/m; iridium: 3268 mJ/m)[62] the subphase completely wets the Wilhelmy plate. Under this condition, the external force F acting on the Wilhelmy plate (Figure 3.5a) and the interfacial tension σ relate as stated in Equation 2;[63] in which L is the contact line of Wilhelmy plate and subphase and $F_{gravity}$ and $F_{buoyancy}$ are the gravitational and buoyancy force, respectively:

$$F = \sigma \cdot L + F_{gravity} - F_{buoyancy} \quad (2)$$

Combining Equations 1 and 2 results in Equation 3 showing that the surface pressure can be measured using the combination of Wilhelmy plate and force gauge shown in Figure 3.5a.

$$\Pi = \sigma_0 - \sigma = (F_0 - F)/\, L \quad (3)$$

Next, the course of a typical Langmuir experiment is outlined based on the consecutive illustrations presented in Figure 3.5.

At the beginning of a Langmuir experiment, the air-water interface is clean, the barriers are completely open, and the surface pressure is zero (Figure 3.5a). Then, an amphiphilic substance of choice is spread to the air-water interface, which causes the surface pressure to increase (Figure 3.5b). After an equilibration time the barriers are set to motion. This reduces the distance between the molecules assembled at the air-water interface and results in a further increase of surface pressure (Figure 3.5c). At the surface pressure of interest, the monolayer film formed at the air-water interface may be transferred to flat substrates by horizontally dipping a blank substrate to the monolayer film (Figure 3.5d). This kind of film transfer -

generally used for quite rigid films[61] - is known as Langmuir-Schaefer deposition, once more referring to Irving Langmuir and Vincent Joseph Schaefer who jointly introduced this approach in 1938.[64]

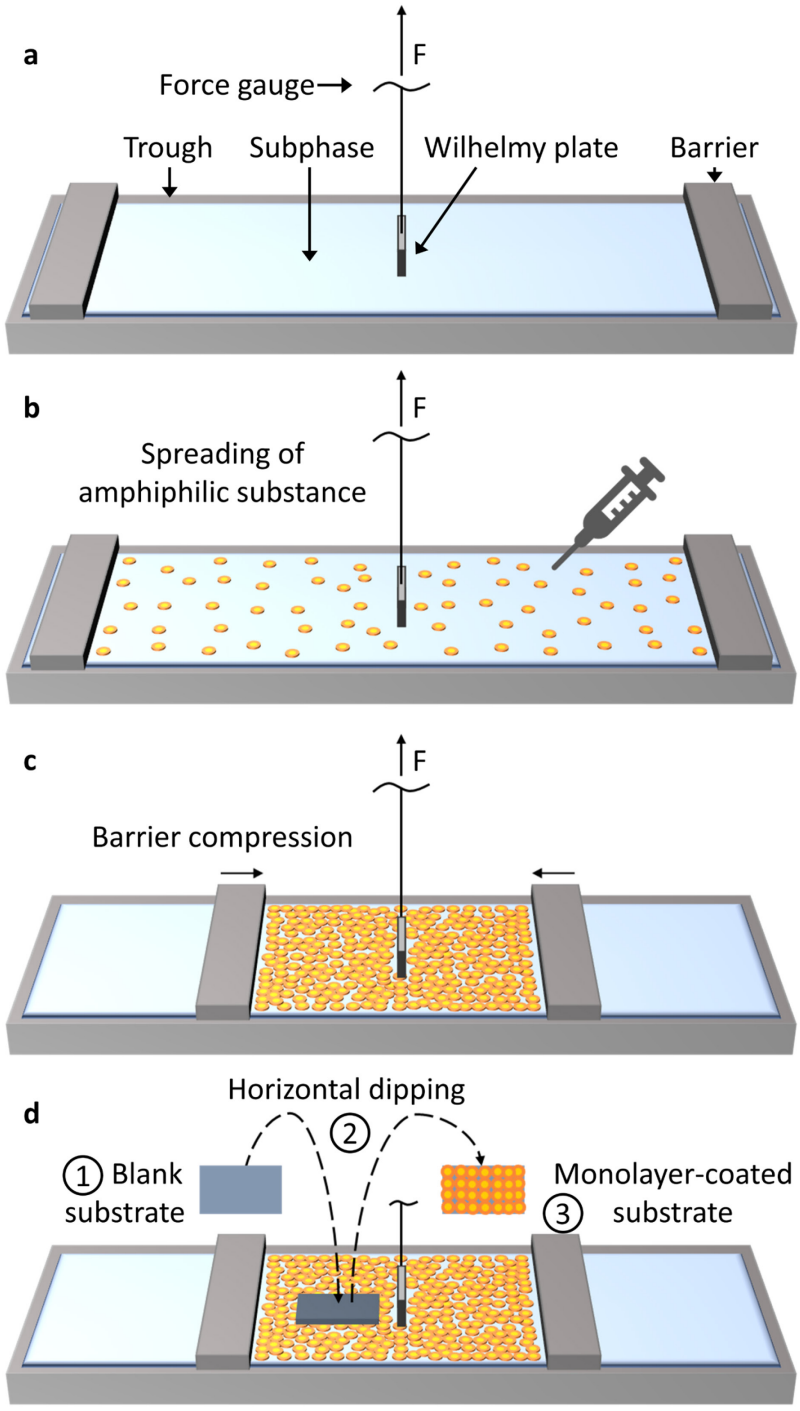

Figure 3.5: Molecular monolayer preparation using a Langmuir trough. (a) Langmuir trough set-up, (b) spreading of an amphiphilic substance to the air-subphase interface, (c) controlled barrier compression until a dense monolayer has formed, (d) monolayer transfer according to the Langmuir-Schaefer method.

Alternatively, Langmuir films can be transferred to flat substrates by slowly dipping the substrate vertically to the film plane,[61] as proposed by Irving Langmuir and Katharine B. Blodgett and therefore commonly denoted as Langmuir-Blodgett transfer.

The graph showing the surface pressure as a function of the area between the barriers is referred to as surface pressure-area isotherm. If the amphiphilic substance spread is known to fully assemble at the air-water interface, the area is typically stated as the area per molecule. Since proteins are known to desorb from the surface into the subphase when exposed to high surface pressures,[65,66] surface pressure-area isotherms shown in this thesis state the area between the barriers (denoted as trough area).

3.3 Bioconjugation using glutaraldehyde

In the previous section, the formation of a molecular monolayer using a Langmuir trough was described, and in the experimental part of this thesis, the Langmuir technique is used to prepare protein monolayer membranes. To be applied in a filtration process, those protein membranes are transferred from the air-water interface to porous supports. While non-covalently linked protein monolayer membranes may be considerably stable at the air-water interface or when transferred to a dense substrate, they would certainly fall apart over the pores of a porous support material. Thus, covalent crosslinking in the protein membranes is required. In the experiments presented in Chapter 5, this is achieved by injecting the protein crosslinker glutaraldehyde to the Langmuir trough subphase. As a theoretical basis, the chemistry of protein crosslinking using glutaraldehyde is summarized below.

Glutaraldehyde is a colorless liquid and a widely used homobifunctional protein crosslinker with the sum formula $C_5H_8O_2$. It consists of a carbon backbone that features one aldehyde group at each end. Aldehyde groups readily react with amino groups to form covalent bonds, and many proteins present amino groups in form of lysine residues at their surface.[67] Still, the chemical nature of the reaction of glutaraldehyde with proteins is not clearly understood,[67] and it is likely that no single mechanism is responsible for this reaction between glutaraldehyde and amino groups. Instead, multiple mechanisms have been proposed in literature, also considering different reaction conditions. This is nicely discussed by Greg Hermanson in two chapters of *Bioconjugate Techniques*.[68,69] He concludes that, depending on the pH value, glutaraldehyde occurs as either monomer or polymer in varying conformations, but always forms covalent bonds with amino groups, either in form of so-called secondary amines or (conjugated) Schiff bases **(Figure 3.6)**.

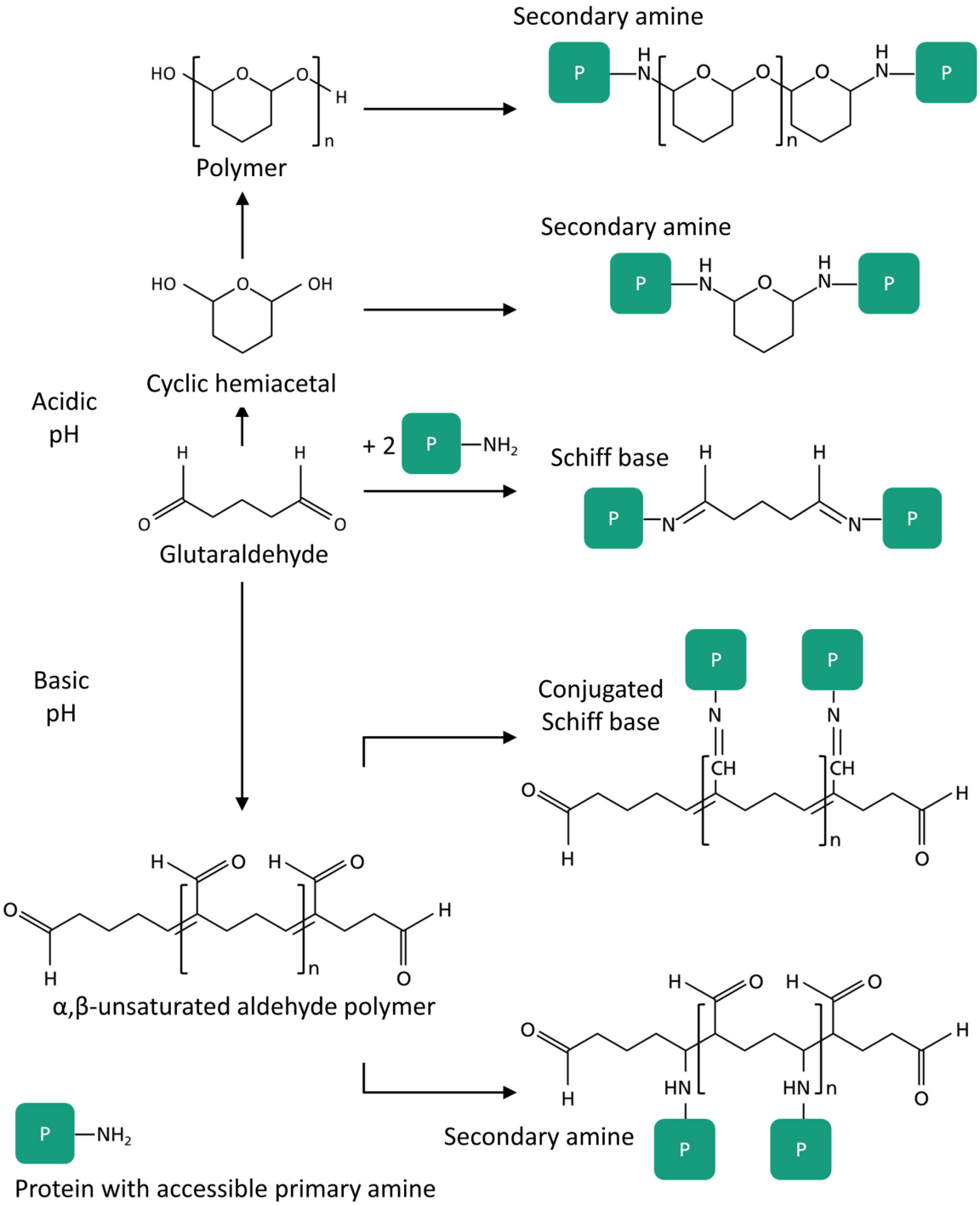

Figure 3.6: Proposed forms of glutaraldehyde in solution and possible reactions with primary amines to form stable crosslinks between proteins [adapted from[68,69]].

Furthermore, Fernandez-Lafuente et al. have reported that, on one hand, one glutaraldehyde molecule bound to an amino group preferentially reacted with another glutaraldehyde molecule bound to an amino group, as compared to a free glutaraldehyde molecule. On the other hand, two glutaraldehyde molecules bound to an amino group showed low tendency to react with another two glutaraldehyde molecules bound to an amino group.[70,71] That is why the authors

conclude that efficient protein crosslinking may be achieved at moderate glutaraldehyde concentrations, suggesting 0.1–1% (v/v) glutaraldehyde at pH 7 for 1 hour.[71]

Next to its application in scientific bioconjugation, glutaraldehyde is widely used for cold sterilization of medical equipment (typically 2–3.5% (v/v) aqueous solution),[72,73] as leather tanning agent[74] and as ingredient in cosmetic products.[73] Glutaraldehyde is toxic, mostly causing irritation and sensitization of the eyes, skin and respiratory tract,[73] which is why direct exposure to the skin and inhalation of its vapor should be minimized.

All in all, its broad use in industry and science, its cheap availability, and most of all its efficiency in crosslinking proteins were the reasons to choose glutaraldehyde for covalently stabilizing protein nanopore membranes in this work.

4 State of the art: Membranes with protein nanopores

The goal of this thesis is to develop an ultrathin membrane that features protein nanopores and allows for energy-efficient nanofiltration. In recent years, research groups around the world have investigated various approaches toward designing similar membranes, some with impressive successes leading to high-ranking publications and creating a dynamic field of research. In order to put the results of the present thesis into perspective, this chapter summarizes the state of the art of protein nanopore membranes, discussing the work of external competitors and coworkers at Fraunhofer IAP. For the sake of clarity, reported approaches toward protein nanopore membranes are here assigned into four strategic categories as outlined in **Figure 4.1**. Each category is first introduced in general and on this basis, selected examples from the literature are discussed.

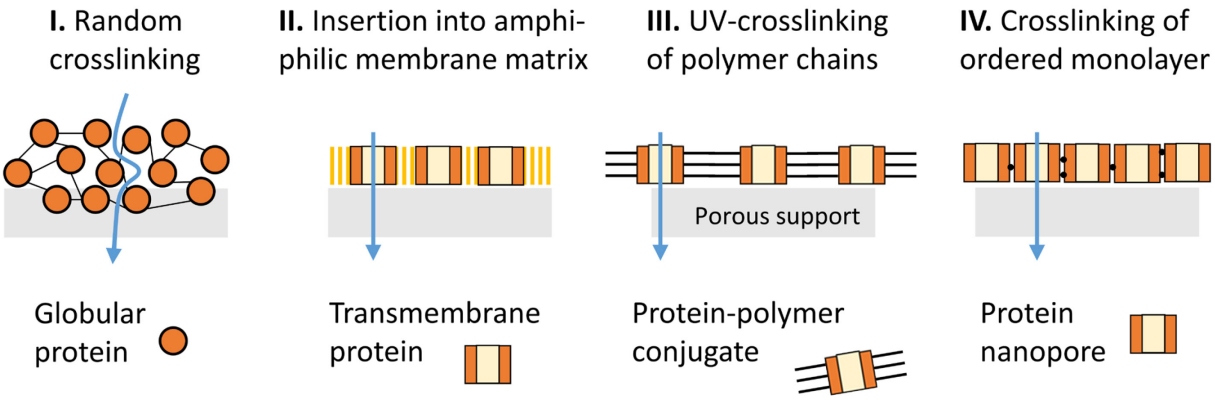

Figure 4.1: Strategies toward protein nanopore membranes. I, Dense, but random crosslinking of globular proteins that do not form a nanopore. Transport occurs through the interstitial space between the proteins (indicated by the blue arrow). **II**, Insertion of transmembrane proteins into lipid bilayer or amphiphilic block copolymer membranes based on hydrophobic interactions. **III**, Synthesis of protein-polymer conjugates, interfacial assembly and subsequent UV-crosslinking of polymer chains. **IV**, Crosslinking of interfacially assembled protein nanopore monolayers.

I. Random crosslinking of globular proteins

Some research groups have developed ultrathin protein nanopore membranes without using nanopores of biological origin as introduced in Chapter 3.1, but globular proteins instead. To prepare membranes, such globular proteins were densely crosslinked as a thin layer on top of microporous support membranes. Transport across the membranes thus takes place through the interstitial space between the proteins, and particles larger than this space will be rejected.

Two examples of membranes of this category are the ferritin membranes[75,76] introduced by Peng et al. in 2009 and the BSA membranes[77] reported by Zhao et al. in 2013. Peng et al.

mixed positively charged cadmium hydroxide nanostrands and ferritin that – due to its negative charge – homogenously attached to the nanostrands. A solution of ferritin-coated nanostrands was then filtered through a microporous polycarbonate membrane filter. As opposed to pure ferritin, ferritin-coated nanostrands were rejected by the polycarbonate membrane and thus accumulated as a thin, homogenous filter cake, which was subsequently stabilized by glutaraldehyde crosslinking (Chapter 3.3). The authors report that ferritin membranes with a thickness of only 60 nm, and estimated pore size of 1.7-2.2 nm showed about 1000 times higher water permeance compared to commercial membranes with comparable rejection properties.

To prepare BSA membranes, Zhao et al. immersed microporous polycarbonate membrane filters into an aqueous BSA solution and subsequently immersed the BSA soaked support into a solution of the protein crosslinker trimesoyl chloride (TMC) in hexane. Because water and hexane do not mix, BSA and TMC interfacially polymerized forming an ultrathin BSA membrane layer on top of the polycarbonate support. This composite membrane effectively rejected dye molecules with a molecular size smaller than 2 nm at a permeance of about 90 L/ (m^2 h bar^{-1}),[77] which is higher than that of commercial nano- or ultrafiltration membranes.[11] It is pointed out that BSA denatures during polymerization at the air-hexane interface so that membranes from proteins that naturally form nanopores cannot be prepared analogously.

Even though these publications lie back about a decade and report outstanding performance, nanofiltration membranes based on randomly crosslinked, globular proteins have not translated into (industrial) applications. It is assumed that this is due to the difficulties in both, scaling up membrane preparation and storage of such membranes, when compared to conventional polymer membranes. Furthermore, these membranes may only be used for size separation and do not enable new membrane applications (because the membrane pores may not be functionally tailored).

II. Insertion of TPs into amphiphilic block copolymer membranes and lipid bilayers

In nature, transmembrane proteins fold into and anchor in phospholipid bilayer membranes based on hydrophobic interactions (Chapter 3.1.1). Consequently, many research groups have investigated strategies that foresee the insertion of TPs into lipid bilayers or block copolymer membranes, which mimic the amphiphilic properties of biological membranes. Typically, those TP-loaded membranes have been vesicles, then referred to as lipo- or polymersomes, or planar nanosheets. Vesicle-spreading or layering of nanosheets on top of membrane supports has

allowed to prepare highly permeable, planar membranes with TPs acting as monodisperse nanopores.

One example of TP-block copolymer membranes prepared by vesicle spreading are the aquaporin-embedded membranes introduced by Zhong et al. in 2012.[23] Aquaporins are TPs that facilitate water transport but - because of their very small pore diameter and unique charge characteristics[23] - even hinder ions to pass. Zhong et al. prepared aquaporin-loaded block copolymer vesicles, which they spread on top of a cellulose acetate membrane support placed into a vacuum filtration unit, softly sucking away excess water from the bottom. Both, the block copolymers and the cellulose acetate support featured UV-crosslinkable end groups, so that the composite membrane was stabilized by covalent crosslinking in a final step. Scanning electron microscopy (SEM) images of the membrane surface show that some vesicles had ruptured, forming a planar membrane layer as intended, but others had not, causing the membrane to appear rather inhomogeneous. Performance assessment of such aquaporin membranes revealed 30% rejection of NaCl, pointing toward significant defects in this kind of aquaporin membrane.

In 2020, Tu et al. published a detailed study of TP membranes prepared from planar, TP-loaded block copolymer nanosheets (TP nanosheets).[11] Therein, such nanosheets are made by mixing TPs (solubilized in a buffer containing the detergent *n*-octyl β-d-glucopyranoside) and block copolymers in a methanol/chloroform mixture, evaporating the solvents to form TP-block copolymer films on a glass surface and subsequent rehydration of the thin films, then (dis-)assembling as TP nanosheets.[11] To prepare stable and homogenous membranes with TP nanopores, microporous polymer supports were coated with six alternate layers of polyethyleneimine (PEI) and TP nanosheets, which were finally crosslinked to stabilize the composite membrane. Incorporating TPs with different pore diameters allowed altering the membranes' molecular weight cut-off accordingly, demonstrating that filtration takes place through the TP pores. Furthermore, such membranes showed water permeances up to 1000 times higher than that of commercially available membranes with similar separation properties.

These two examples nicely highlight the challenges and chances of preparing membranes from lipid bilayer or block copolymer membranes loaded with TPs. Time will show if the membrane preparation can be made sufficiently simple and inexpensive to allow their translation to industry. It should further be pointed out that membrane preparation based on lipid or block copolymer membranes is solely suited for TPs and not for other interesting biological nanopores, such as VLPs derived from TMV (Chapter 3.1.2).

III. Crosslinking of protein-polymer conjugates

The third strategy of fabricating protein nanopore membranes mentioned here uses so-called protein-polymer conjugates as membrane building blocks, and has been essentially researched by present co-workers and predecessor under supervision of Prof. Alexander Böker. As the name says, protein-polymer conjugates are proteins featuring covalently attached polymer chains. The polymer chains are either pre-synthesized and grafted to, or grafted from the protein surface by polymerization of suitable monomers.[78,79] Protein-polymer conjugates were shown to have high interfacial activity, and interfacially-assembled films of protein-polymer conjugates with UV-crosslinkable groups have been transferred into covalently stabilized, ultrathin protein-polymer membranes. Nanopores in such membranes have been either formed by denaturation of the proteins, or by using a pore-forming TP in the first place.

Two examples of membranes of this category are the ferritin membranes introduced by van Rijn et al. in 2014,[38] and the FhuA membranes/micro-compartments proposed by Charan et al. in 2017[40] (both works were supervised by Prof. Alexander Böker).

Rijn et al. synthesized protein-polymer conjugates using ferritin and a statistical, thermoresponsive copolymer incorporating UV-crosslinkable groups. The amount of protein-polymer conjugates estimated to cover a microporous polycarbonate or polyethersulfone membrane support as a monolayer was diluted in water and placed on top of the membrane support in form of a droplet covering the full support. The interfacially assembled monolayer of protein-polymer conjugates was crosslinked by UV-light irradiation, which also caused the water to evaporate, leaving behind a dry, crosslinked protein-polymer monolayer membrane on top of the support. This membrane had a thickness below 10 nm and upon ferritin denaturation membrane pores were formed. The resulting membrane was characterized for water permeation at varying temperatures, confirming thermoresponsive characteristics. Considering its size selectivity for particles below 20 nm, the monolayer membrane showed outstanding water permeance of up to 25 000 L m^{-2} h^{-1} bar^{-1}.[38]

Inspired by the work of Rijn et al., Charan et al. further developed membrane formation on basis of protein-polymer conjugates using the TP FhuA instead of ferritin.[40] FhuA-polymer conjugates were assembled at the interface of an oil-water emulsion, thus forming a so-called Pickering emulsion. Upon UV-crosslinking, lots of stable FhuA-polymer micro-compartments (crosslinked Pickering emulsion droplets) were formed, with a membrane thickness of down to

11 nm. The authors suggest that such micro-compartments may serve as carrier for controlled drug-delivery when further optimized.

Combining the membrane formation presented by Rijn et al. and the synthesis of FhuA-polymer conjugates investigated by Charan et al., formation of planar FhuA-polymer membranes has been investigated in a doctoral thesis by Maria Mathieu-Gaedke,[80] in parallel to the present dissertation. Finally, it is pointed out, that controlled synthesis of protein-polymer conjugates that does not compromise the protein conformation is highly challenging, and so is the proof of proper protein conformation in protein-polymer conjugates and membranes. The latter remains a key-challenge of this third strategic category toward protein nanopore membranes.

IV. Crosslinking of ordered monolayers of protein nanopores

The highest pore-density in protein nanopore membranes could be achieved by directly forming covalent bonds between protein nanopores assembled as a crystalline 2D monolayer sheet, not featuring any polymer matrix as proposed in strategies II and III. To the author's knowledge, a publication by Zhang et al. from 2018 is the only one presenting such direct crosslinking of interfacially assembled and highly ordered monolayer membranes from nanopores of biological origin.[33]

Zhang et al. used TMV discs (Chapter 3.1.2) laterally presenting cysteine residues. Such TMV discs were found to self-assemble as an ordered monolayer on top of a planar, nanowire-haired copper mesh (when the gird was immersed into a TMV disc solution). The authors assume the vertical and collective orientation of TMV discs in such monolayer is fostered by the formation of disulfide bridges (Chapter 3.1.1) between cysteine residues from neighboring TMV discs, catalyzed by Cu^{2+} ions released from the copper mesh. Furthermore, crosslinked TMV disc sheets (typical dimensions 5−10 μm) were reported to easily detach from the copper mesh and float in aqueous solution. By vacuum filtration of such solutions, TMV disc sheets were layered on top of a ceramic membrane support to form larger, planar TMV membranes with a thickness ranging between 25 nm and 210 nm. The study reports precise size selectivity of TMV disc membranes, resembling the 4 nm TMV pore diameter and water permeance an order of magnitude superior to conventional membranes with similar rejection properties. [33]

While this approach certainly resulted in very homogenous and functional TMV disc membranes, it is presumably not transferable to TPs as building blocks, and it is further questionable, if a scale-up of copper mesh-mediated membrane formation is applicable.

In this thesis, therefore, a straightforward and scalable Langmuir-Schaefer approach to prepare well-ordered monolayer membranes of directly crosslinked protein nanopores (strategy IV) is proposed, as presented in the following Chapter 5.

5 Membrane formation by a Langmuir approach

Engineering and extraction of the FhuA variants used in this study were done by our collaboration partners; Dr. Daniel Sauer, Dr. Marco Grull, Dr. Mehdi Davari Dolatabadi and others in the group of Prof. Schwaneberg at the RWTH Aachen University.

5.1 Overview

As stated in the Introduction (Chapter 2), a new approach for implementing uniform protein pores into a membrane for nanofiltration is presented in this thesis. The goal was to create an ultrathin protein membrane that can be operated by applying low transmembrane pressures and that thus allows for highly energy-efficient nanofiltration through the protein pores.

The strategy followed in this thesis is based on the Langmuir technique well-known for molecular monolayer fabrication (Chapter 3.2) and the homobifunctional crosslinker glutaraldehyde, being an efficient protein crosslinker (Chapter 3.3), known not to impact the protein conformation in many cases.[68,71,81] For demonstration, two variants of the monomeric β-barrel TP FhuA were used (Chapter 3.1.1): The naturally occurring FhuA WT with an almost closed pore and the engineered FhuA ΔCVF^{tev} variant with an open pore (**Figure 5.1**a). Both variants have an elliptical cross-section of 3.9-4.6 nm and a height of 6.9 nm.[42] The FhuA ΔCVF^{tev} pore has an inner diameter of (2.6 ± 0.6) nm,[82] yet engineering of FhuA variants with larger pore diameters is possible.[82,83] FhuA WT and FhuA ΔCVF^{tev} have 37 and 28 lysine residues, respectively, distributed over their lateral surface and allowing for dense chemical crosslinking with glutaraldehyde. Additionally, FhuA ΔCVF^{tev} has an accessible cysteine residue inside the open pore, which enables chemical modification with thiol-reactive groups. FhuA is an amphiphilic protein characterized by a hydrophobic transmembrane region and a hydrophilic loop region. Due to its pronounced amphiphilicity, FhuA has a strong tendency to assemble at interfaces, as demonstrated with tensiometry measurements by Charan et al.[40] In the present thesis, FhuA molecules were spread at the air-water interface of a Langmuir trough (Figure 5.1b(i)). Upon compression with the two movable barriers of the Langmuir trough, a dense 2D film was formed and stabilized by glutaraldehyde crosslinking. Single or multiple layers of crosslinked FhuA membranes were transferred to various substrate materials using the Langmuir-Schaefer method (Figure 5.1b(ii)).[64] FhuA membranes covered holes in substrates without tearing and elastically stretched when loaded with a point force in AFM measurements, which demonstrates great mechanical stability. Membranes were prepared from either FhuA WT or FhuA ΔCVF^{tev} naturally forming almost closed or completely open

pores, respectively (Figure 5.1c). Even membranes with almost closed FhuA pores showed outstanding water permeance, two orders of magnitude superior to state-of-the-art thin-film composite nanofiltration membranes. This is attributed to their low thickness of only a few molecular layers. Moreover, membranes prepared using the open pore variant showed higher ion permeability over those prepared using the closed pore variant (Figure 5.1d).

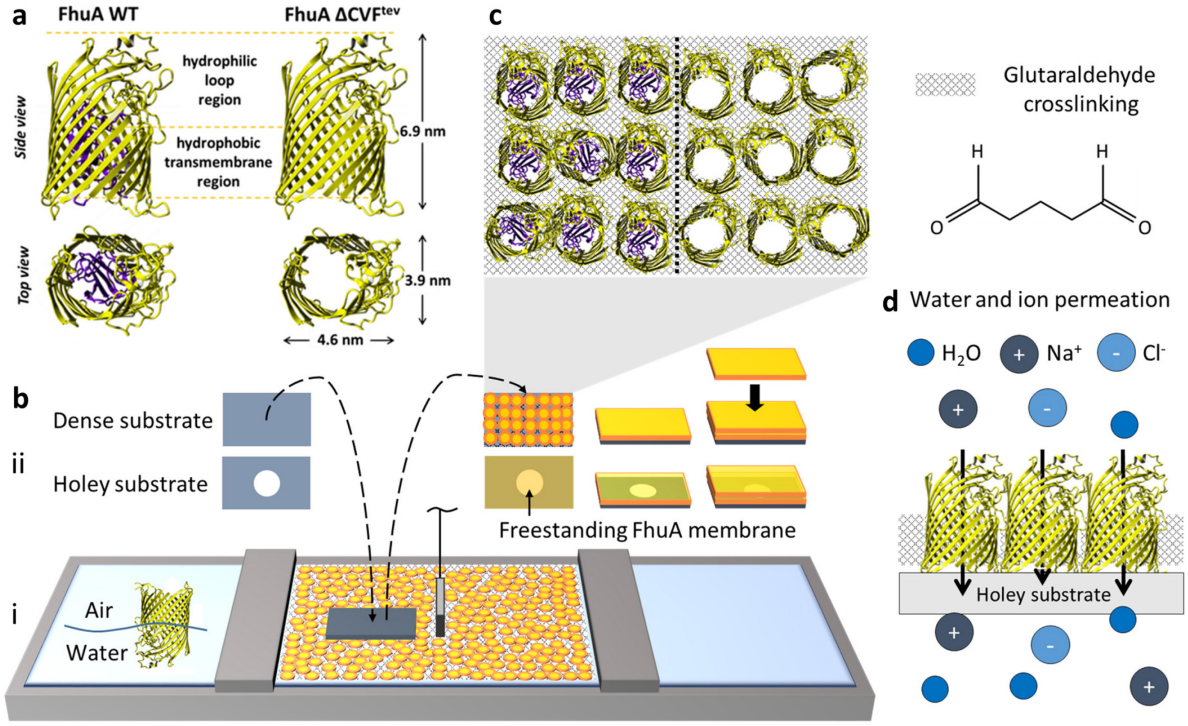

Figure 5.1: Crosslinked 2D membrane sheets of transmembrane protein FhuA. a, Two variants of the ß-barrel protein FhuA were used: In FhuA WT, a cork domain blocks most of the pore interior while this cork domain was biotechnologically removed to form the open pore variant FhuA ΔCVF^{tev}. Both FhuA variants have identical dimensions and are characterized by a hydrophilic loop region in the upper part of the protein and a hydrophobic transmembrane region in the lower part of the protein. b, The Langmuir technique was applied to form ultra-large 2D FhuA membrane sheets. (i) Due to their amphiphilicity, FhuA molecules occupy a largely upright orientation when spread to the air-water interface. (ii) When densely compressed between the barriers of the Langmuir trough and crosslinked with glutaraldehyde, FhuA membrane sheets can be layered on top of substrates by repeated horizontal dipping. By using holey substrates, freestanding FhuA membranes can be fabricated. c, Schematic top view of membranes made of FhuA WT (left) or FhuA ΔCVF^{tev} (right) and structural formula of glutaraldehyde. d, FhuA membranes were characterized in terms of water and ion permeation.

The following sections present the experiments and findings related to the development of the new protein nanopore membranes. First, the quality of FhuA as a membrane building material is discussed analyzing the results of sodium dodecyl sulfate polyacrylamide gel electrophoresis (SDS-PAGE), circular dichroism (CD) spectroscopy and TEM investigations. Next,

experiments studying FhuA Langmuir films at the air-water interface are presented covering Brewster-angle microscopy (BAM), sum-frequency generation (SFG) spectroscopy and FhuA membrane fabrication by glutaraldehyde crosslinking of FhuA Langmuir films. Subsequent sections focus on the investigation of FhuA membranes transferred to either dense or holey substrates by Langmuir-Schaefer method exploiting advanced imaging techniques such as TEM, helium ion microscopy (HIM) and atomic force microscopy (AFM). Then, water and ion permeation measurements on FhuA membranes covering substrates with a single hole are illuminated. The final sections describe the transfer of FhuA membranes to larger, ceramic membrane supports and nanoscale rejection properties of the resulting composite membranes. At the end, transferability of membrane preparation demonstrated throughout this work using FhuA to TMV-derived VLPs is discussed.

5.2 Assessment of FhuA as building material

As part of this doctoral project, ultrathin protein nanopore membranes were prepared using variants of the transmembrane protein FhuA. Ideally, those membranes would be fabricated from pure and monodisperse FhuA pores. However, non-denaturing extraction and purification of β-barrel proteins form bacterial cultures is expensive and rather suited to produce low protein amounts (information from discussion with biotechnologists). For the investigations in this thesis and potential applications of FhuA membranes in future, larger amounts of FhuA are required. Hence, FhuA used in this study was extracted in a denaturing process, purified, and then refolded by dialysis against a buffer containing the stabilizing agent MPD (Chapter 3.1.1). During refolding and storage in aqueous media, amphiphilic MPD molecules attach to and thus stabilize the hydrophobic transmembrane region of FhuA. While this is a more affordable and straightforward procedure to provide large amounts of β-barrel proteins in solution, established MPD refolding protocols are known to not result in perfect refolding of all the β-barrel proteins present.[53] As basis for the investigations presented in this thesis, experiments assessing the quality of MPD-refolded FhuA samples are therefore summarized in this chapter.

5.2.1 SDS-PAGE

The proposed Langmuir approach for FhuA membrane preparation requires pure FhuA samples and covalent crosslinking of MPD-stabilized FhuA molecules with glutaraldehyde. To test dialyzed FhuA samples for these criteria, SDS-PAGE was performed. SDS-PAGE[84] allows to qualitatively determine the purity and roughly the molecular weight of protein samples. While pure proteins show a narrow molecular weight distribution, protein crosslinking may be

detected by a more diffuse molecular weight distribution and a shift of the band toward higher molecular weights.

The following six samples were investigated in one SDS-PAGE gel (performed under kind supervision of Maria Mathieu-Gaedke): FhuA WT, FhuA ΔCVF^{tev} and FhuA A2a, each dialyzed in MPD buffer according to the refolding protocol, as well as the same samples each mixed with glutaraldehyde 24 hours in advance. If mixed, the concentration of glutaraldehyde in the FhuA solution was 0.5 vol%, which is the same concentration as later used for FhuA membrane stabilization in Chapter 5.3.2. An image of the resulting SDS-PAGE gel stained with Coomassie brilliant blue is shown in **Figure 5.2**.

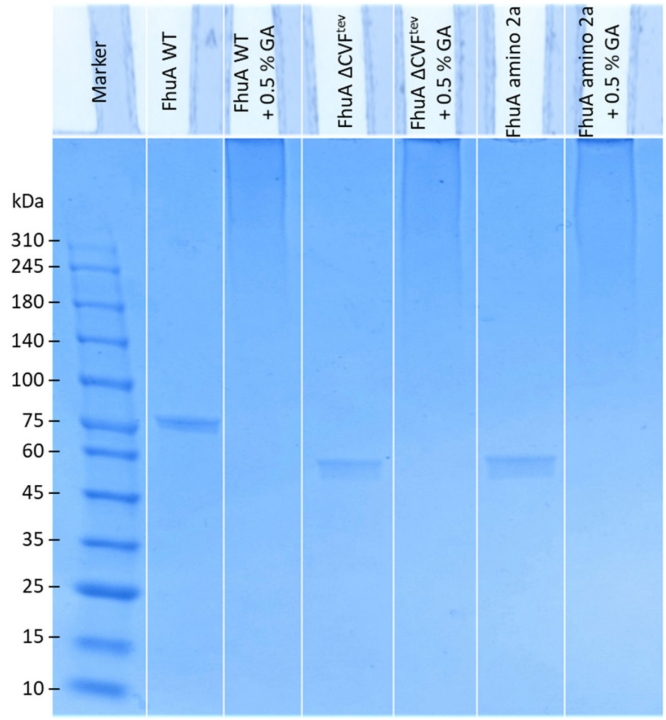

Figure 5.2: Verification of FhuA purity and glutaraldehyde crosslinking in solution. Image of an SDS-PAGE gel showing the molecular weight distribution of pure, MPD-refolded FhuA WT, FhuA ΔCVF^{tev} and FhuA A2a samples and the molecular weight distribution of the same samples after crosslinking at a glutaraldehyde concentration of 0.5 vol% for 24 hours.

The stained SDS-PAGE gel shows narrow bands for the FhuA WT, the FhuA ΔCVF^{tev} and the FhuA A2a sample matching their respective molecular weights of 78.9 kDa, 63.7 kDa and 63.2 kDa. This indicates high purity of the dialyzed FhuA samples. In contrast, all three samples of FhuA variants mixed with glutaraldehyde show a highly diffused band at the very top of the gel inlet, suggesting that FhuA oligomers have formed. This demonstrates that a concentration of 0.5 vol% of glutaraldehyde in MPD buffer reliably crosslinks the three FhuA variants tested here.

SDS-PAGE thus indicated high purity of all three FhuA samples and proved that FhuA molecules stabilized with MPD may be crosslinked at a moderate glutaraldehyde concentration. Next, structural features of the FhuA samples after dialysis were investigated.

5.2.2 CD spectroscopy

CD spectroscopy on FhuA samples was conducted by Maria Mathieu-Gaedke at the University of Potsdam.

For the preparation of membranes with functional FhuA nanopores, effective refolding of denatured FhuA variants to their β-barrel structure is mandatory (Chapter 3.1.1). While the determination of tertiary protein structures usually requires advanced crystallographic or small-angle scattering techniques, optically active secondary protein structures such as β-sheets or α-helices may be detected straightforwardly using circular dichroism (CD) spectroscopy.[85] CD spectroscopy relies on the property of optically active or chiral structures to differently absorb left- and right-hand circular polarized light. If linear polarized light is passed through an optically active substance it will thus turn into elliptically polarized light. The graph showing the ellipticity of polarization for different wavelengths is referred to as CD spectrum and the CD spectra of different optically active secondary protein structures have assignable shapes. CD spectra corresponding to SDS-denatured FhuA A2a before refolding and FhuA A2a, FhuA ΔCVF^{tev} and FhuA WT samples after refolding in MPD buffer are shown in **Figure 5.3.**

The CD spectrum of FhuA A2a in SDS has a minimum between 200 and 210 nm (not around 215 nm as typically associated with β-sheets)[86], indicating that FhuA was properly denatured before dialysis. After refolding, in contrast, the CD spectra of all three FhuA variants have minima around 215 nm and the typical shape associated with β-sheets.[86] Since the structure of FhuA in its native state is dominated by β-sheets, CD spectroscopy clearly suggests that at least partial refolding of FhuA was achieved by dialysis against MPD buffer.[54] However, to use FhuA as a nanopore in a membrane, it is essential that the refolded β-sheets actually arrange as a β-barrel. This was investigated by TEM measurements presented in the next section.

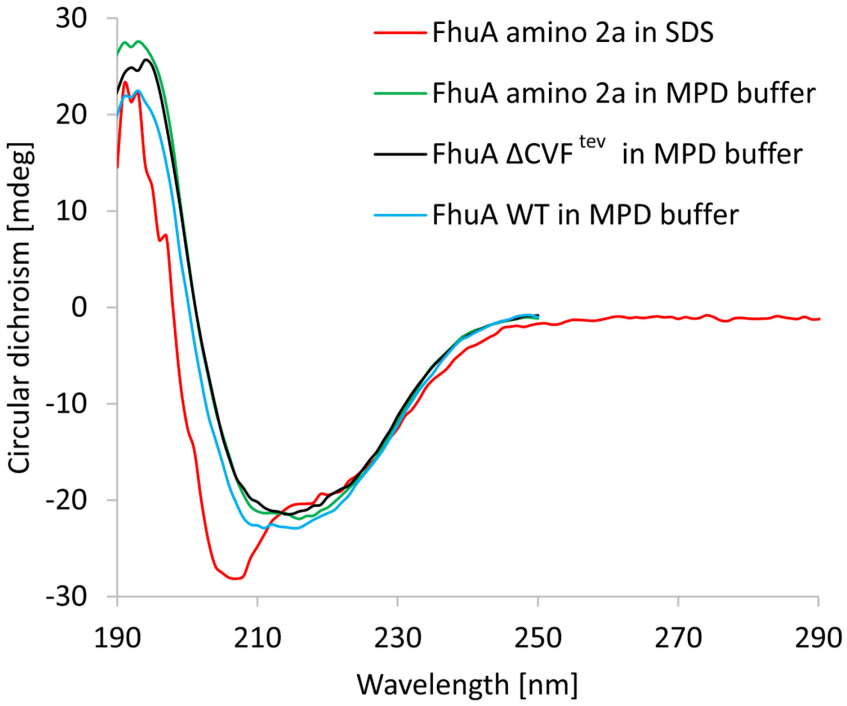

Figure 5.3: Verification of structural integrity of FhuA variants refolded in MPD buffer I. Circular dichroism (CD) spectra of FhuA A2a, FhuA ΔCVF^{tev} and FhuA WT refolded in MPD buffer. The CD spectrum of FhuA A2a denatured in SDS is shown as reference.

5.2.3 TEM

TEM measurements were performed by Thomas Bick from the group of Prof. Petra Wendler at the University of Potsdam.

In the previous section, CD spectroscopic investigations suggested successful refolding of FhuA's secondary β-sheet structure upon dialysis against MPD buffer. To determine whether dialysis against MPD buffer further induces refolding to FhuA's tertiary protein structure, TEM was used. Contrary to the indirect structure determination of CD spectroscopy, TEM enables actual visualization of down to Ångström-sized structures as a 2D-projection when suspended on a TEM grid. Here, the goal was to verify the size of single, refolded FhuA molecules and to visualize the pronounced pore of FhuA, especially in the open channel variants FhuA ΔCVF^{tev} and FhuA A2a. To enhance contrast when investigating biological samples in TEM, negative staining with uranyl acetate is an established method.[87] In case of FhuA, the stain was expected to surround the single molecules and to accumulate in the central pores, thus, highlighting these features of interest due to enhanced electron scattering of the stain. TEM images of uranyl acetate-stained FhuA WT, FhuA ΔCVF^{tev} and FhuA A2a samples in two magnifications are shown in **Figure 5.4**. The TEM overview images of all samples show both, irregular particles significantly larger than single FhuA molecules (> 10 nm) and small particles of similar size in the order of magnitude of single FhuA molecules (< 10 nm) (Figure 5.4 a(i), b(i), c(i)**)**. Considering the SDS-PAGE results (Chapter 5.2.1), which indicated great FhuA sample purity, it can be concluded that the larger, unregular features are FhuA aggregates while the smaller particles are single FhuA molecules. Solvent evaporation during TEM sample preparation could contribute to the formation of aggregates. The TEM image magnifications (Figure 4.4 a(ii), b(ii), c(ii)**)** allow a closer view of the single FhuA molecules, which in size and shape indeed look similar to single, purified and properly folded FhuA WT molecules on TEM images published by Breyton et al. in 2013.[88] Most single FhuA ΔCVF^{tev} and FhuA A2a molecules, in particular, are characterized by a black dot in their center indicating uranyl acetate agglomeration. This suggests the presence of cavities in the FhuA molecules, which may be interpreted as FhuA pores.

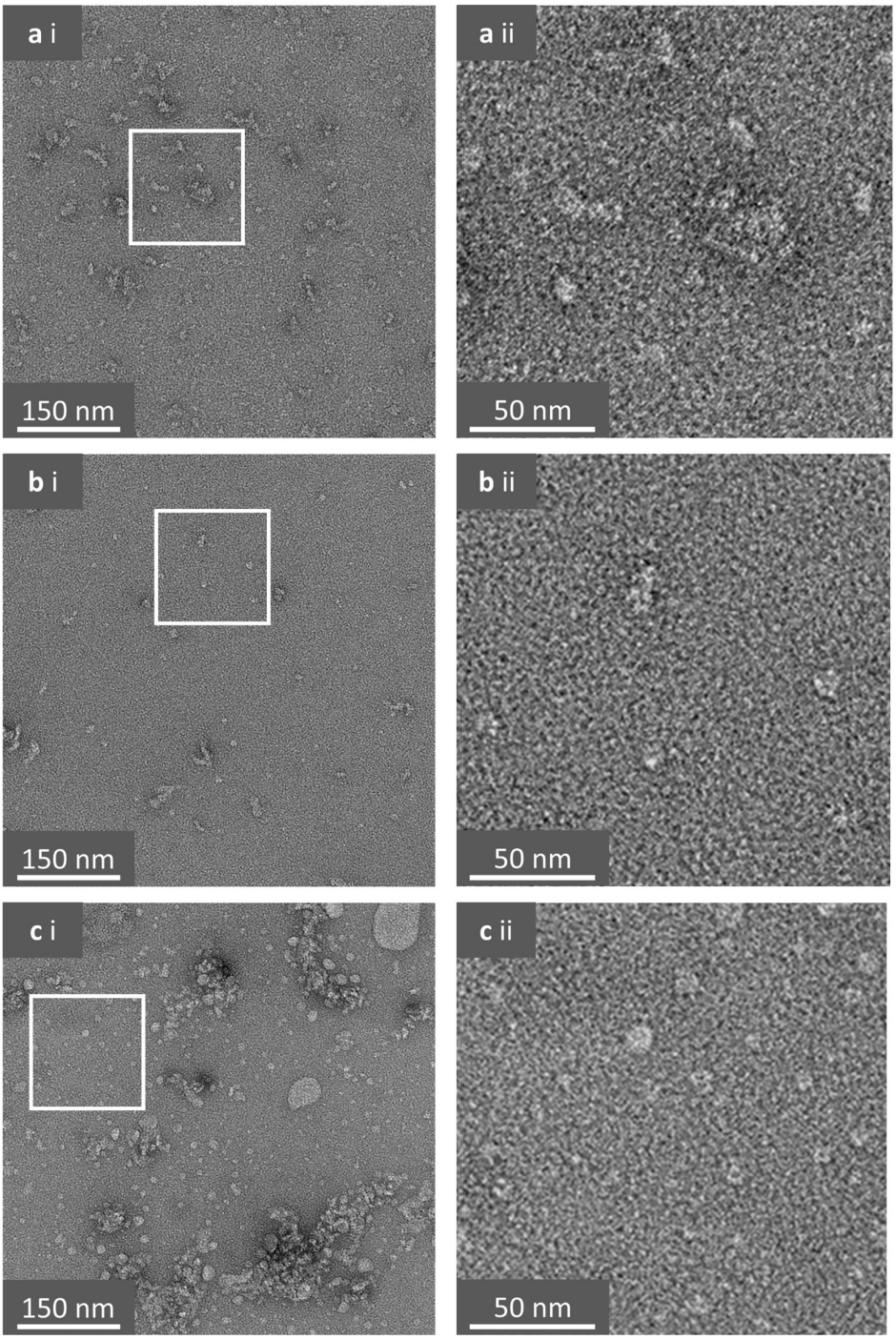

Figure 5.4: Verification of structural integrity of FhuA variants refolded in MPD buffer II. TEM images of a, FhuA WT, b, FhuA ΔCVF^{tev} and c, FhuA A2a samples stained with uranyl acetate. In a, b and c, (ii) shows the magnification of the white box in i.

TEM thus strongly suggested that refolding of FhuA to its native β-barrel structure may be achieved by dialysis against MPD buffer. However, it also revealed considerable agglomeration of FhuA molecules refolded in MPD buffer when suspended on a TEM grid. The latter was considered for the discussion of experiments related to FhuA membrane preparation and characterization presented hereinafter.

5.3 Langmuir experiments and FhuA membrane preparation

After quality assessment of FhuA samples used as membrane building material, preparation of FhuA monolayer membranes was investigated following the Langmuir-Schaefer approach described in the project overview (Chapter 5.1). Briefly, FhuA molecules were self-assembled at the air-water interface of a Langmuir trough, compressed using the Langmuir trough barriers until forming a dense monolayer, which was then stabilized as a membrane by glutaraldehyde crosslinking of the lysine residues present on the lateral surface of FhuA (Chapter 3.1.1). General descriptions of the Langmuir technique used to study/fabricate molecular monolayers and of protein crosslinking using glutaraldehyde are given in the Chapters 3.2 and 3.3, respectively. This chapter focuses on FhuA membrane formation at the air-water interface, which was investigated applying BAM, recording Langmuir isotherms and using SFG spectroscopy.

5.3.1 BAM

BAM measurements were performed together with Aleksei Chumakov in the lab of Prof. Svetlana Santer at the University of Potsdam.

In tensiometry experiments by Charan et al., FhuA was shown to have high tendency to assemble at interfaces.[40] Nonetheless, this thesis reports for the first time the investigation of FhuA spread to the air-water interface of a Langmuir trough. Furthermore, investigations of Langmuir films of solely TPs at the interface (without being in a mixture with lipids) were, to the best of my knowledge, only published for TP bestrophin-1 before, when molecular mechanisms underlying specific pathologies linked to this protein were studied.[89,90] To get fundamental insights into FhuA film formation, FhuA WT in MPD buffer was first spread to the clean air-water interface of a Langmuir trough featuring a Brewster Angle Microscope.

BAM is a method frequently used to visualize Langmuir films on the micro-scale.[91] The method applies Brewster's law, which predicts that p-polarized electromagnetic waves directed towards the clean air-water interface in so-called Brewster angle (~ 53° for the air-water interface) are fully refracted at the air-water interface and no reflection may be detected. The BAM image is thus simply black when the air-water interface is clean. If, however, particles adsorb to the air-water interface, the refractive index of the air-water interface changes so that reflection occurs, which is detected and transformed into a microscale image of the air-water interface.[91]

Here, BAM was performed simultaneously to recording a compression isotherm after spreading 0.88 nmol FhuA WT in MPD buffer to the air-water interface of the Langmuir trough. After an equilibration time of 15 min, almost no rise in surface pressure was detected. In the compression isotherm shown in **Figure 5.5,** the surface pressure at maximum trough area of 232 cm^2 is thus close to zero (0.05 mN m^{-1}). However, upon reducing the trough area by barrier compression, the isotherm shows a monotone increase in surface pressure. This indicates an increasing surface concentration and thus the formation of a denser FhuA film at the air-water interface.

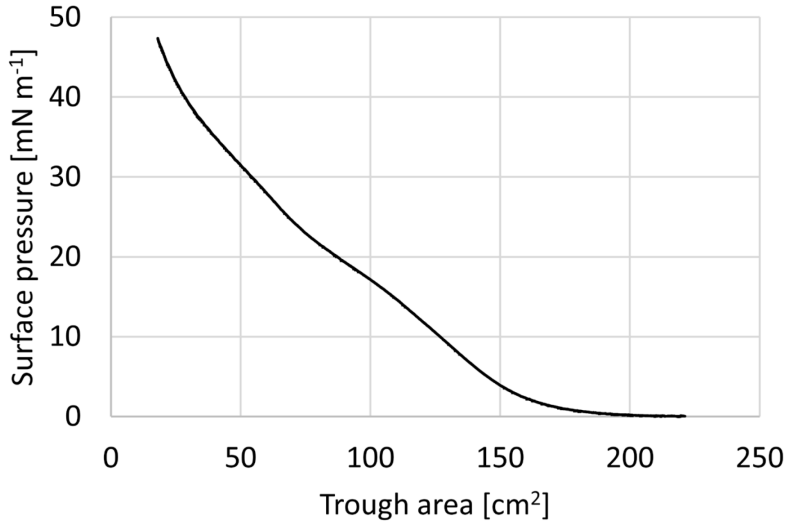

Figure 5.5: FhuA WT at the air-water interface of a Langmuir trough I. Langmuir isotherm recorded after spreading 0.88 nmol FhuA WT to the air-water interface (70 µl FhuA WT in MPD buffer at a concentration of 12.6 µM, subphase Millipore pure water, compression rate 1 mm min^{-1}, room temperature).

The latter is also reflected in the corresponding BAM images compiled in **Figure 5.6**. The black reference BAM image in Figure 5.6a was taken before spreading of FhuA WT, verifying that the air-water interface was sufficiently clean. Immediately after spreading, however, BAM shows a dense and homogenous film adsorbed to the air-water interface (Figure 5.6b). This demonstrates great sensitivity of BAM, as the initial increase of surface pressure detected in the isotherm was still almost negligible at this point. The adsorbed FhuA WT film was compressed to surface pressures up to 25 mN m^{-1} without showing inhomogeneities (Figure 5.6c-d). At surface pressures of 30 mN m^{-1} and higher, elongated cracks perpendicular to the direction of compression were visible in the FhuA WT film (Figure 5.6f). To prevent cracks but form a densely packed FhuA membrane, membrane stabilization with glutaraldehyde was performed at a surface pressure of 25 mN m^{-1}, as described in the next section.

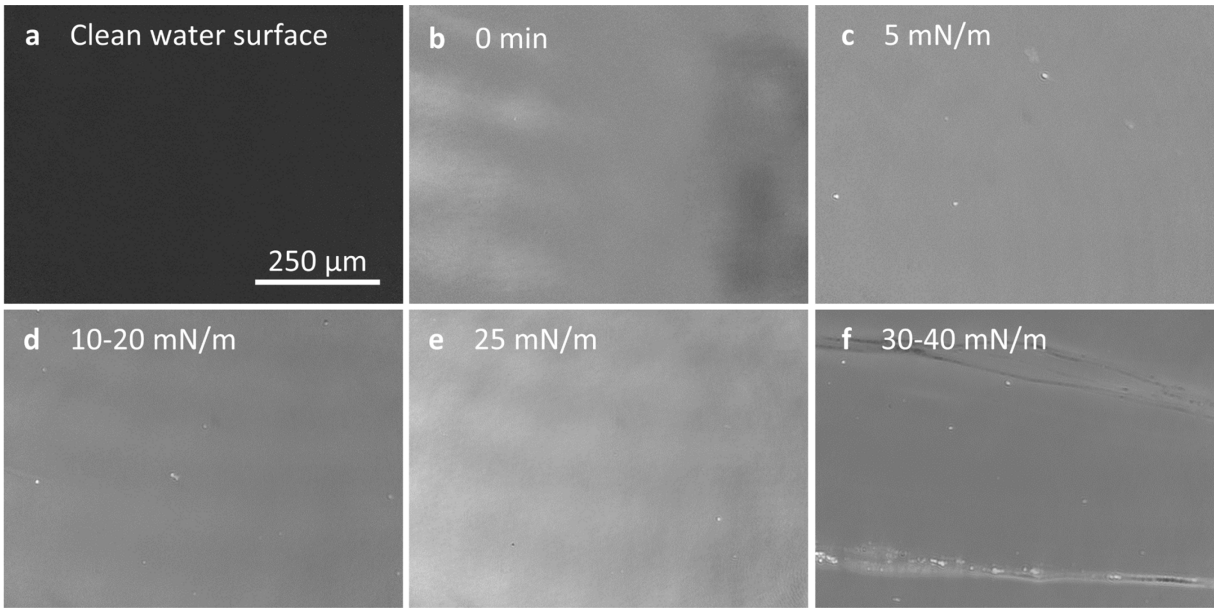

Figure 5.6: FhuA WT at the air-water interface of a Langmuir trough II. BAM images of the air-water interface of the Langmuir trough (a) before and (b) immediately after spreading FhuA WT to the air-water interface of a Langmuir trough; and (c-f) at different surface pressures upon barrier compression (corresponding Langmuir isotherm shown in Figure 5.5).

5.3.2 Membrane stabilization: Glutaraldehyde crosslinking of FhuA Langmuir films

In the previous section, BAM showed that FhuA instantly forms a homogenous film when spread at the air-water interface of a Langmuir trough, reaching its maximum density at a surface pressure around 25 mN m^{-1}. This insight was the basis for further developing a protocol for FhuA membrane formation.

To prepare FhuA membranes, typically 0.32 nmol of monodisperse FhuA WT or FhuA ΔCVF^{tev} in MPD buffer were spread to the air-water interface of the Langmuir trough. This is less FhuA than needed to fully cover the initial trough area and ensures that the adsorbed FhuA film rather consists of one than multiple molecular layers (as estimated based on the area occupied by upright oriented FhuA molecules in a crystal (Figure S1, Appendix)). FhuA adsorption was monitored as a function of surface pressure over time (**Figure 5.7**a(i), b(i)), showing an initial rise in surface pressure until asymptotically approaching an equilibrium between 2 and 2.5 mN m^{-1} after 2 hours. This higher equilibrium surface pressure - as compared to the initial surface pressure of the isotherm recorded during BAM imaging (Figure 5.5) - is associated with the different subphases used. In BAM measurements, this was pure water while FhuA membranes were formed on top of phosphate buffer. Referred to as “salting up” effect, salts were shown to strongly enhance the adsorption of BSA from highly diluted bulk solutions to the air-water interface.[92] For the purpose of FhuA membrane formation, using phosphate

buffer as subphase on the one hand leads to an increase of the interfacial activity of FhuA and consequently the incorporation yield of spread FhuA into a membrane. On the other hand, it prevents a drop in pH upon injection of acidic glutaraldehyde solution, which could otherwise adversely affect the ß-barrel conformation of FhuA.

To prevent cracks (as observed by BAM for high surface pressures) but form a densely packed FhuA membrane, spread FhuA films were compressed to and crosslinked with glutaraldehyde at a surface pressure of 25 mN m^{-1} (Figure 5.7a(ii), b(ii)). Injection of glutaraldehyde into the buffer subphase was carried out reaching a final concentration of 0.5 vol% and is visible as a small irritation in the compression isotherms at trough areas around 115 cm^2 (marked with an arrow in Figure 5.7a(ii)). Efficient FhuA crosslinking at this glutaraldehyde concentration in solution was verified by SDS-PAGE (Chapter 5.2.1). The plateaus in the compression isotherms indicate that keeping the surface pressure constant requires further reduction of the trough area (Figure 5.7a(ii), b(ii)). However, the kinks in the trough area-time isotherms (Figure 5.7a(iii), b(iii)) illustrate that, shortly after the injection of glutaraldehyde (marked with an arrow in Figure 5.7a(iii)), the membrane area stabilizes at a trough area of around 100 cm^2. For reference, additional isotherms corresponding to FhuA WT membrane formation carried out without injection of glutaraldehyde are shown in red color in Figure 5.7b(ii) and (iii). Without the addition of glutaraldehyde, the trough area reduces at high rates, which is attributed to FhuA molecules desorbing into the subphase as a result of the high surface pressure.[65,66] When glutaraldehyde is added, however, the trough area soon reduces at significantly lower rates (Figure 5.7a(iii), b(iii), black isotherms), which is associated with covalent bonds forming between the lysine residues of adsorbed FhuA molecules and consequent stabilization of the FhuA film at the air-water interface. Generally, FhuA WT and FhuA ΔCVF^{tev} samples showed similar adsorption behavior and membranes of both variants were prepared in an analogous manner (Figure 5.7). After 8 hours of crosslinking, the FhuA WT and the FhuA ΔCVF^{tev} membranes covered an area of 95.7 cm^2 and 97.4 cm^2, respectively.

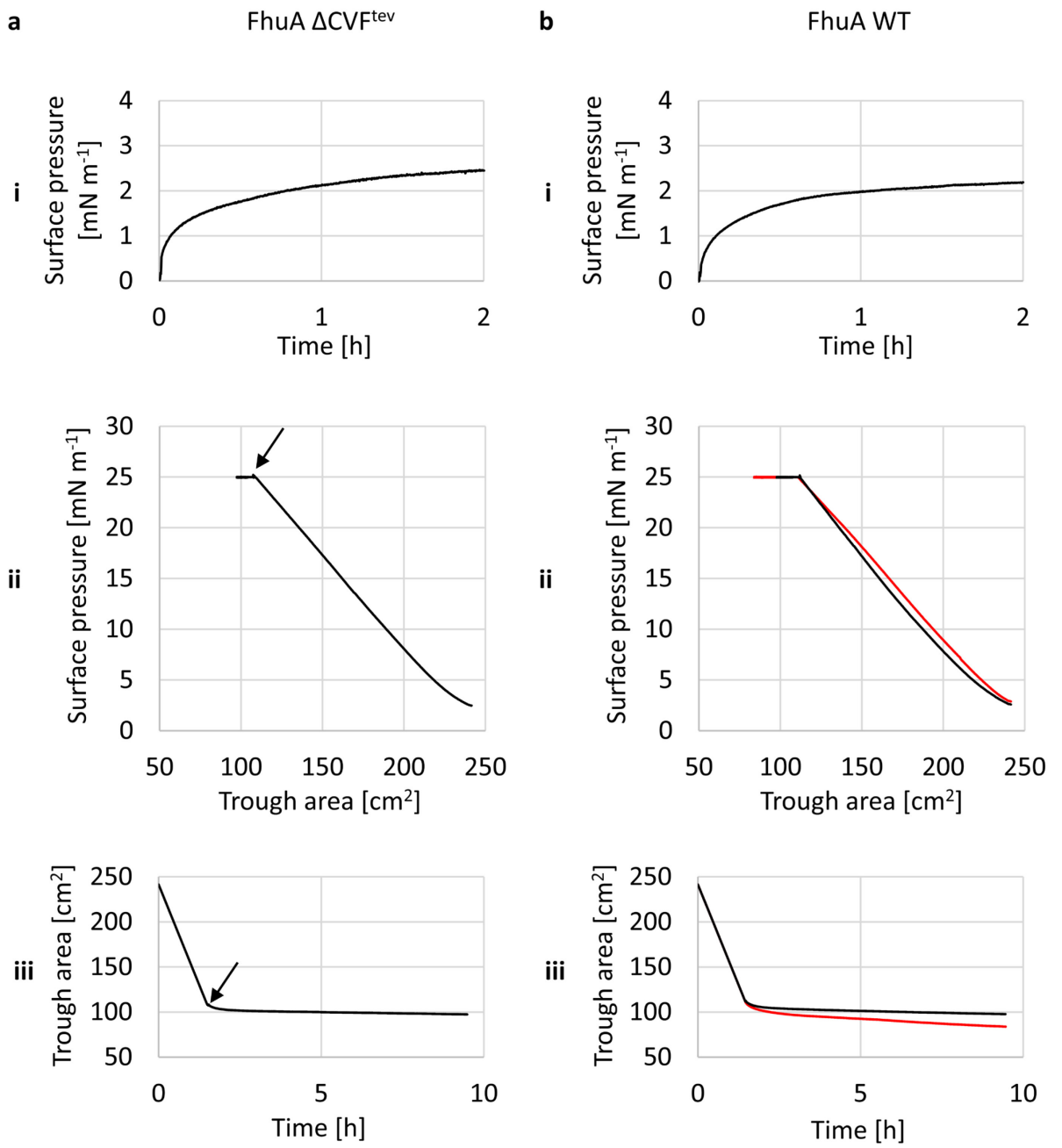

Figure 5.7: FhuA at the air-water interface of a Langmuir trough III. Representative set of Langmuir (i) adsorption, (ii) compression and (iii) trough area-time curves measured during membrane fabrication from 0.32 nmol (a) FhuA ΔCVF^{tev} and (b) FhuA WT spread on top of phosphate buffer (pH 7.4) (50 µl FhuA WT in MPD buffer at a concentration of 6.3 µM, compression rate 1 mm min^{-1}, at room temperature). In a(ii) and a(iii), the injection of glutaraldehyde is marked with an arrow. Similarly, glutaraldehyde was injected during measurement of the black curves in b, while measurement of the curves marked red was done without injection of glutaraldehyde.

5.3.3 SFG spectroscopy and packing density

SFG measurements and analysis were carried out by Daizong Qi, Dr. Hao Lu and Dr. Konrad Meister from the group of Prof. Mischa Bonn at the Max Planck Institute for Polymer Research in Mainz.

In the project overview (Chapter 5.1), it was proposed that FhuA molecules will occupy a largely upright orientation when spread to the air-water interface, with their hydrophilic loop region oriented toward the water phase and their hydrophobic transmembrane region oriented toward the air phase. Only such collective and upright orientation of FhuA during membrane preparation will result in well-ordered, functional FhuA membranes, with pores aligned vertically to the membrane plane.

To investigate the alignment of FhuA molecules at the air-water interface before and after crosslinking at a surface pressure of 25 mN m^{-1}, sum-frequency generation (SFG) spectroscopy was used. SFG is a surface-sensitive vibrational spectroscopy technique, which provides the vibrational spectrum of the interfacial region for which symmetry is broken. In this approach, visible and infrared laser pulses impinge upon the surface, and SFG light, at a frequency given by the sum of the visible and infrared frequencies, is generated when the infrared is resonant with interfacial vibrations – in this case the protein amide mode.[93] Here, the good match of measured and calculated SFG spectra (computed for upright oriented FhuA molecules) demonstrated upright and collective orientation of FhuA molecules at the air-water interface, and crosslinking did not impact this constitution (**Figure 5.8**).

Combining knowledge of upright FhuA orientation with an approximation of the area occupied by uprightly oriented FhuA molecules as derived from its crystal structure (Figure S1, Appendix), the maximum packing density of FhuA molecules in FhuA membranes was estimated. If all spread FhuA molecules (0.32 nmol) arranged in upright fashion at the air-water interface (neglecting desorption into the subphase), they would cover an area of about 78 cm^2 (Figure S1, Appendix). Relating this area to the final FhuA membrane area of about 96 cm^2 (Chapter 5.3.2), results in a maximum packing density of 80%, the other 20% being interstitial space between the FhuA molecules. However, the interstitial space in this upper bound scenario is at least partly filled with glutaraldehyde. Therefore, the interstitial space may contribute to water flux and ion permeability through FhuA membranes (Chapter 5.5), but is presumably blocked for transport of larger molecules or particles during filtration experiments.

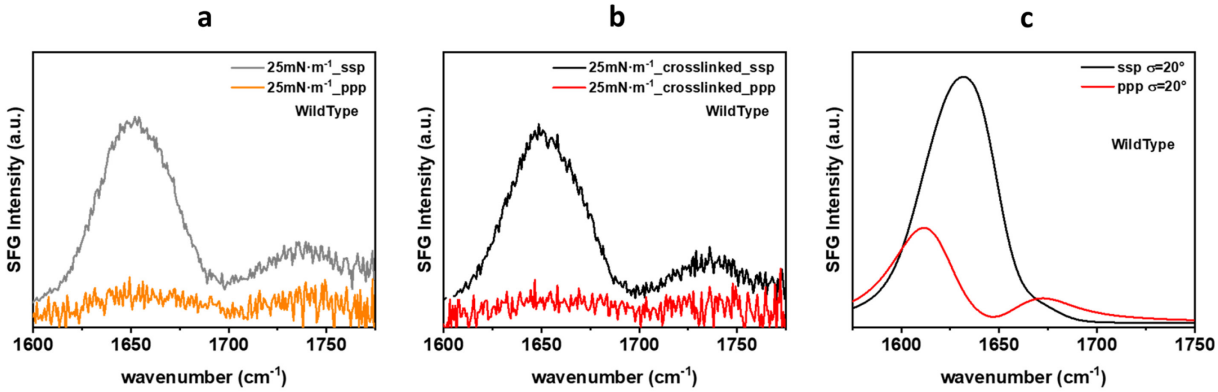

Figure 5.8: Sum-frequency generation spectroscopy data from FhuA monolayers. Spectra for FhuA WT (a), self-assembled at the air-water interface (surface pressure 25 mN/m) and (b), spectra following crosslinking at the same surface pressure are indistinguishable, indicating that crosslinking does not affect protein orientation or conformation. SFG spectra were recorded for two different polarization combinations (PPP and SSP, where the first letter corresponds to the polarization of the sum-frequency light, the second to that of the visible, and the third to that of the infrared beam; polarization is defined relative to the plane of incidence). The large SSP signal, relative to other proteins at interfaces,[93] indicates a very high degree of preferential orientation of proteins at the interface. (c), Calculations of the expected signal for an ensemble of oriented FhuA proteins, arranged with their backbone perpendicular to the water-air interface, following ref.[94], are in qualitative agreement with experiments. For the calculations, a 20° full-width at half maximum, Gaussian angular distribution around the surface normal was assumed. The calculations assume the structure described in the Protein Database (PDB), which are inferred from low-temperature x-ray diffraction experiments on crystals. The fully hydrated protein at the air-water interface at room temperature likely has some structurally subtle differences to the PDB structure, possibly accounting for the observed discrepancies between experiment and theory.

5.4 Transfer to supports

The previous chapter described the preparation of membranes from uprightly oriented FhuA molecules at the air-water interface of a Langmuir trough. Even though crosslinked with glutaraldehyde, FhuA membranes are highly flexible and not self-supporting when removed from the air-water interface. To enable membrane characterization and application off the air-water interface, FhuA membranes were therefore transferred to various support materials using the Langmuir-Schaefer method (Chapter 3.2). The first section of this chapter summarizes investigations on FhuA membranes transferred to dense substrates, which shine light on the membrane thickness and structural integrity of FhuA pores incorporated in a membrane in the dry state. The second part of this chapter presents experiments on FhuA membranes transferred to porous support materials, revealing considerable mechanical strength of the ultrathin membranes when freestandingly covering holes with microscale diameters.

5.4.1 Transfer to dense substrates

Advanced techniques for the investigation of supported thin films, such as AFM or nano-scale X-ray studies, typically require super flat substrates that do not interfere with the measurement set-up. For such investigations, FhuA membranes were transferred to silicon substrates, which were plasma-activated shortly in advance to enhance membrane attachment.

5.4.1.1 AFM

The goal of FhuA membrane fabrication using a Langmuir trough was to prepare homogenous, well-ordered, molecular monolayer membranes. Therefore, the membrane thickness was expected to correspond to the known dimensions of single FhuA molecules. Furthermore, FhuA membrane bi-layers prepared by repeated Langmuir-Schaefer transfer should have doubled thickness. Verification of FhuA membrane thickness was first conducted using AFM, which, in contrast to other high-resolution microscopic techniques such as SEM or TEM, creates a height-scan of the sample surface. AFM images of FhuA WT mono- and bi-layer membranes on top of silicon substrates, half scratched away with a syringe tip, show dense and homogenous films with consistent thicknesses of 5 nm and 9 nm, respectively (**Figure 5.9**). The irregular features protruding the membranes (white spots in the images) are attributed to lose membrane fragments caused and deposited when half of the membrane was scratched away. Generally, FhuA monolayer membranes prepared from each variant had a thickness of 5 nm complying with the dimensions of native FhuA molecules (in upright position: max wide – 4.6 nm, max. height – 6.9 nm, Chapter 3.1.1), which suggests that FhuA membrane sheets are indeed molecular monolayers. Thus, the partially large FhuA aggregates observed in

TEM analysis do not seem to dominate or prevent the formation of homogenous FhuA membranes. However, considering possible drying and deposition effects as well as limited accuracy of AFM with respect to sub-nanometer resolution, this AFM analysis may not be interpreted regarding orientation of FhuA molecules in the membrane plane either. To demonstrate collective and upright FhuA orientation, SFG spectroscopy applied to FhuA membranes in Chapter 5.3.3 was thus a more appropriate method.

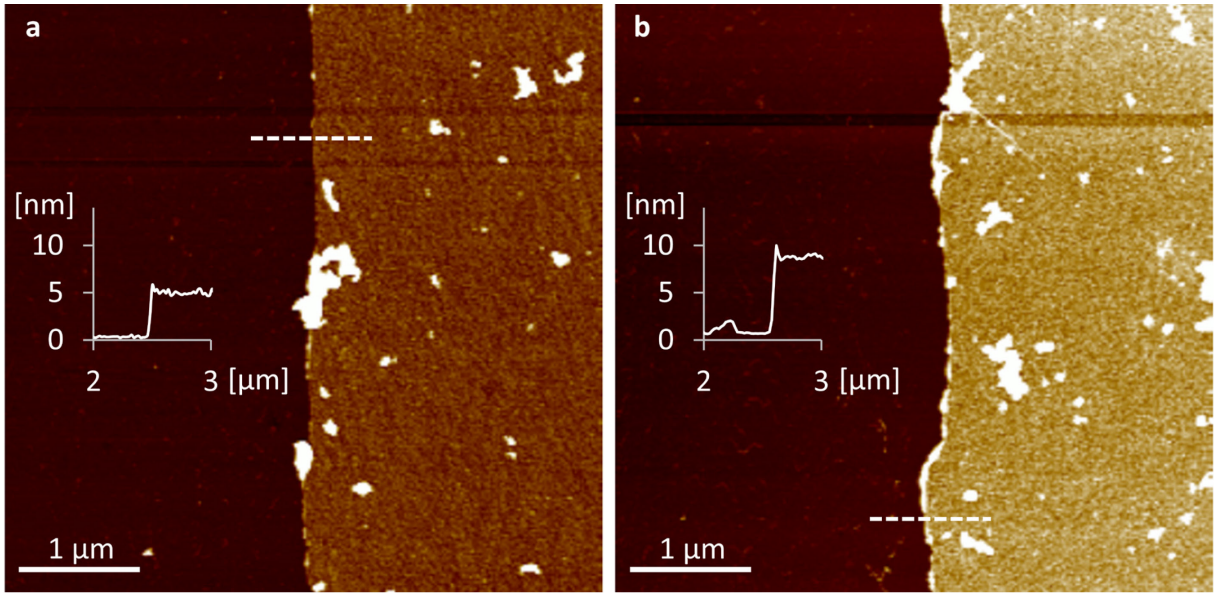

Figure 5.9: AFM images of (a) one or (b) two FhuA membrane sheets layered on top of a silicon substrate (left half scratched away with a syringe tip). The height profiles belong to the dashed lines in the images and indicate membrane thicknesses of (a) 5 nm and (b) 9 nm.

The almost doubled thickness of the FhuA WT membrane prepared with two subsequent Langmuir-Schaefer transfers measured by AFM (Figure 5.9), on the other hand, clearly confirms that FhuA membranes may be layered on top of each other. This finding was later used to prepare more robust membranes suited to assess permeation properties of FhuA membranes rather than molecular monolayer membranes.

The next sections describes X-ray reflectivity (XRR) and grazing-incidence small-angle X-ray scattering (GISAXS) experiments performed on FhuA mono- and bi-layer membranes to measure the membrane thicknesses with an alternative method and to access the FhuA arrangement in the membrane layers, respectively.

5.4.1.2 XRR and GISAXS

XRR and GISAXS experiments were performed at Synchrotron SOLEIL collaborating with Dr. Stephanie Taßler.

The AFM study presented in the previous section suggests that FhuA membranes are molecular monolayers, in other words 2D films made from FhuA molecules. Further studies on the structure of FhuA films regarding thickness and protein arrangement were carried out using sophisticated X-ray-based techniques at Synchrotron SOLEIL (beamtime: 29.05.-03.06.2019). Analogous to the AFM analysis, mono- and bi-layer membranes prepared from FhuA WT and FhuA A2a were investigated on silicon substrates.

First, specular X-ray reflectivity (XRR) was performed and the measured reflectivity curve was analyzed to estimate the membrane thickness. The reflectivity curve is the graph showing the intensity of X-ray reflection of a sample for a range of angles around the critical angle (angle between substrate and incident X-ray at which total external reflection occurs). Furthermore, in specular XRR, the angle of incidence equals the angle in which the reflection intensity is detected. In case of FhuA membranes on top of solid silicon wafers, the incident X-rays are partially reflected and partially refracted at the air-membrane interface and at the membrane-silicon substrate interface. Depending on the angle of incidence, the reflected X-rays interfere differently, which determines the intensity of the detected reflectivity and thus the shape of the reflectivity curve. To estimate the membrane thickness, the reflectivity curve data was analyzed using StochFit[95] analysis software. The program is suited for the analysis of XRR reflectivity curves of homogenous films (which holds true for FhuA membranes, as indicated by AFM) and estimates the scattering length density based on the elemental composition and the density of the film material. On this basis, StochFit was used to first deduce electron density profiles from the reflectivity curves of FhuA mono- and bi-layer membranes and then to fit the electron density profiles to estimate the membrane thickness, as shown in **Figure 5.10**. The box fits[96] indicate FhuA A2a as well as FhuA WT mono- and bilayer membranes to have thicknesses of about 5 nm and 9 nm, respectively, closely resembling the values obtained by AFM.

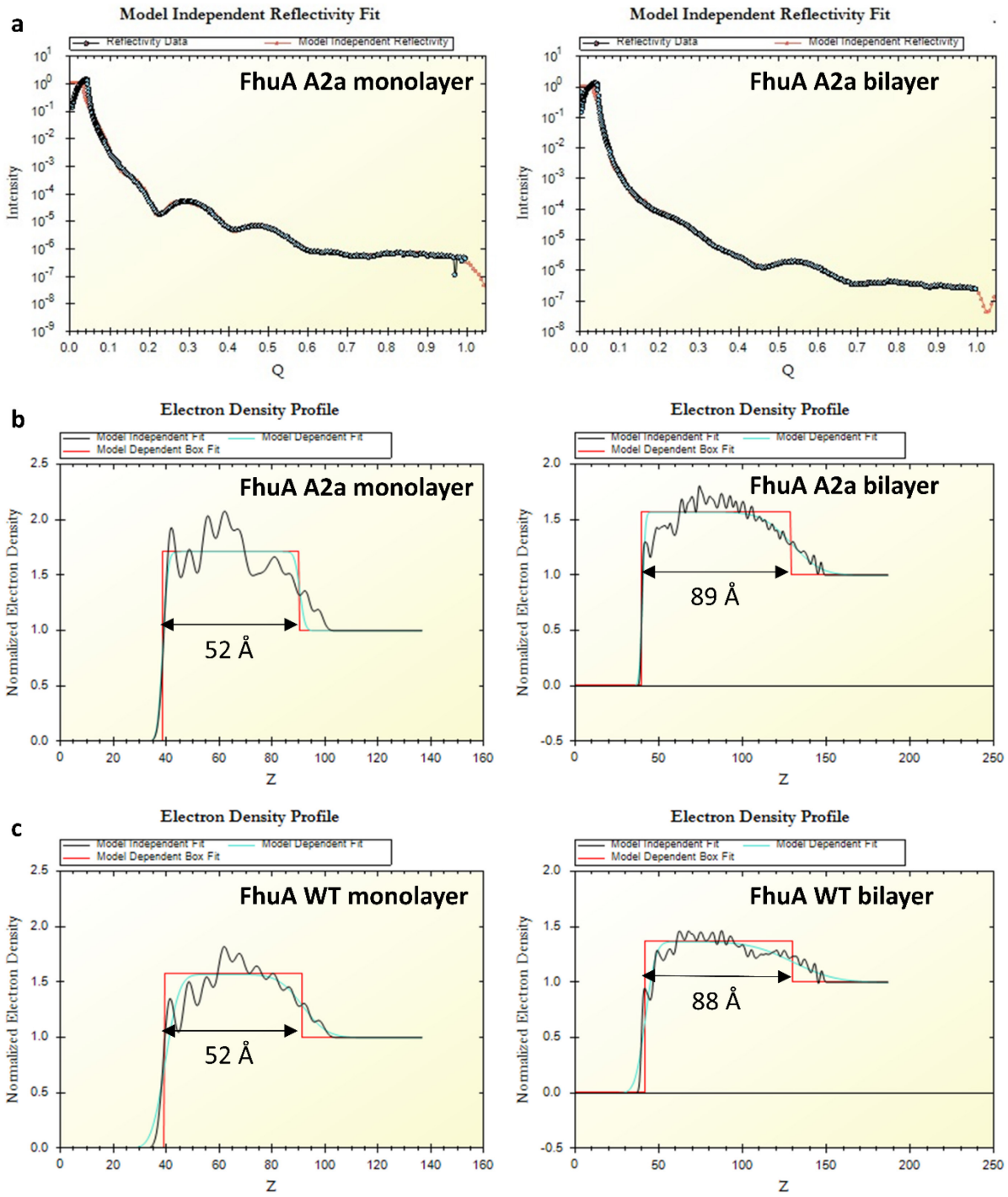

Figure 5.10: Determination of FhuA membrane thickness. a, XRR-reflectivity curves of FhuA A2a mono- and bilayer membranes on top of silicon substrates fitted using the software StochFit. b, c, Electron density profiles deduced from the fitted reflectivity curves of FhuA A2a and FhuA WT mono- and bilayer membranes. StochFit was used to perform box fits to estimate the membranes' thicknesses.

Using AFM and XRR, the thickness of FhuA mono- and bi-layer membranes was determined, the films were thus studied in direction normal to the silicon substrate. Next, grazing-incidence small-angle X-ray scattering (GISAXS) was performed testing the membrane structure in the

horizontal plane to determine if the FhuA molecules are arranged crystalline-like. For GISAXS, the samples were irradiated with X-rays under an incidence angle about 3 mrad in order to only penetrate the protein film, but not the silicon wafer ($\alpha_{critical}$ = 3.9 mrad). The reflection intensity in GISAXS then recorded with a two-dimensional Pilatus detector placed vertically behind the sample, and not punctually as in XRR. The GISAXS diffraction patterns corresponding to FhuA WT mono- and bi-layer membranes on top silicon substrates shown in Figure 5.10c do not indicate a defined repeating distance (**Figure 5.11**), neither do the GISAXS diffraction patterns of FhuA A2a membranes (data not shown). Hence, the proteins in the thin films do not have a crystalline-like ordering.

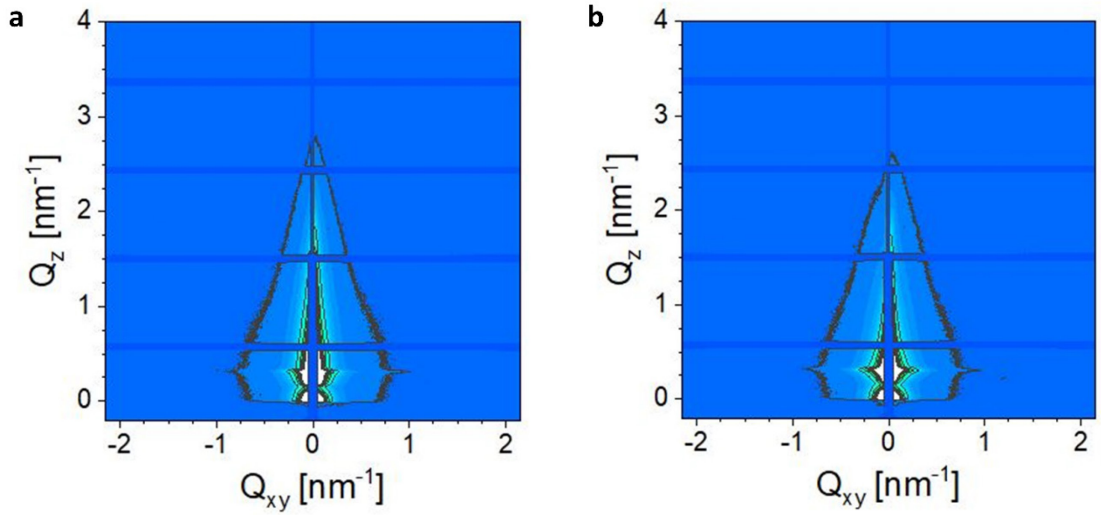

Figure 5.11: Investigation of the protein order in FhuA membranes. Grazing-Incidence Small-Angle X-ray Scattering (GISAXS) pattern of a, a FhuA WT monolayer and b, a FhuA WT bilayer membrane on top of silicon substrates. No diffraction pattern indicating a crystalline-like ordering in the FhuA membranes was observed.

GISAXS experiments have shown that the FhuA molecules do not have a crystalline-like ordering when incorporated into the membrane. It is pointed out that a non-crystalline FhuA arrangement does not contradict the presence of collective and upright oriented FhuA molecules in the membrane that was indicated by SFG measurements in Chapter 5.3. The structural integrity of FhuA molecules in dried membranes was thus further investigated with other methods, e.g., CD spectroscopy as elaborated in the following section.

5.4.1.3 CD spectroscopy

CD spectroscopy on FhuA membranes was conducted by Dr. Daniel Sauer at the RWTH Aachen University.

Before membrane preparation, CD spectroscopy on dialyzed FhuA variants in MPD buffer (Chapter 5.2.2) indicated successful protein refolding as it showed the typical CD spectrum associated with ß-sheets, the major motif of the secondary structure of FhuA. To test whether this structure is maintained during membrane fabrication and drying, multiple FhuA ΔCVF^{tev} membrane layers were transferred to a cuvette glass. As thin films are difficult to investigate by CD spectroscopy, a multilayer film on the glass substrate was aimed at in order to improve signal sensitivity. The membrane thickness was measured using AFM that indeed proved successful Langmuir-Schaefer transfer of at least six membrane layers (**Figure 5.12**).

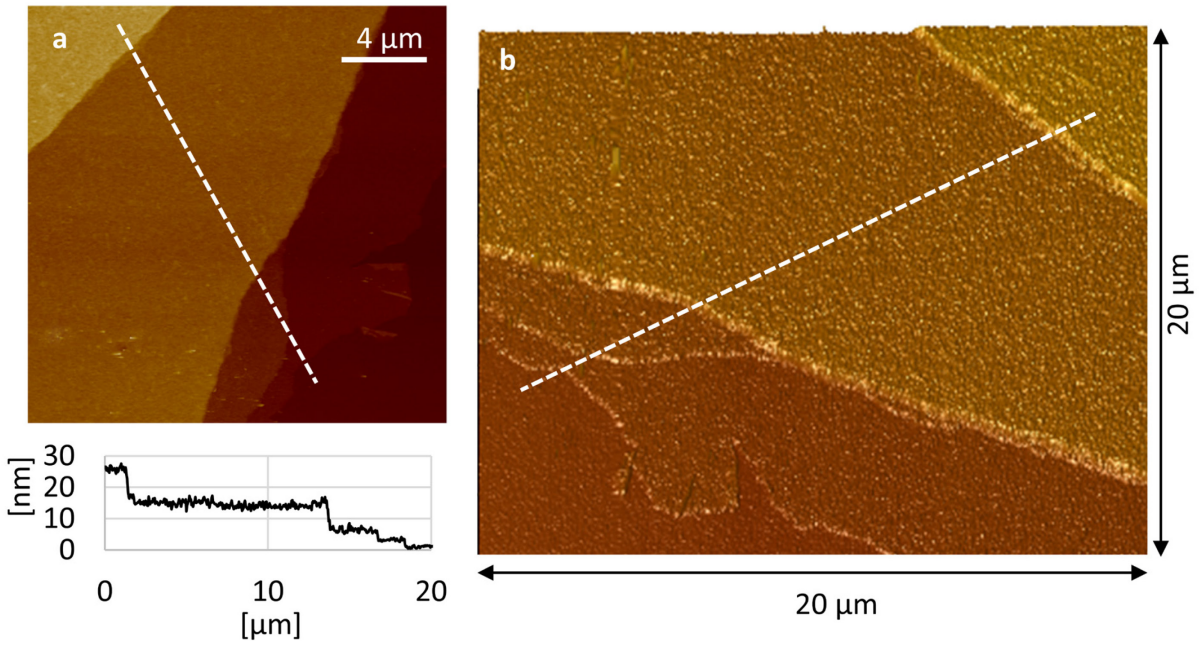

Figure 5.12: Layered structure of FhuA membranes. AFM image of six FhuA ΔCVF^{tev} membrane sheets layered on top of a cuvette glass, a, 2D view and b, 3D view. The image was taken at the edge of the cuvette glass where the membranes rupture during transfer from the air-water interface (Langmuir-Schaefer transfer). The height profile belongs to the line in the image and clearly shows how the membrane thickness discreetly increases by about 5 nm with every FhuA membrane sheet added. The two top steps have a thickness of 10 nm and represent either two FhuA membrane sheets ruptured at the same edge or one FhuA membrane sheet that has folded forming a double layer.

Next, the CD spectrum of the FhuA ΔCVF^{tev} membrane-coated cuvette glass was measured showing a minimum at 215 nm, just like the CD spectrum of refolded FhuA in MPD buffer associated with ß-sheets. Due to the low amount of FhuA in the nanothin membrane, the

CD signal was weak and noisy. For comparison with the CD spectrum of FhuA ΔCVF^{tev} in MPD buffer (**Figure 5.13)**, it was therefore multiplied by factor 10 and smoothed.

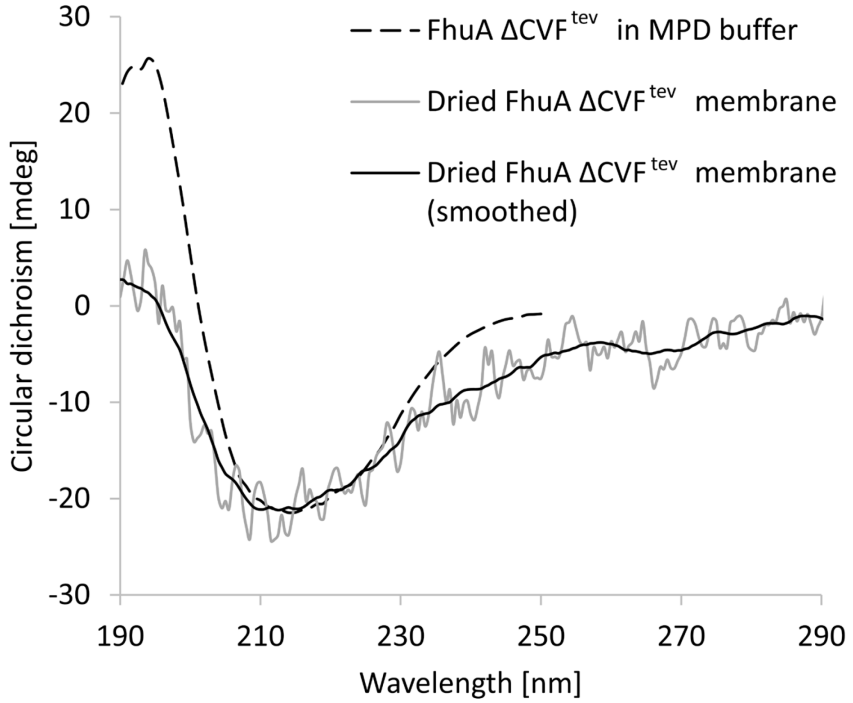

Figure 5.13: Verification of structural integrity of FhuA as part of the membrane. Circular dichroism (CD) spectra of FhuA ΔCVF^{tev} in MPD buffer and of multiple FhuA ΔCVF^{tev} membrane layers dried on top of a CD cuvette glass. For better comparability, the data of the FhuA ΔCVF^{tev} membrane layers were multiplied by factor 10 and smoothed. The CD spectra of FhuA ΔCVF^{tev} in solution and as part of the FhuA membrane match and show a minimum around 215 nm indicating proper secondary protein structure in both cases.[54,97]

CD spectroscopy thus indicated the secondary FhuA structure to be maintained during membrane fabrication and transfer. Evidence of intact tertiary FhuA structure was obtained indirectly using fluorescence microscopy, as illuminated in the next section.

5.4.1.4 Fluorescence microscopy

Indirect verification of FhuA pore structure as part of FhuA membranes was obtained following a fluorescence microscopic protocol first implemented by Garakani et al. to test FhuA ΔCVF^{tev} presence and pore structure in spread polymersomes.[28] Garakani et al. labelled the free cysteine residue accessible inside the open pore of FhuA ΔCVF^{tev} after insertion into polymersome membranes with a fluorescence dye (ThioGlo1) and found the polymersomes to shine bright when illuminated with light in the dye's excitation wavelength. This not only proved FhuA presence in the polymersomes, but also cysteine accessibility inside the FhuA pores indicating preserved pore structure. Following this procedure, FhuA ΔCVF^{tev} membranes

transferred to silicon substrates were fluorescence-labelled by light-protected incubation in a ThioGlo1 solution, thoroughly washed, air-dried and investigated using confocal fluorescence microscopy. Corresponding fluorescence microscopy images (**Figure 5.14)** show FhuA membranes to homogenously shine bright indicating significant covalent dye attachment and thus accessibility of the cysteine residue, which in properly folded FhuA ΔCVF^{tev} molecules is located inside the open pore. Cysteine accessibility itself is not a definite proof of native FhuA ΔCVF^{tev} structure in the membrane though, as the cysteine - although less likely - may also be accessible in partially folded or even unfolded proteins. In the light of the SFG measurements indicating high protein order in FhuA membranes (Chapter 5.3.3), however, it can be assumed that here indeed cysteines inside functional FhuA ΔCVF^{tev} pores were modified. Furthermore, the fluorescence microscopy images demonstrate the wide lateral expansion of FhuA membranes as compared to their very low thickness determined in AFM and XRR measurements.

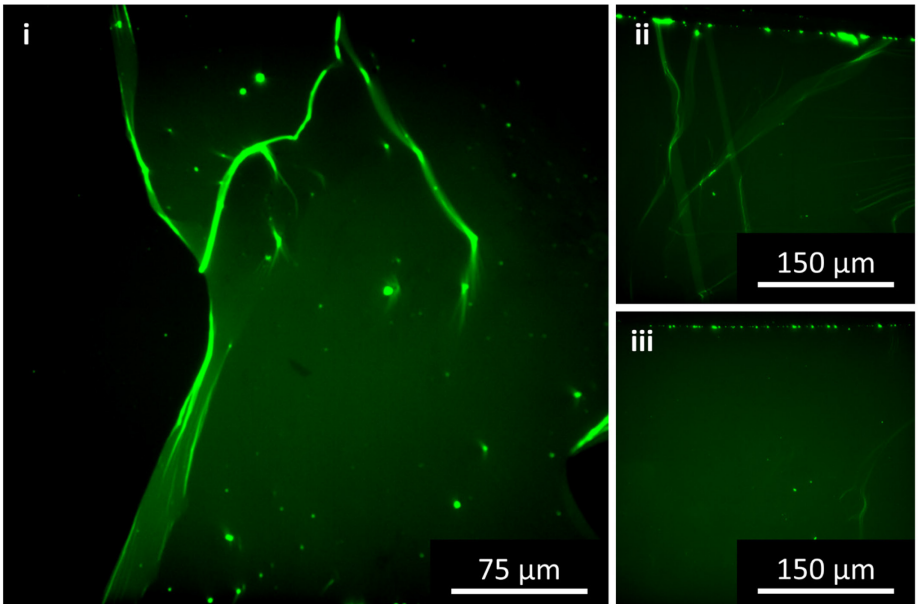

Figure 5.14: Confocal fluorescence microscopy images acquired at three spots (i-iii) of a single FhuA ΔCVF^{tev} membrane sheet labeled with a fluorescence marker on top of a silicon substrate.

5.4.2 Transfer to TEM grids

Investigations of FhuA membranes transferred to dense substrates revealed FhuA membranes to be the desired molecular monolayers. To enable filtration applications, however, such FhuA membranes are required to cover porous supports without rupturing. For demonstration, FhuA membranes were transferred to holey TEM grids and analyzed using AFM and TEM, as summarized in this section.

5.4.2.1 AFM

Analogous to dense substrates, holey TEM grids were first plasma activated and subsequently coated with FhuA membranes according to the Langmuir-Schaefer method. Successful transfer was verified by comparison of the FhuA membrane-coated grid with a blank reference grid using AFM (**Figure 5.15**). The used Quantifoil® Multi A TEM grids have different sized round and elliptical holes with diameters of up to 8 µm. The presence of holes is clearly confirmed by the indentations in the height profile of the reference measurement, the indentations' V-shape being a projection of the pointed cantilever geometry (Figure 5.15a**)**. The reference measurement also shows small elevations of the carbon film around the holes, which according to the manufacturer inevitably occur during hole fabrication. These elevations can also be seen in the height profile belonging to the AFM image of the TEM grid coated with a FhuA membrane (Figure 5.15b**)**. In this profile, by contrast to the reference, only few indentations indicating open holes are visible, while the FhuA membrane covers the majority of the holes without noticeable defects. On top of holes, the FhuA membrane recedes about 30-40 nm into the supporting carbon film.

AFM analysis thus proved that FhuA membranes cover microscale holes in a carbon film of a TEM grid and slightly recede into the hole. It is very remarkable that monolayers of around 5 nm thickness are stable enough to freestandingly cover holes up to 8 µm diameter, hence orders of magnitude larger than the membrane thickness. However, AFM resolution is limited by the cantilever tip radius, which was 7-10 nm in this case. Minor membrane defects in size below 20 nm would thus not be visible in AFM. To assure that FhuA membranes are free of nano-sized defects and to further study the membrane structure, TEM was used as presented in the section below.

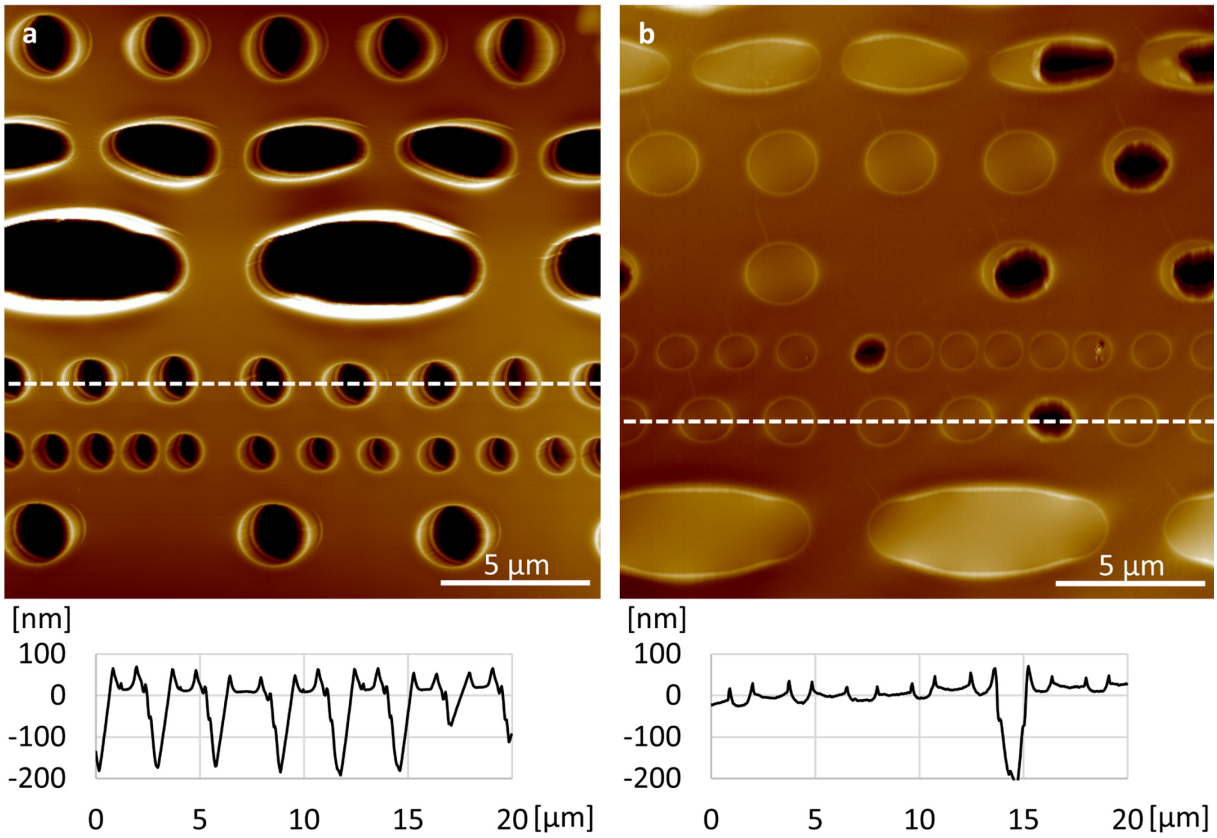

Figure 5.15: FhuA membranes cover holes in porous supports. AFM images of a Quantifoil® Multi A TEM grid with a structured hole pattern in the carbon film. In a, the TEM grid is not covered with a FhuA membrane and the existence of open holes in the carbon film is indicated by the indentation in the height profile belonging to the dashed line in the image. In b, the TEM grid is covered with a FhuA WT membrane and only holes with defects in the FhuA WT membrane appear as indentations in the corresponding height profile.

5.4.2.2 TEM

TEM measurements were performed by Thomas Bick from the group of Prof. Petra Wendler at the University of Potsdam.

In TEM single particle analysis of the FhuA variants, uranyl acetate (UA) negative staining was used for contrast enhancement and allowed visualizing the open pores in FhuA molecules (Chapter 5.2.3). For the same purpose, FhuA membranes on top of holey TEM grids were stained with UA right after Langmuir-Schaefer transfer. Representative TEM images of freestanding FhuA ΔCVF^{tev} membranes in different magnifications are compiled in **Figure 5.16**. Consistent with the AFM analysis in the previous section, the overview TEM image in Figure 5.16a shows many holes covered with an intact membrane and few cracks in membranes, especially over larger holes. Close-up imaging of single holes was challenging as FhuA membranes ruptured immediately when exposed to high intensity electron beams (Figure 5.16b). The rupturing FhuA ΔCVF^{tev} membrane in Figure 5.16c shows a homogenous

nanoscale pattern that is very similar to the one of UA stained carbon films (Figure 5.16d). Furthermore, UA stained FhuA WT and FhuA A2a membranes show the same pattern as well. This limits the interpretation of the pattern regarding structural features of the FhuA membranes.

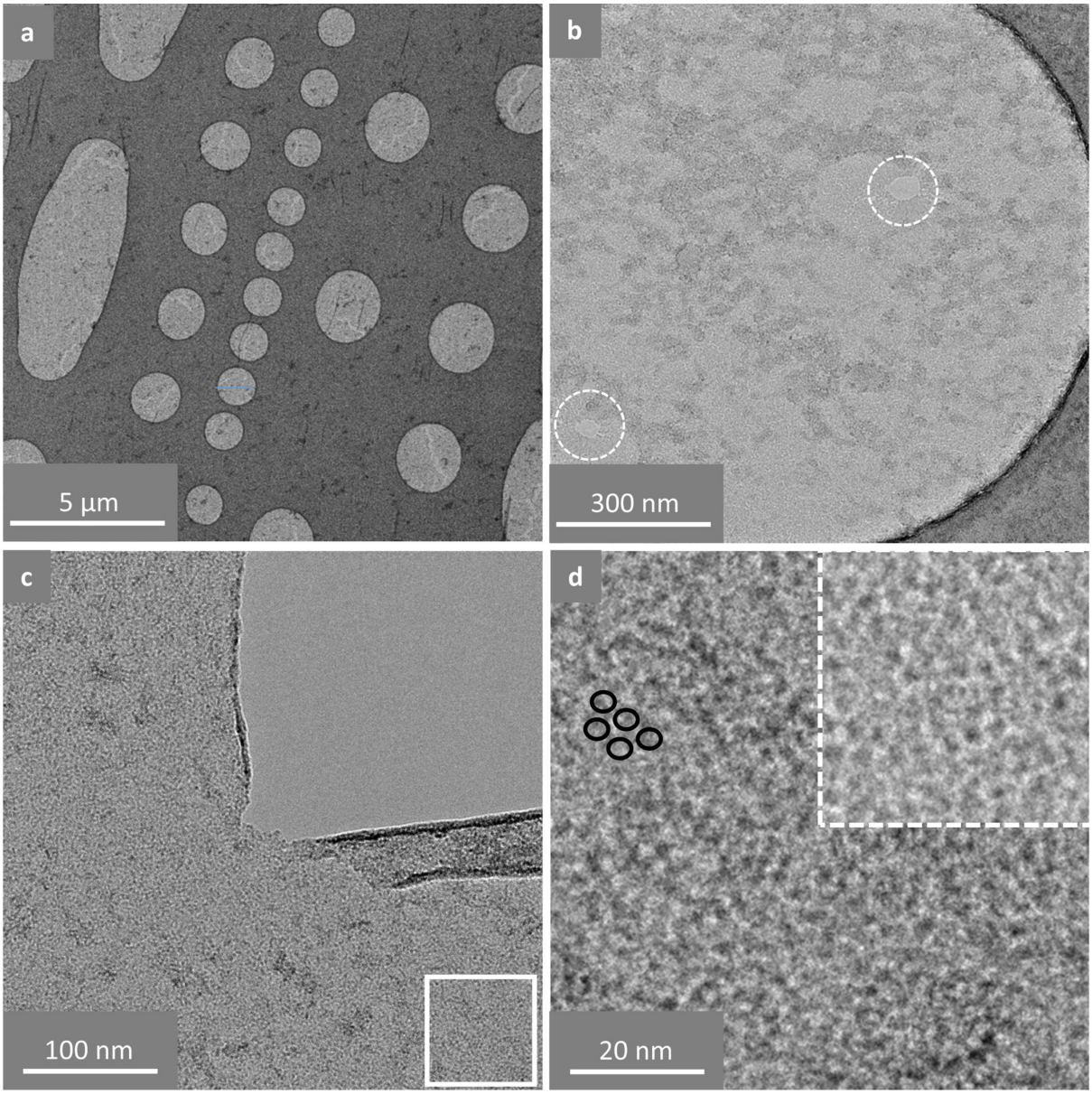

Figure 5.16: TEM images of FhuA ΔCVF^{tev} membranes on top of holey carbon grids stained with UA. a, Grid overview showing many holes covered with the FhuA membrane. b, Single hole close-up; origins of membrane rupture due to electron beam exposure are marked with the dashed circles. c, Ruptured FhuA membrane that has rolled up close to the crack edge. d, Magnification of the area marked with a white box in c, revealing the nanoscale pattern of the UA-stained FhuA ΔCVF^{tev} membrane. The ellipses drawn in the image mark the theoretical size of upright oriented FhuA molecules. As reference, a TEM image of an UA-stained carbon film is shown in the top right of the image marked with the dashed line.

Unstained FhuA membranes dried at room temperature, on the other hand, were even more sensitive to electron irradiation and corresponding TEM investigations did not result in further insight about the membrane structure. The latter also applies to high-resolution cryo-TEM imaging that once more showed FhuA membranes to be very homogenous (**Figure 5.17**), but lacked contrast to reveal information about the presence of FhuA pores as well.

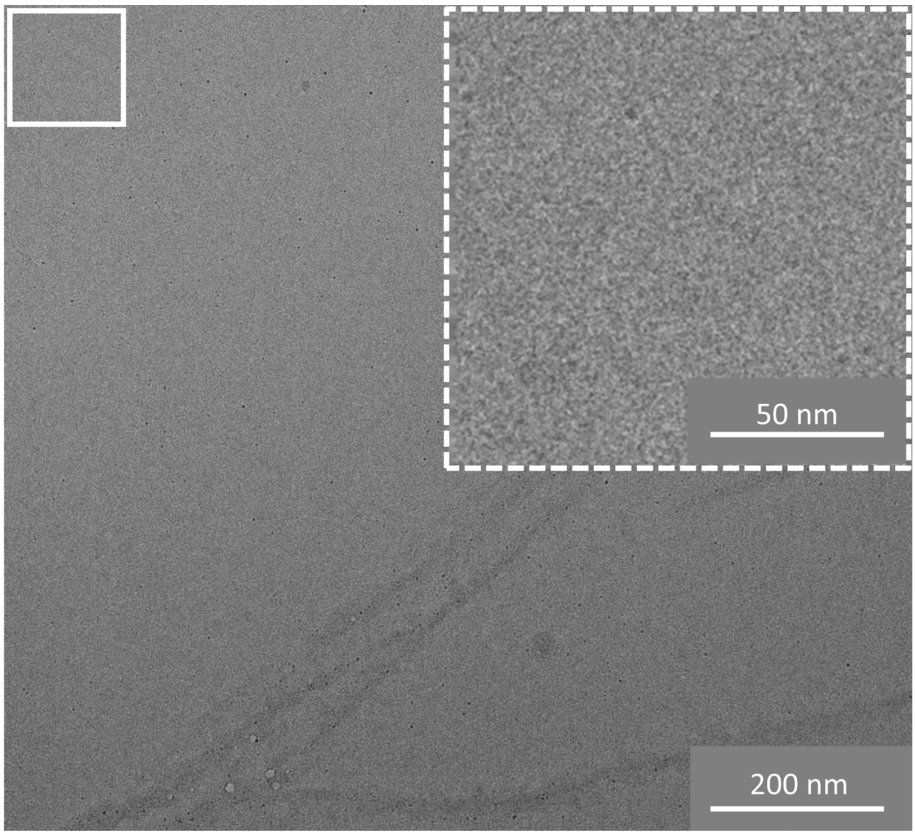

Figure 5.17: Cryo-TEM image of a freestanding FhuA ΔCVF^{tev} membrane. The black dots in the otherwise homogenous pattern are attributed to FhuA that has burned when exposed to the electron beam. The image in the top right shows a magnification of the white box marked in the top left.

Overall, TEM clearly proves that FhuA membranes are indeed very dense films and – if not ruptured due to the electron beam – do not even have defects on the nanoscale. This is crucial as the membranes' molecular selectivity is intended to be determined by the FhuA pores and not by membrane defects.

5.4.3 Transfer to silicon nitride membrane windows

AFM and TEM showed FhuA membranes to freestandingly cover holes in the carbon film of TEM grids. However, in all cases FhuA membranes on top of some holes were broken or broke during imaging, which emphasized the fragility of ultrathin FhuA membranes. That is why assessment of water and ion permeation properties of FhuA membranes was carried out using

FhuA membrane-coated substrates with a single hole, so that the membrane integrity could be easily verified after the respective permeation experiment. Suited substrates with a single, micro-sized hole were found in so-called silicon nitride membrane windows, which are commercially available through Silson Ltd, UK. A schematic illustration of the silicon nitride membrane windows can be seen in **Figure 5.18**a. Silicon nitride membrane windows were purchased with various hole diameters in the range between 1-7 µm, and in either squared (5 x 5 mm) or rounded (Ø 3.05 mm, TEM grid size) form to fit the experimental set-up used for water permeation and ion conductivity measurements, respectively. For comparison, a photo of both versions is shown in Figure 5.18b. The silicon nitride membrane windows were coated with either one or several FhuA membrane layers, the preparation of one FhuA membrane at the air-water interface of the Langmuir trough being sufficient to coat multiple silicon nitride membrane windows with multiple FhuA membrane layers. This is exemplarily illustrated with the two images in Figure 5.18c, showing the subsequent Langmuir-Schaefer transfer of two FhuA membrane layers to seven silicon nitride membrane windows at the same time. In the images, the air-water interface between the Langmuir trough barriers is covered with a FhuA membrane and each time the silicon nitride membrane windows touch the FhuA membrane, another FhuA membrane layer attaches to the silicon nitride membrane windows. Interestingly, the difference between silicon nitride membrane windows coated with one or several FhuA membrane layers was already visible using the digital camera of the AFM (Figure 5.18d), even though the individual membrane layers are only 5 nm thick. Results of the AFM analysis of FhuA membranes on top of holes in silicon nitride membrane windows are presented in detail in the following section. Next to AFM, HIM was found a suited method to differentiate intact from defect FhuA membranes as demonstrated with the HIM images shown in Figure 5.18e. However, like in TEM analysis, freestanding FhuA membranes frequently ruptured when exposed to ion beams of higher intensity so that images could not be acquired at maximum magnification.

Water and ion permeation experiments on FhuA membranes on top of silicon nitride membrane windows are described in Chapter 5.5. First, a detailed AFM investigation providing insights into mechanical properties of FhuA membranes over the hole in silicon nitride membrane windows is presented in the next section.

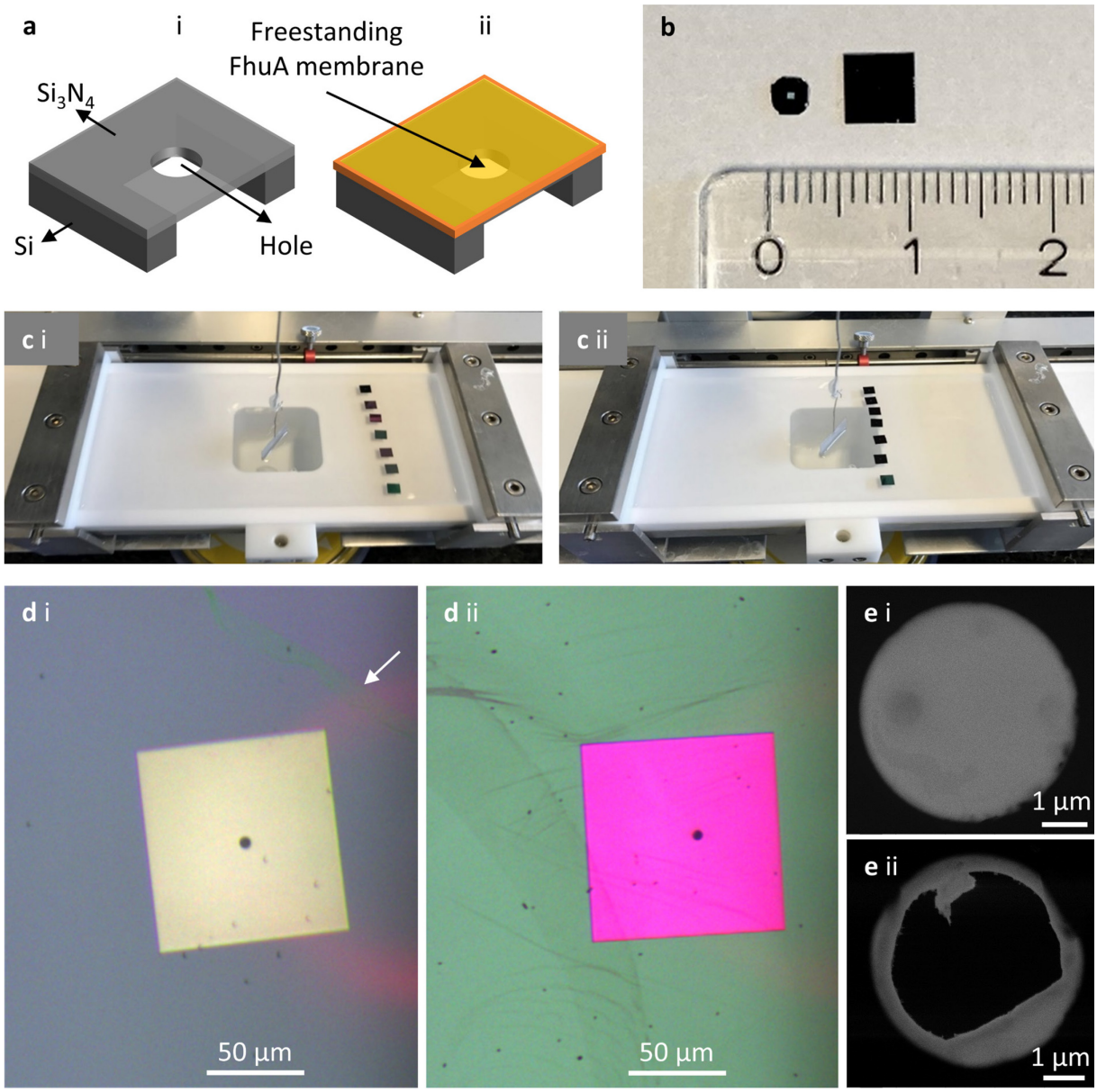

Figure 5.18: Transfer of FhuA membranes to silicon nitride membrane windows. a, Schematic illustration of a silicon nitride membrane window with a single hole in its center when (i) not covered and (ii) covered with a FhuA membrane. b, Photo of silicon nitride membrane windows in either squared or rounded (TEM-grid size) form as used in water permeation and ion conductivity measurements, respectively. c, Lateral view on the Langmuir trough during subsequent Langmuir-Schaefer transfer of two FhuA membrane layers to seven silicon nitride membrane windows at the same time ((i) first and (ii) second layer). d, AFM-camera image of (i) a single FhuA membrane layer and (ii) several FhuA membrane layers on top of a silicon nitride membrane window. The white arrow in (i) marks the edge of the FhuA membrane; the top right of the image thus shows the blank substrate while the rest is covered with a FhuA membrane. e, HIM images of (i) an intact and (ii) a defect FhuA WT membrane on top of the 5 µm hole in a silicon nitride membrane window.

5.4.3.1 AFM / PeakForce QNM

In preparation of water permeation and ion conductivity measurements (Chapter 5.5), FhuA membranes were transferred to silicon nitride membrane windows with a single hole in their center (Ø 5 µm or Ø 7 µm), as described in the previous section and once more illustrated in **Figure 5.19**a(i) and (ii). To verify successful transfer and test the deformability of FhuA membranes, coated silicon nitride membrane windows were analyzed using the AFM PeakForce quantitative nanomechanical property mapping (PeakForce QNM) mode in liquid.[98]

In PeakForce QNM, the AFM cantilever is moved toward the sample until a certain peak force is reached (Figure 5.19a(iii)) and with each cantilever-sample interaction a so-called force-distance curve is measured. Software-controlled analysis of such curves allows to simultaneously acquire both, the typical AFM height image and an AFM deformation image, showing the local sample deformation upon cantilever loading at the peak force.[98]

Corresponding AFM height images clearly allow discriminating the open hole in a silicon nitride membrane from holes covered with defect or intact FhuA monolayer membranes (Figure 5.19b, c, e, f). The height profiles of intact FhuA ΔCVF^{tev} membranes in Figure 5.19b and c show that the membranes recede about 500 nm into the hole. This is exactly the thickness of the silicon nitride membrane and similar behavior was reported by Mueggenburg et al. for monolayer membranes of close-packed gold nanoparticles covering a hole in a silicon nitride membrane with a thickness of 100 nm.[99] The AFM deformation image in Figure 5.19d corresponds to the height image of the FhuA ΔCVF^{tev} membrane on top of the 5 µm hole (Figure 5.19c) and was measured at a peak force of 2 nN. The circular hole area is brighter than the surrounding area, visualizing increased deformability of freestanding over supported parts of the FhuA membrane. Repeated imaging did not change the results, which demonstrates mechanical stability as well as elastic behavior of FhuA membranes made from a single protein layer.

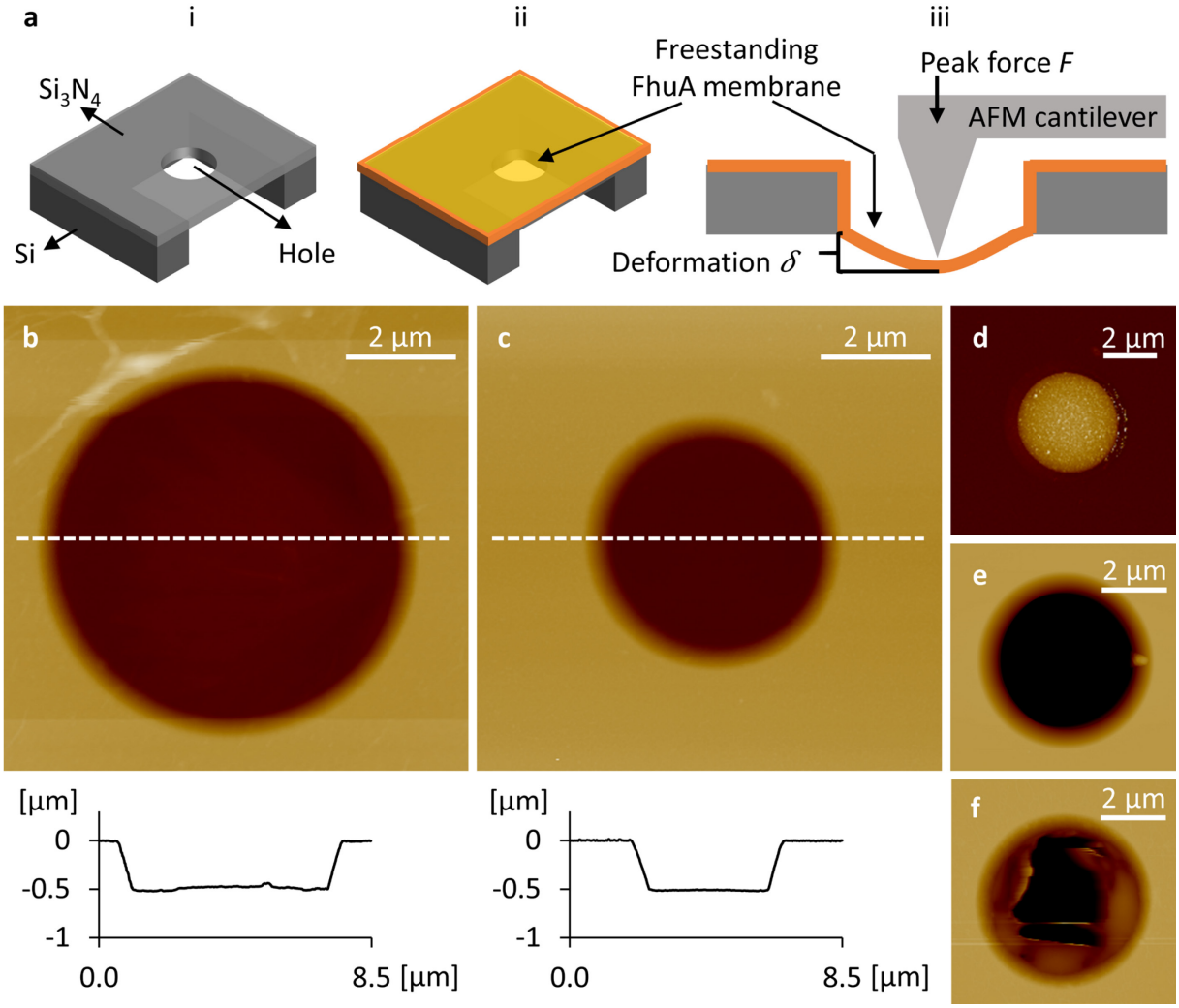

Figure 5.19: AFM measurements on FhuA monolayer membranes I. a, Schematic illustration of a silicon nitride membrane window with a single hole in its center when (i) not covered and (ii) covered with a FhuA membrane. (iii) Cross-section of the FhuA membrane coated silicon nitride membrane window during AFM imaging in PeakForce QNM mode, in which the cantilever deforms the freestanding membrane until a set peak force is reached. b, c, AFM height images of holes in silicon nitride membrane windows with a diameter of 7 µm and 5 µm, respectively, when covered with a FhuA ΔCVF^{tev} membrane. The height profiles below the images belong to the dashed lines in the images. d, AFM deformation image showing the membrane deformation at a peak force of 2 nN (corresponding to the height image in c). e, f, AFM height images of holes in silicon nitride membrane windows when, e, the hole was not covered with a FhuA membrane and, f, the hole was covered with a defect FhuA ΔCVF^{tev} membrane (shown as reference). All images were measured in water.

Elasticity of FhuA membranes was further investigated with additional PeakForce QNM measurements. To do so, two silicon nitride membrane windows with a 5 µm or 7 µm hole were coated with FhuA ΔCVF^{tev} monolayer membranes and measured multiple times, the peak force being gradually increased with every measurement. A series of AFM deformation images corresponding to the FhuA membrane over the 5 µm hole measured at peak forces of 2 nN, 5 nN, 10 nN and 20 nN is shown in **Figure 5.20**a. In the images, the color of the hole area shades brighter with increasing peak force, which indicates increasing FhuA membrane deformation. At a peak force of 20 nN, the deformation became so pronounced, that - presumably - the cantilever oscillation was disturbed and the sample was moved on the sample stage. This happened again when the 20 nN measurement was repeated on the same sample. However, the membrane did not break as verified with a second measurement at a peak force of 2 nN, which showed an intact membrane and nicely corresponded to the first measurement at 2 nN. As basis for quantitative analyses, deformation profiles extracted from the series of deformation images in Figure 5.20a are plotted in Figure 5.20b. The deformation profiles confirm that the freestanding FhuA ΔCVF^{tev} membrane elastically stretched about 70 nm, 80 nm, and 130 nm, when the membrane was loaded with a peak force of 2 nN, 5 nN, and 10 nN in the hole center, respectively. Deformation profiles extracted from an analogous series of deformation images belonging to the FhuA membrane-coated silicon nitride membrane window with a 7 µm hole are shown in Figure 5.20c. In the center of the 7 µm hole, the freestanding FhuA ΔCVF^{tev} membrane elastically stretched about 75 nm, 130 nm, and 250 nm, when loaded with a force of 2 nN, 5 nN, and 10 nN, respectively.

Studying their gold nanoparticle membranes, Mueggenburg et al. deduced a mathematical model from elastic theory to estimate the Young's modulus of homogenous membranes covering a hole and loaded with a point force in central position.[99–101] Filling this model with data from the PeakForce QNM measurements described above and shown in Figure 5.20a-c, results in an average Young's modulus of FhuA ΔCVF^{tev} membranes of 7 GPa (for calculation see Experimental). All Young's moduli calculated can be overseen in the bar chart in Figure 5.20d and range between 1.5 GPa and 11.5 GPa. Interestingly, these values closely resemble the range of Young's moduli (3-39 GPa) stated by Mueggenburg et al. when measuring 19 gold nanoparticle monolayer membranes in their study. This suggests similar elastic properties of the two freestanding monolayer membranes when probed by AFM, even though the gold nanoparticle membranes were not covalently crosslinked and the bulk material gold is assumed to be significantly stiffer than proteins.

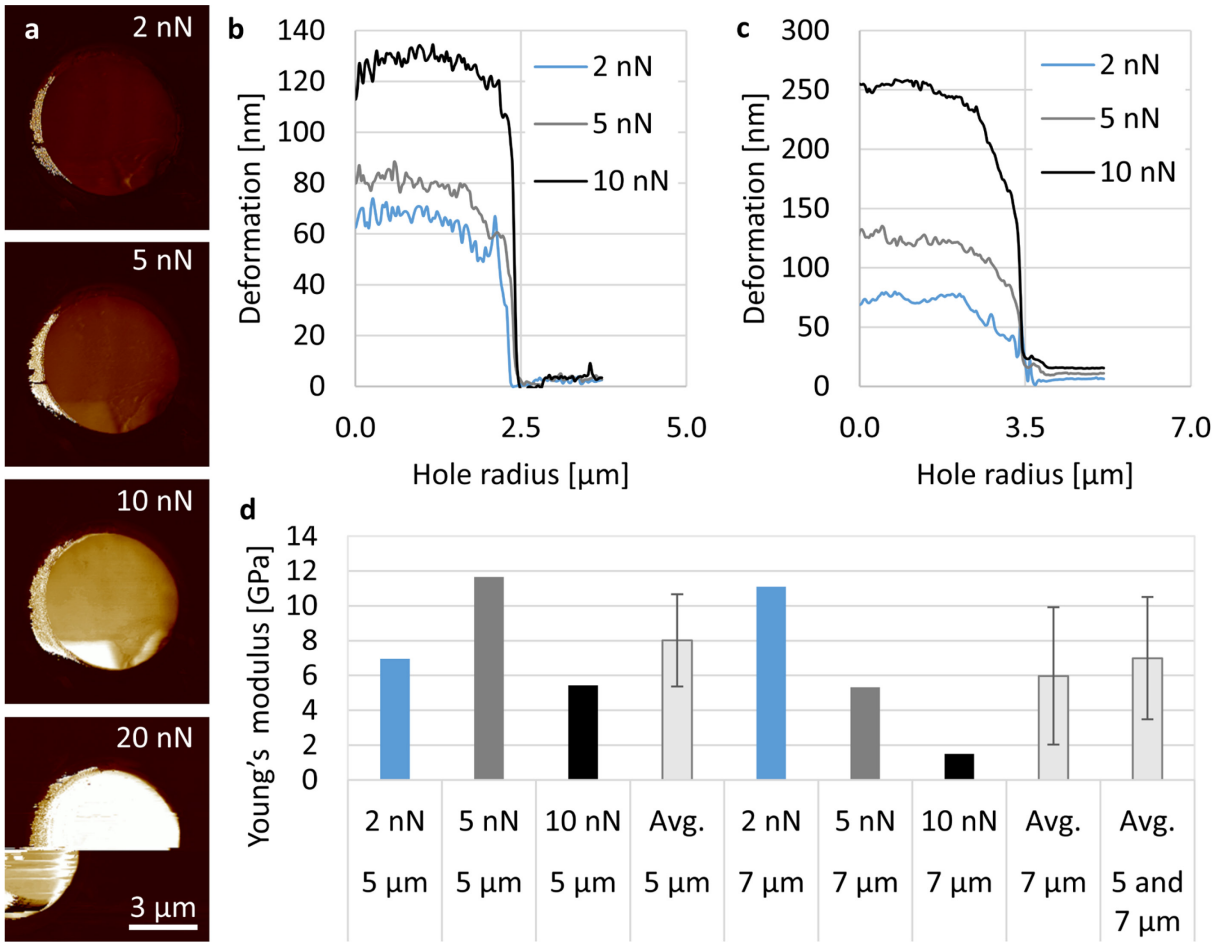

Figure 5.20: AFM measurements on FhuA monolayer membranes II. a, Series of AFM deformation images of a FhuA monolayer membrane over the hole in a silicon nitride membrane window measured at various peak forces (hole diameter 5 µm). b, Plotted deformation profiles belonging to the images in a. c, Plotted deformation profiles belonging to a series of AFM deformation measurements of a FhuA monolayer membrane over the hole in a silicon nitride membrane window measured at various peak forces (hole diameter 7 µm). d, Young's moduli of the two FhuA membranes from a and b, calculated on the basis of the deformations in the hole center using the model deduced by Mueggenburg et al. from point force elastic theory.[99]

FhuA monolayer membranes thus demonstrated remarkable mechanical strength towards the point force applied by the AFM cantilever, when measured in liquid. When measured dry in PeakForce QNM or other AFM measurement modes though, not a single FhuA monolayer membrane over holes in silicon nitride membranes remained stable, in contrast to when transferred to TEM girds (Chapter 5.4.2). This difference may be based on the fact that FhuA membranes attach to the inner wall of the silicon nitride membranes (Figure 5.19b, c) and are thus likely to be under extra tension when spanning the hole. In this state, FhuA membranes may be more sensitive towards the drying process or AFM imaging than when covering holes in TEM grids.

However, intact, dried FhuA multilayer membranes on top of silicon nitride membrane windows were successfully measured in AFM tapping mode, even after water permeation and ion conductivity measurements (**Figures 5.22 and 5.24**) that are described in the next two chapters.

5.5 FhuA membrane permeation properties

Experiments presented in the previous sections focused on FhuA membrane preparation using a Langmuir trough and showed that the ultrathin membranes may cover micron-sized holes in silicon nitride membrane windows without tearing. The latter was a basic requirement to evaluate the permeation properties of FhuA membranes in a next step. Designed to enable low-pressure filtration through the protein nanopores, FhuA membranes were expected to have very high water permeance when compared to conventional nanofiltration membranes. Furthermore, membranes made from FhuA variants with open pores should be more permeable than membranes prepared from FhuA variants with closed pores. Both was verified in water and ion permeation experiments, as presented in the two following sections.

5.5.1 Water permeance

Water permeation measurements were conducted under kind supervision of Raphael Dalpke and Dr. André Beyer in the lab of Prof. Armin Gölzhäuser at the University of Bielefeld. HIM measurements were performed by Michael Westphal.

The water permeance of FhuA WT membranes was measured with a mass loss method.[102] First, the single hole (Ø 5 µm) in a silicon nitride membrane window was coated with one, two or five FhuA WT membrane layers, as described in Chapter 5.4.3. Next, the coated chips were glued to container caps, which in return were screwed on top of containers filled with 400 µl of water. Subsequent cup assembly is shown in a series of images in **Figure 5.21**a. Assembled cups were weighted and placed into an oven, keeping temperature and relative humidity constant during the experiment. The only way for water to evade the container was thus to permeate the FhuA WT membrane on top of the hole. The driving force of this permeation process is the difference in water vapor pressure from the container inside to the outside, which was kept constant during the experiment (Figure 5.21b). FhuA membrane water permeance was calculated by relating the mass of permeated water to the duration of the experiment, the water vapor pressure difference and the FhuA WT membrane area. To distinguish intact from defect FhuA WT membranes, samples were analyzed by AFM and HIM after the experiment. This revealed that all single layer FhuA WT membranes broke during or had broken before the

experiment. Considering the fragility of dry FhuA monolayer membranes over the holes in silicon nitride membranes described before (Chapter 5.4.3), this was not surprising. Here, membrane drying was inevitable though to properly glue the chips to the containers. In contrast to the monolayers, several FhuA WT membranes consisting of two or five layers remained stable (**Figure 5.22**) showing permeances of average 3.87 x 10^{-4} mol Pa^{-1} m^{-2} s^{-1}. Compared to reference measurements in which the hole remained uncovered, FhuA WT membranes reduced water evaporation from the cup by a factor of 6.5. Furthermore, permeances of defect FhuA WT membranes lay between the permeances measured for references and intact FhuA WT membranes. Additionally, these results are summarized in the bar chart in Figure 5.21c. The measured water permeance of FhuA WT membranes falls within the range of water permeances reported for other biomimetic membranes with nanopores (FhuA 1.11 x 10^{-4} mol Pa^{-1} m^{-2} s^{-1};[11] TMV 10.76 x 10^{-4} mol Pa^{-1} m^{-2} s^{-1};[33] Aquaporin Z 0.92 x 10^{-4} mol Pa^{-1} m^{-2} s^{-1} and 0.05 x 10^{-4} mol Pa^{-1} m^{-2} s^{-1} [23,25]) and ultrathin carbon nano membranes (CNM 1.1 x 10^{-4} mol Pa^{-1} m^{-2} s^{-1},[14] tested in the same set-up). FhuA WT membranes thus show more than 150 times greater water permeance than the polyamide thin-film composite membrane FilmTec™ NF270 (0.023 x 10^{-4} mol Pa^{-1} m^{-2} s^{-1}, MWCO 400 Da, DuPont de Nemours Inc., USA), which performed best in a water permeance comparison among eight commercial membranes in the sub-nanometer to few-nanometer separation range in 2020.[11] Here, FhuA WT membranes (with "closed" pores) were investigated showing extremely high permeances. It should be pointed out that the pore of FhuA WT is blocked by a cork domain, but not closed in a sealed way. In fact, the cork domain is known to allow water transport.[103] Additionally, considering the FhuA membrane packing density of maximum 80% (as estimated in Chapter 5.3.3), water permeation will very likely also occur through the interstitial spaces between the crosslinked FhuA molecules. In conclusion, the presented mass loss method nicely highlights the overall very high water permeance of FhuA membranes.

To test if FhuA membranes made of either FhuA open- or closed-pore variants show different permeation properties, ion conductivity measurements were performed as presented in the subsequent section.

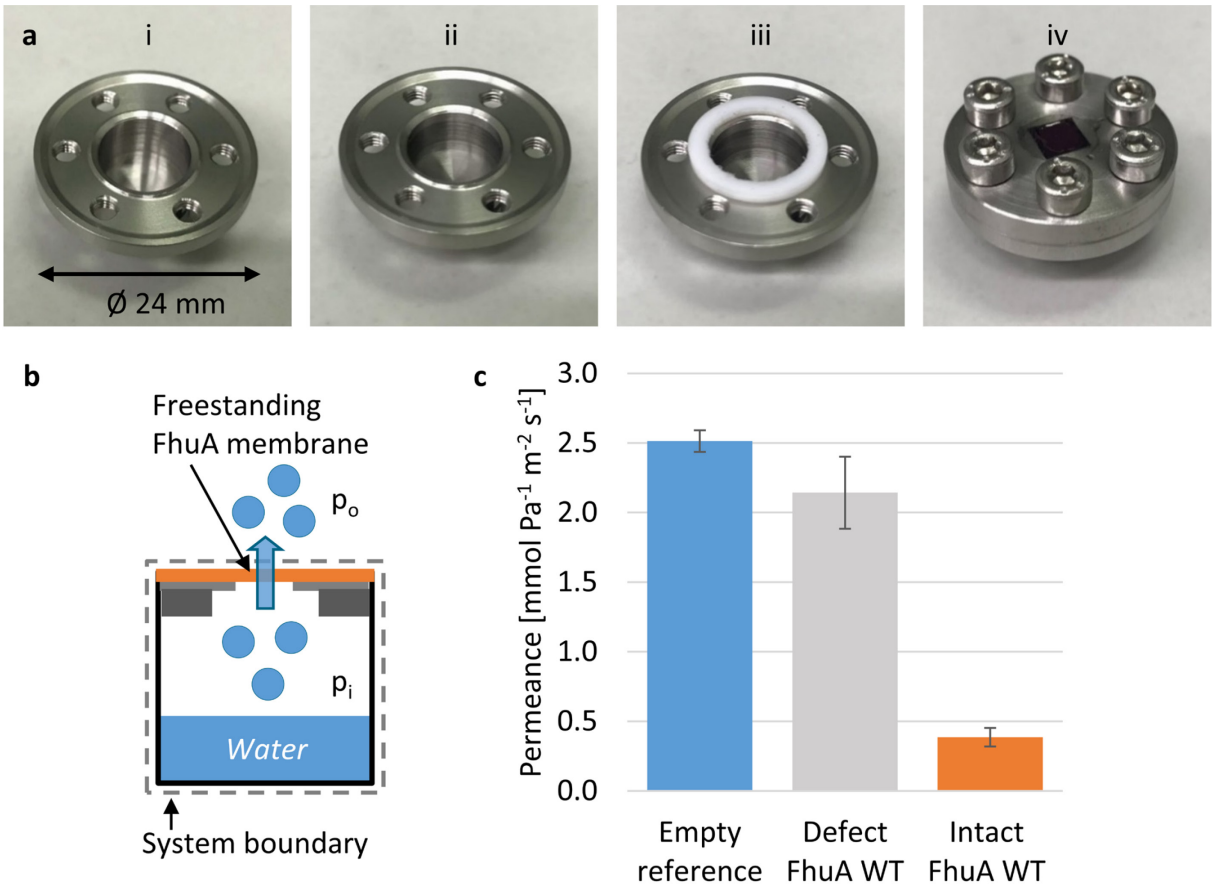

Figure 5.21: Water permeation through FhuA membranes. a, Image series showing the assembly of sealed cups used to measure the water permeance of FhuA WT membranes: (i) empty container, (ii) container filled with water, (iii) PFTF sealing ring on top of water filled container, and (iv) sealed, water filled container with silicon nitride membrane window glued to the container cup. b, Schematic illustration of the water-filled container pictured in a iv. Driven by the water vapor pressure difference from the cup inside to the outside (p_i-p_0), the only way for water to evade the cup was to permeate the FhuA WT membrane. c, The water permeance of FhuA WT membranes was 3.87 x 10^{-4} mol Pa^{-1} m^{-2} s^{-1} (empty reference 25.13 x 10^{-4} mol Pa^{-1} m^{-2} s^{-1}). Error bars indicate the standard error of mean of at least three samples.

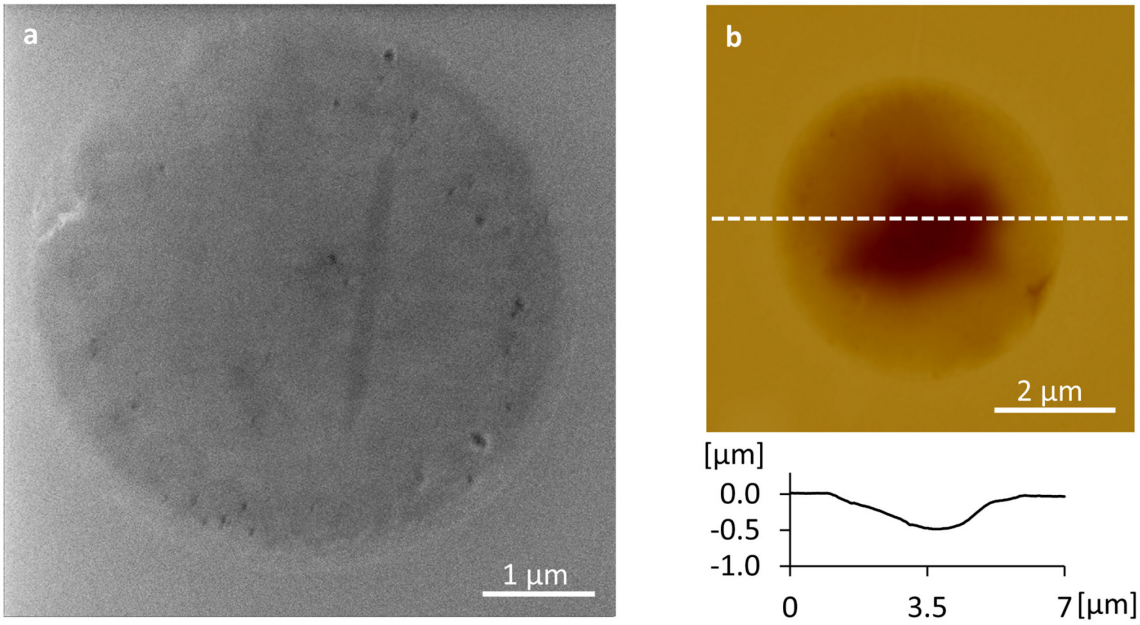

Figure 5.22: Verification of FhuA membrane intactness after water permeation measurement. a, HIM and b, AFM image of the hole in a silicon nitride membrane window covered with a FhuA WT membrane after being used in water permeation measurements. The height profile in b belongs to the dashed line in the image. After being used in water permeation measurements, this sample showed an intact FhuA WT membrane. Only permeances measured on samples showing an intact FhuA membrane after the permeation measurement were included to calculate the averaged permeance.

5.5.2 Ion permeability

Ion permeation measurements were carried out by Maxim Dirksen in the lab of Prof. Thomas Hellweg at the University of Bielefeld.

Black lipid membrane experiments by Killmann and coworkers have demonstrated that open pore variants of FhuA form an ion-permeable, water-filled diffusion pore. The experiments also suggest that the cork domain in FhuA WT significantly reduces FhuA's ion permeability by about 80% (factor 6), so that only minor current fluctuations were detected.[20] To test if the different ion permeabilities transfer to membranes prepared from FhuA WT and FhuA ΔCVF^{tev}, conductance measurements were performed as follows: Five FhuA membrane sheets were layered on top of a silicon nitride membrane chip having a single hole with a diameter of 1 µm. The resulting FhuA membrane thickness of a little more than 20 nm was verified by AFM before the experiment to only include FhuA WT and FhuA ΔCVF^{tev} membranes of identical thickness (**Figure 4.24**(iii)). As reference, silicon nitride membrane windows without FhuA membranes on top were used. The samples were mounted between two parts of a microfluidic measurement chamber filled with a phosphate buffer. Two electrodes connected to a voltage source were immersed into the phosphate buffer (including NaCl) on both sides of the membrane and the resulting current was measured, while successively increasing the voltage (**Figure 5.23**). After the experiment, the integrity of FhuA membranes on top of the hole was verified by AFM (Figure 4.24(i), (ii)).

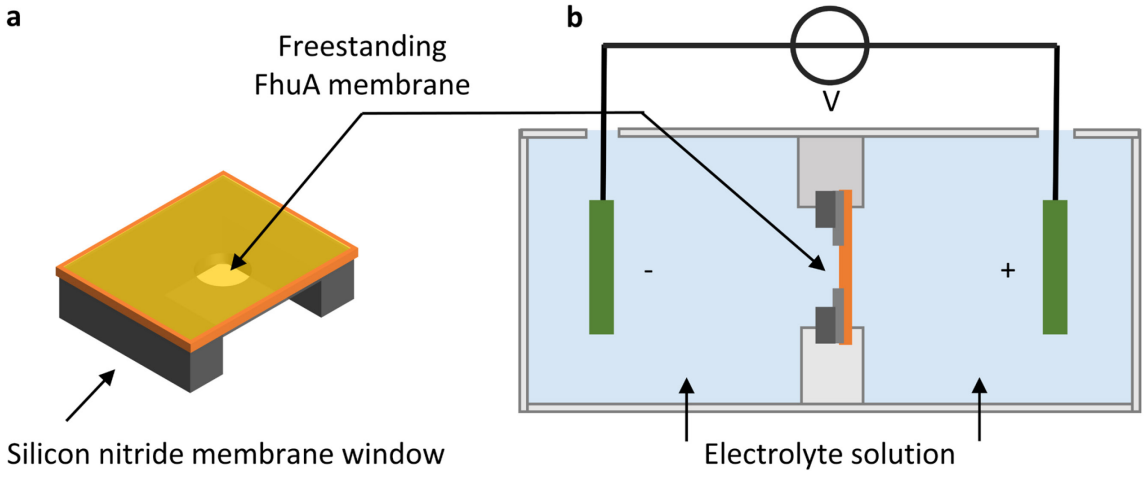

Figure 5.23: Ion permeation through FhuA membranes I. a, Schematic illustration of the FhuA membrane-coated silicon nitride membrane window that was placed between two reservoirs containing an electrolyte solution, as shown in b. Two electrodes connected to a voltage source were placed on either side so that the only way for ions to diffuse between the electrodes was to permeate the FhuA membrane.

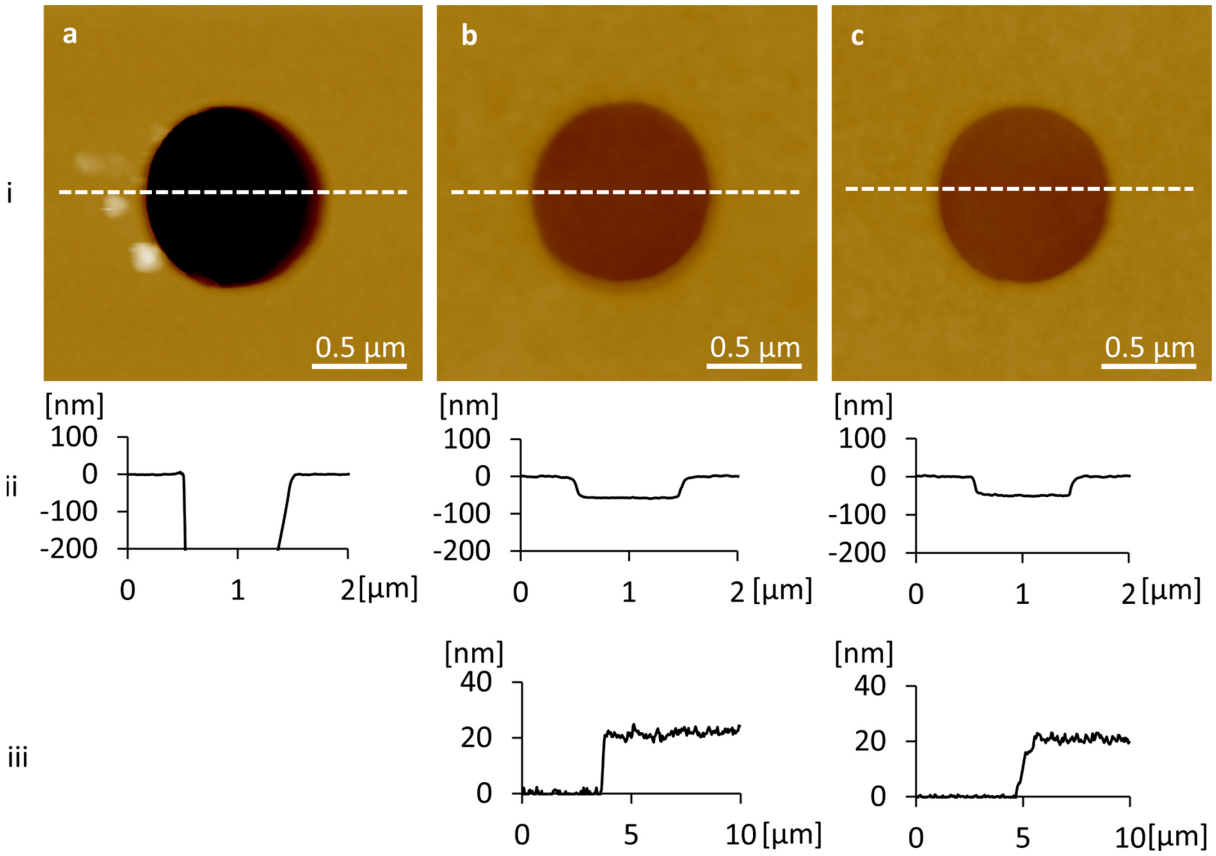

Figure 5.24. Verification of FhuA membrane intactness after ion permeability measurement. (i) AFM images of the 1 µm hole in silicon nitride membrane windows after examination in ion permeability measurements: a, empty reference, b, hole covered with five FhuA WT membrane sheets and c, hole covered with five FhuA ΔCVF^{tev} membrane sheets. (ii) Height profiles belonging to the dashed lines in the images above and indicating that the FhuA membranes covering the holes were intact during and not damaged by the examinations. (iii), height profiles showing the thicknesses of the FhuA membranes measured close to the holes. To measure the thicknesses, parts of the FhuA membranes were scratched away with a syringe needle. Both, the FhuA WT membrane in (b) and the FhuA ΔCVF^{tev} membrane in (c) were 21 nm thick matching the height of five layered FhuA membrane sheets. Only ion permeability measurements on intact FhuA membranes with identical thicknesses were considered for data analysis in Figure 5.25.

The current-voltage curves (I-V curves) of each three references, FhuA WT and FhuA ΔCVF^{tev} membranes were measured and the averaged results are shown in **Figure 5.25**. The measurement set-up allowed to register currents up to ± 20 nA. Within this range, the I-V curves for the references as well as for FhuA WT and FhuA ΔCVF^{tev} membranes are linear. The constant slopes of the I-V curves correspond to constant conductances of 4.0 mS when the hole was not covered with a membrane and 3.4 mS or 2.3 mS when a FhuA ΔCVF^{tev} or FhuA WT membrane covered the hole, respectively. Compared to the reference, FhuA ΔCVF^{tev} or FhuA WT membranes are permeable for 85% or 58% of the ions. These findings indicate

that the different ion permeabilities of FhuA WT and FhuA ΔCVF^{tev} demonstrated in black lipid membrane experiments indeed transfer to FhuA membranes made from each variant to some extent. This strongly suggests the incorporation of structurally intact FhuA pores into a 2D membrane. However, even FhuA WT membranes showed rather high ion conductivity, which was not 80% lower (as reported from the FhuA variants tested in black lipid membranes) but only 30% lower than that of FhuA ΔCVF^{tev} membranes. While such direct comparison has limited meaning, because black-lipid membrane experiments were done using a different buffer and voltage, influence of ion permeation through the interstitial space between the FhuA molecules is very likely to have contributed to ion permeation of both FhuA WT and FhuA ΔCVF^{tev} membranes as well. Nonetheless, FhuA membranes were layered to increase the mechanical stability of the membrane and - from a statistical point of view - it is thus likely that most ions passed at least one channel when permeating the multilayer membranes.

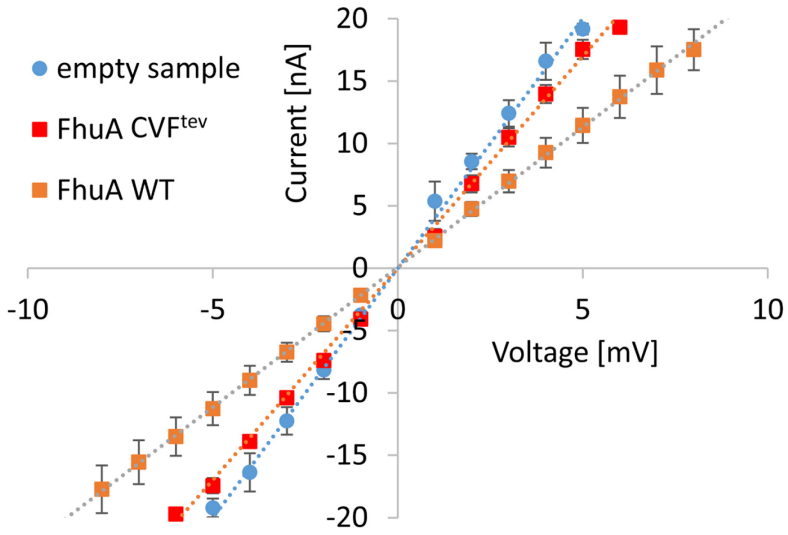

Figure 5.25. Ion permeation through FhuA membranes II. Current-voltage curves of FhuA WT and FhuA ΔCVF^{tev} membranes measured in phosphate buffer (10 mM NaCl, 10 mM sodium phosphate (NaPi), pH=7). The constant slopes correspond to constant conductances between the electrodes of 4.0 mS (empty reference), 3.4 mS (FhuA ΔCVF^{tev} membrane, 5 layers) and 2.3 mS (FhuA WT membrane, 5 layers). Error bars indicate the standard error of mean of at least three samples.

5.6 Transfer to membrane supports

SEM measurements were performed by Minh Thu Tran at Fraunhofer IAP.

In the previous chapters, water and ion permeation of FhuA membranes was investigated when covering substrates with a single, micron sized hole. This was beneficial, as membrane intactness and thickness could be readily verified using AFM after the respective experiment. However, standard filtration scenarios require significantly larger membrane areas to achieve sufficient membrane flux and economic membrane application. Consequently, transfer of FhuA membranes to scalable membrane supports was sought.

Due to cost-effective availability and wide use in industry, polymeric membranes such as track-etched polycarbonate membranes or polyethersulfone membranes with random, spongy pore structure were the first candidates considered as FhuA membrane supports. Handling these polymeric membranes during Langmuir-Schaefer transfer was not feasible though, because the flexible membranes uncontrolledly bend while touching down and peeling off from the air-water interface.

Alternatively, Langmuir-Schaefer transfer of FhuA membranes to stiff, ceramic membrane supports was investigated. First, commercially available aluminum oxide membranes with honeycomb pore structures, and laterally stabilized with a transparent polypropylene ring (Whatman® Anodisc inorganic filter membrane, pore size 0.2 µm) were used. From now on these supports are referred to as Anodisc supports. Principally, FhuA membrane transfer to Anodisc supports was successful and centimeter-sized FhuA membrane fragments on top of the support were even recognizable with the eye when holding the wet support against daylight (**Figure 5.26**a). Successful transfer was additionally verified with AFM measurements, clearly showing the difference between blank and FhuA membrane-coated Anodisc supports (Figure 5.26b). However, even though stabilized with the polypropylene ring, the brittle Anodisc supports often broke during repeated Langmuir-Schaefer transfer performed to cover the full support with FhuA membranes. For this reason, another support membrane was considered.

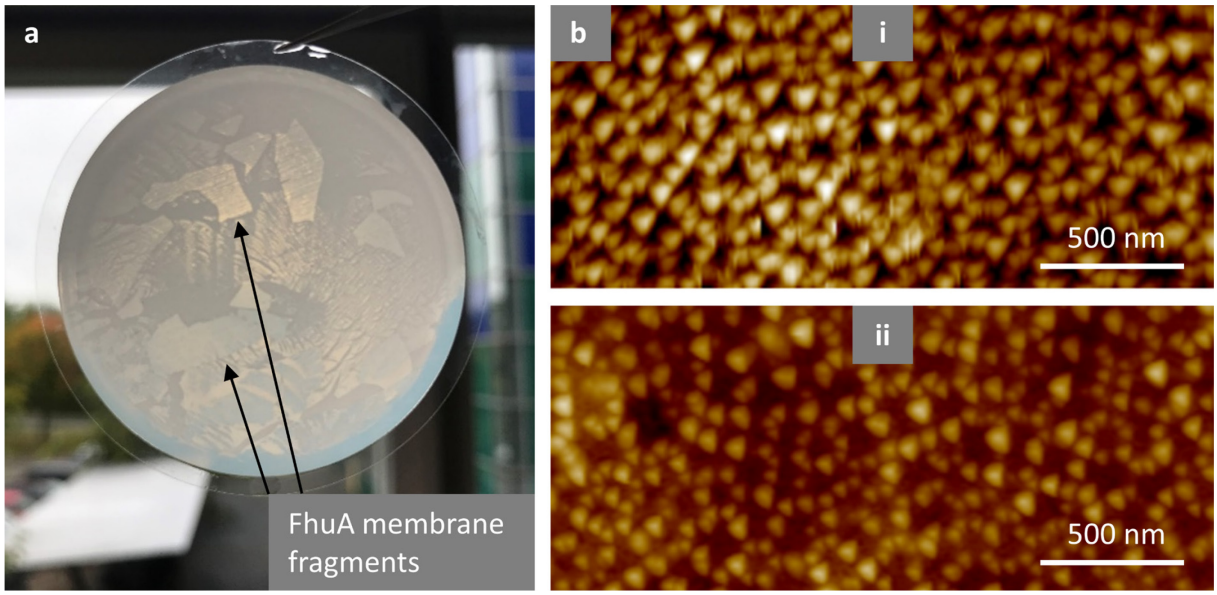

Figure 5.26: FhuA membranes on top of Anodisc supports. a, Photo of the polypropylene ring-stabilized Anodisc support after Langmuir-Schaefer transfer. Centimeter-sized FhuA WT membrane fragements were visible when holding the wet support against daylight. b, AFM images of the surface of the Anodisc support when (i) blank or (ii) coated with a FhuA WT membrane.

A third, more stable membrane support was found in ceramic microfiltration membranes provided by Fraunhofer IKTS, therefore referred to as IKTS membrane from now on. Compared to the Anodisc supports, the IKTS membrane is much thicker with overall dimensions comparable to those of a Euro coin (**Figure 5.27**a). The IKTS membrane consists of sintered aluminum oxide granules of different size, with larger granules forming the membrane foundation and smaller granules on top, defining the membrane's minimum pore size of 70 nm. SEM images of the IKTS membrane's cross-section are shown in Figure 5.27b. The gradual design of the IKTS membrane ensures both, high permeance for aqueous solutions during filtration and considerable stability, e.g., when handled with tweezers during repeated Langmuir-Schaefer transfer (Figure 5.27c). AFM images of the IKTS membrane surface before and after 10, 20, and 30 Langmuir-Schaefer transfers of FhuA WT membranes are pictured in Figure 5.27d. The more transfers were performed; the less pronounced appeared the aluminum oxide granules in AFM, which suggests successful coating of the IKTS membranes with FhuA membranes.

To test if FhuA membranes on top IKTS membranes are capable of separating small molecules from a solution and if they remain stable when exposed to the conditions of a pressure-driven filtration process, a series of filtration experiments was carried out as described in the following section.

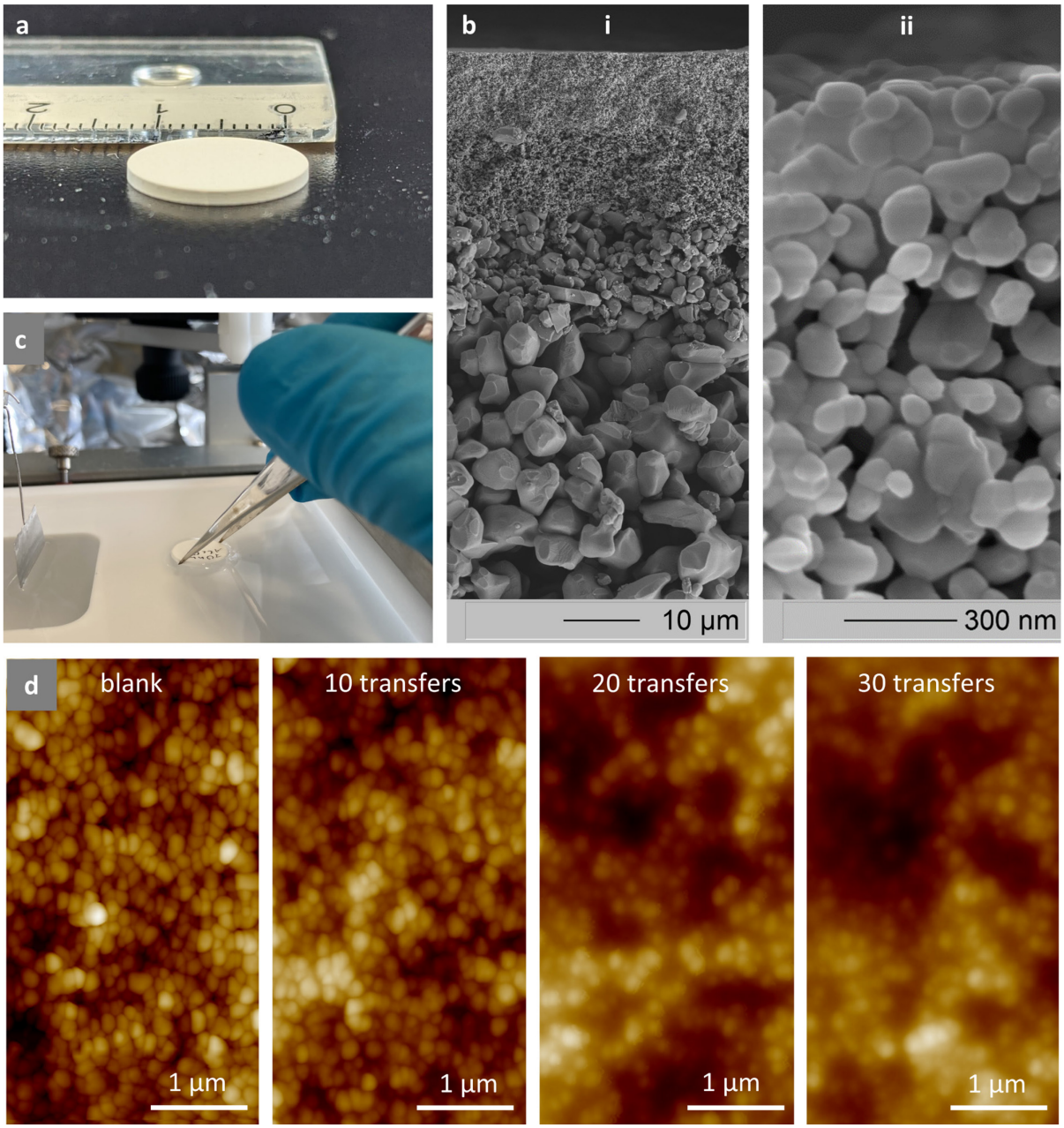

Figure 5.27: Ceramic membrane support and coating with multiple FhuA membrane layers. a, Photo of the ceramic membrane support with dimensions similar to a Euro coin as provided by Fraunhofer IKTS. b, SEM images of the cross-section of the ceramic membrane support in different magnifications: (i) overview image showing the pore size gradient across the membrane and (ii) magnification of the upper, sintered membrane structure with pore size around 70 nm. c, Photo showing the ceramic membrane support handled with tweezers during Langmuir-Schaefer transfer of a FhuA membrane present at the air-water interface of the Langmuir trough. d, AFM images of the surface of the ceramic membrane support before and after 10, 20, or 30 Langmuir-Schaefer transfers of a FhuA ΔCVF^{tev} membrane performed as shown in c.

5.7 FhuA membrane rejection properties

SEM measurements were performed by Minh Thu Tran at Fraunhofer IAP.

In the previous section, successful coating of ceramic IKTS membrane supports with FhuA membranes was demonstrated. To verify if FhuA membranes cover the complete IKTS membrane surface and if FhuA membranes transferred to IKTS membranes remain stable during filtration, rejection of the FhuA-IKTS composite membrane toward BSA was measured. BSA molecules have a molecular size (hydrodynamic radius ~ 3.5 nm)[104] similar to that of FhuA molecules, and complete and stable FhuA membrane coverage of the IKTS membrane should thus result in full BSA rejection (no matter if the membranes are made from FhuA WT or FhuA ΔCVF^{tev}; here, mostly FhuA ΔCVF^{tev} membranes were investigated though). Furthermore, determination of BSA concentration in feed, permeate and retentate could be straightforwardly carried out using UV-vis spectroscopy.

Controlled filtration of a solution of BSA in water through FhuA-IKTS membranes was done using the set-up of a syringe pump shown and described in **Figure 5.28**.

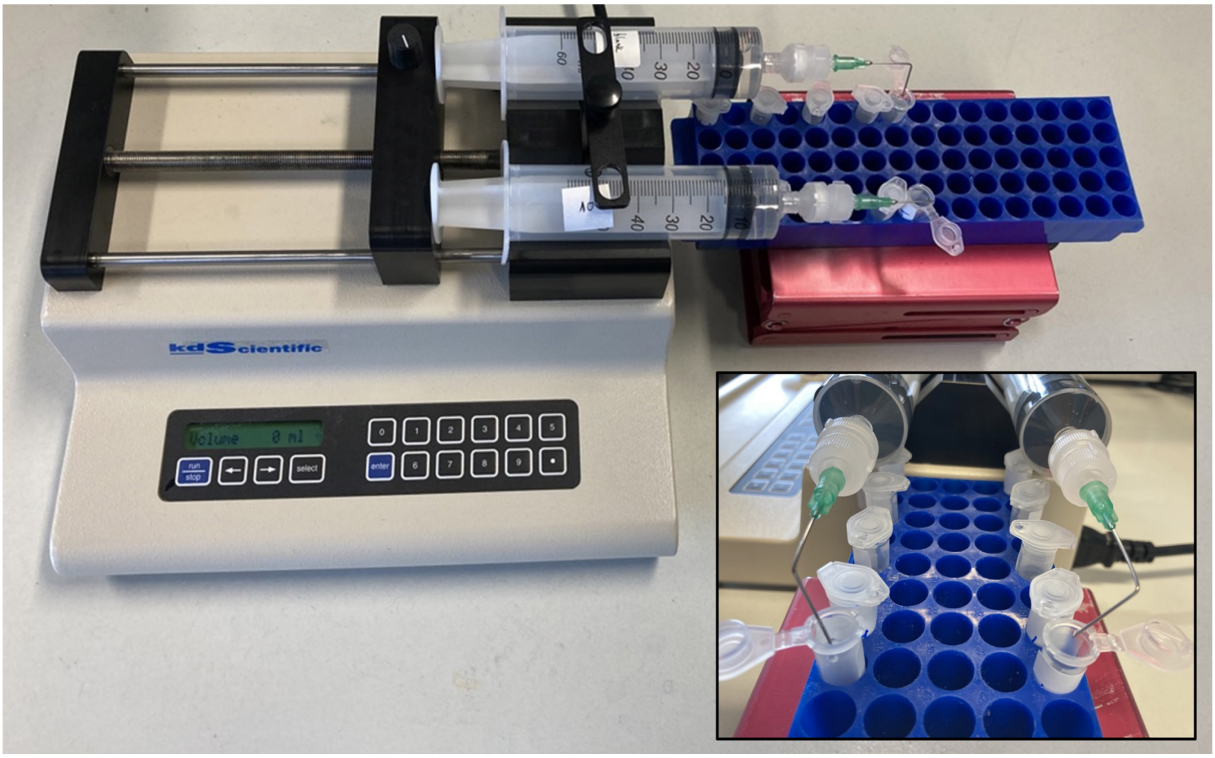

Figure 5.28: Experimental set-up of BSA rejection measurements. The photo shows a syringe pump equipped with two syringes filled with a solution of BSA in water. The syringe outlets are connected to filter holders each holding a ceramic membrane support coated with serveral FhuA membrane layers. The permeate is collected in fractions in 1 ml reaction vessels.

In all cases, the two syringes of the syringe pump were loaded with exactly 10 ml of BSA solution (~ 0.5 mg ml^{-1}) and exactly 5 ml of that feed solution were filtered through the respective membrane sample at a constant flow rate of 0.1 ml min^{-1}. The permeate was collected in five 1 ml fractions and the BSA concentrations in each permeate fraction and in the retentate (5 ml BSA solution remaining in the syringe) were measured.

First, as reference, three blank IKTS membranes were investigated and the results are presented in **Figure 5.29**. Within the scope of the accuracy of the UV-vis-concentration determination (e.g. dilution errors), the BSA concentrations in permeate and retentate were the same as in the respective feed solution. This suggests that BSA does not unspecifically adsorb to the ceramic IKTS membrane to significant extent and that measuring the BSA rejection is a valid method for the assessment of FhuA-IKTS membranes.

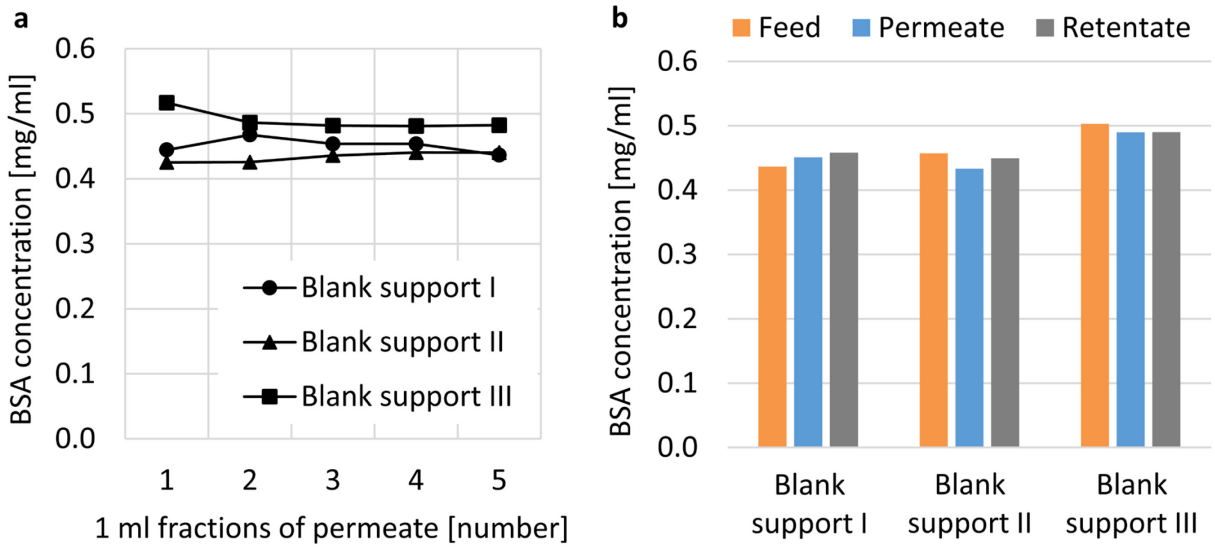

Figure 5.29: BSA rejection of blank ceramic membrane supports. a, Diagram showing the BSA concentration in five 1 ml-permeate fractions collected after filtration trough blank ceramic membrane supports (Reference measurements were performed on different days with freshly prepared BSA feed solutions having slightly different BSA concentrations). b, Bar chart comparing feed (10 ml), permeate (5 ml) and retentate (5 ml) concentrations corresponding to the filtrations described in a.

To screen how many Langmuir-Schaefer transfers are required to achieve BSA rejection, the three FhuA-IKTS membranes prepared with 10, 20, and 30 transfers (previously analyzed by AFM, Chapter 5.6, Figure 5.27d) were investigated next. All three membranes did reject BSA to some extent, but none entirely, as indicated by the results presented in **Figure 5.30**. Interestingly, the sample prepared with only 10 transfers showed the highest overall rejection of about 63%, followed by the samples prepared with 30 and 20 transfers showing rejections of

55% and 19%, respectively (Figure 5.30b). BSA rejection resulted in almost equivalent BSA concentration in the retentate, suggesting that filter cake formation played a minor role in this experiment. The five permeate fractions corresponding to the membrane prepared with 10 transfers had comparable concentrations ranging between 0.15 mg ml^{-1} and 0.2 mg ml^{-1} (Figure 5.30a). The other two membranes, however, showed comparably low BSA concentrations in the first, but higher BSA concentrations in the subsequent fractions. The latter could be an indication of FhuA membrane rupture or FhuA membrane detachment from the IKTS membrane support. It is pointed out that the flow rate and not the transmembrane pressure was kept constant in this experiment, so that thicker membranes were exposed to higher transmembrane pressures as compared to thinner membranes. This could explain why thicker membranes may have ruptured rather than thin membranes (even though thicker membranes were generally assumed to have higher mechanical stability than thin membranes). Exemplary, the constitution of the FhuA-IKTS membrane prepared with 30 transfers was investigated after BSA filtration by SEM and AFM (**Figure 4.31**).

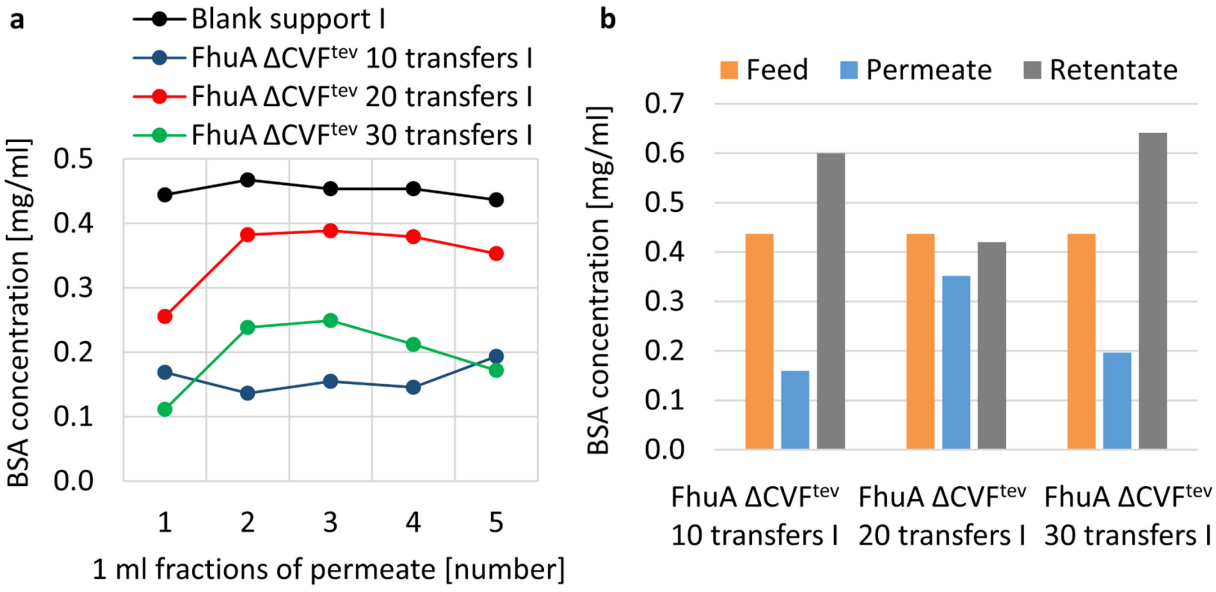

Figure 5.30: BSA rejection of ceramic membrane supports coated with FhuA membranes I. a, Diagram showing the BSA concentration in five 1 ml-permeate fractions collected after filtration through IKTS membrane supports coated with FhuA ΔCVF^{tev} membranes by performing 10, 20 or 30 Langmuir-Schaefer transfers. b, Bar chart comparing feed (10 ml), permeate (5 ml) and retentate (5 ml) concentrations corresponding to the filtrations described in a.

SEM images of the upper cross-section of the FhuA-IKTS membrane after BSA filtration show the FhuA membrane as a thin, homogenous film that settles against the rough, sintered surface of the IKTS support (**Figure 5.31**a). As reference, a blank IKTS membrane was investigated

using the same SEM settings and not showing a film covering the sintered granules at the top of the membrane support (Figure 5.31b). Similarly, the series of AFM images in Figure 5.31c allows comparing the topography of the blank IKTS membrane and the FhuA-IKTS membrane prepared with 30 transfers, before and after BSA filtration. The AFM images before and after filtration clearly distinguish from the blank membrane and both indicate coverage of the IKTS membrane surface. After filtration, the granules seem slightly more pronounced than before filtration. This could be an indication that the FhuA membrane is pressed towards and settles to the support during filtration. However, neither AFM nor SEM suggest broad membrane damage or detachment during filtration.

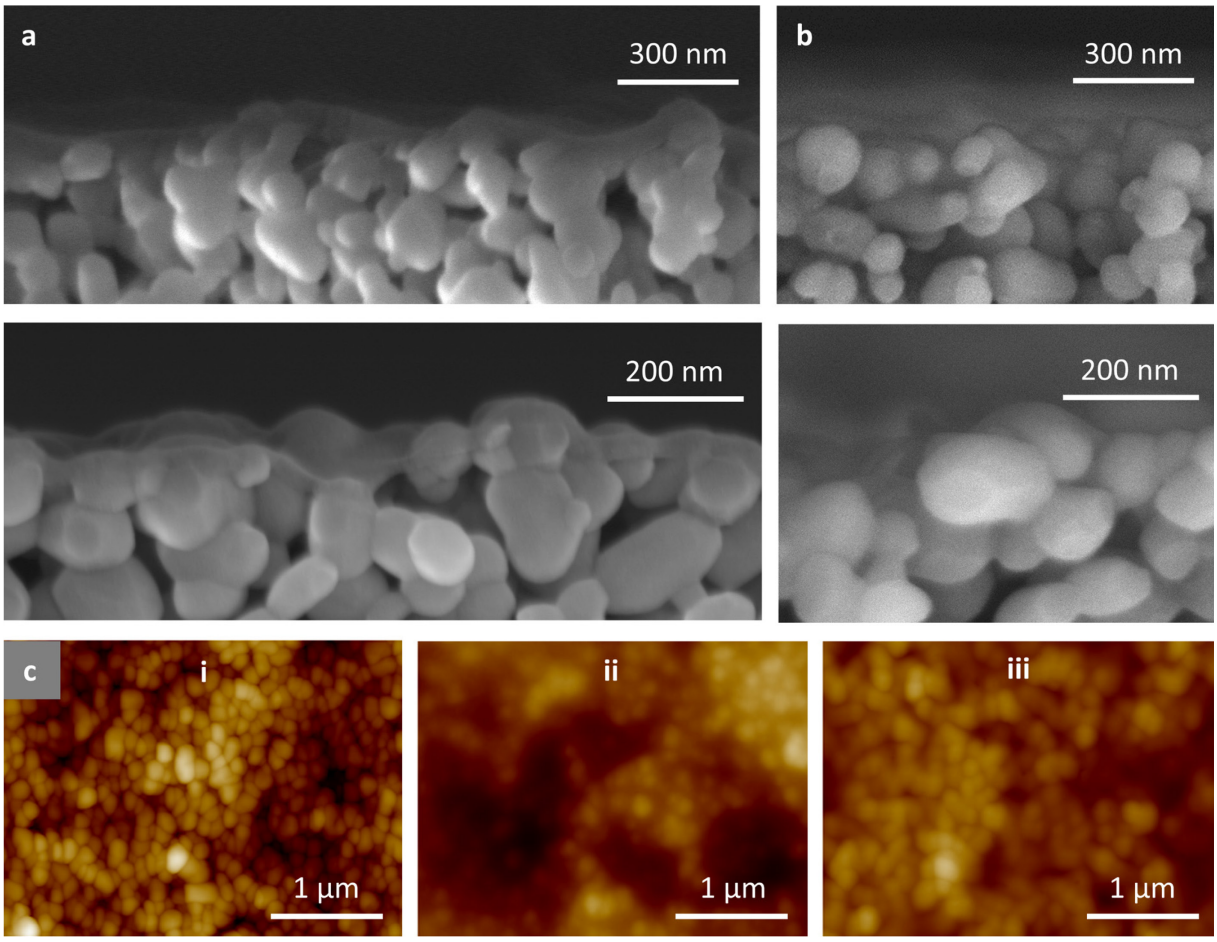

Figure 5.31: Membrane investigation after filtration of BSA solution. a, SEM images showing the upper cross-section of the ceramic membrane support coated with multiple FhuA membrane layers (FhuA ΔCVF^{tev} 30 transfers I), after BSA filtration, in two magnifications. The FhuA membrane is visible as a thin, homogenous film that settles against the rough, sintered surface of the support. For reference, SEM images of the upper cross-section of a blank ceramic membrane support in same magnification are shown in b. c, AFM images of the surface of the ceramic membrane supports when (i) not coated with a FhuA membrane or when coated with multiple FhuA layers (FhuA ΔCVF^{tev} 30 transfers I) (i) before and (iii) after BSA filtration.

To support the previous findings with more data, BSA rejection of eight additional FhuA-IKTS membranes prepared with either 10, 20 or 30 Langmuir-Schaefer transfers was measured. All data are shown Figure S2 in the Appendix, overall indicating low reproducibility. The latter may be explained by the manual execution of the Langmuir-Schaefer transfers, presumably resulting in IKTS membranes that were sometimes well and sometimes less well covered with FhuA membranes. FhuA-IKTS membranes prepared with 20 or 30 transfers did not outperform those prepared with 10 transfers though. It is thus concluded that the quality of the first transfers is relevant to achieve good support membrane coverage and simply performing more transfers is not suited to compensate poor first transfers. BSA rejection results of the three best-performing FhuA-IKTS membranes investigated in this study are summarized in **Figure 5.32**. BSA concentrations are stated in percent of the BSA feed solution and the BSA rejection in the three first fractions collected lay between 61% and 75%. BSA concentrations in the subsequent fractions did, surprisingly, not remain at the same level or follow a clear trend (Figure 5.32a). Solely subsequent fractions of one sample (FhuA ΔCVF^{tev} 10 transfers III) showed monotonously declining BSA concentrations, which could indicate BSA filter cake formation on top of the respective FhuA IKTS membrane. However, the latter was a single observation and the average BSA concentration of permeate and retentate sums up to 91%, suggesting that maximum 9% of the BSA contributed to filter cake formation. The average BSA concentration of permeate and retentate of the two other samples was 96% and 87%, respectively, again, suggesting that filter cake formation played a minor role in this experiment. Sample FhuA ΔCVF^{tev} 10 transfers III showed the highest overall BSA rejection of 82%.

In conclusion, FhuA-ITKS membranes showed significant BSA rejection and considerable stability in a real filtration process. The low performance reproducibility is traced back to not very reproducible and presumably incomplete coating of the IKTS membrane supports with FhuA membranes during manual Langmuir-Schaefer transfer. As basis for more detailed investigations of the molecular weight cut-off and a comparison of FhuA open and closed pore membranes, IKTS membrane coating with FhuA membranes has to be optimized in future, e.g., by automation.

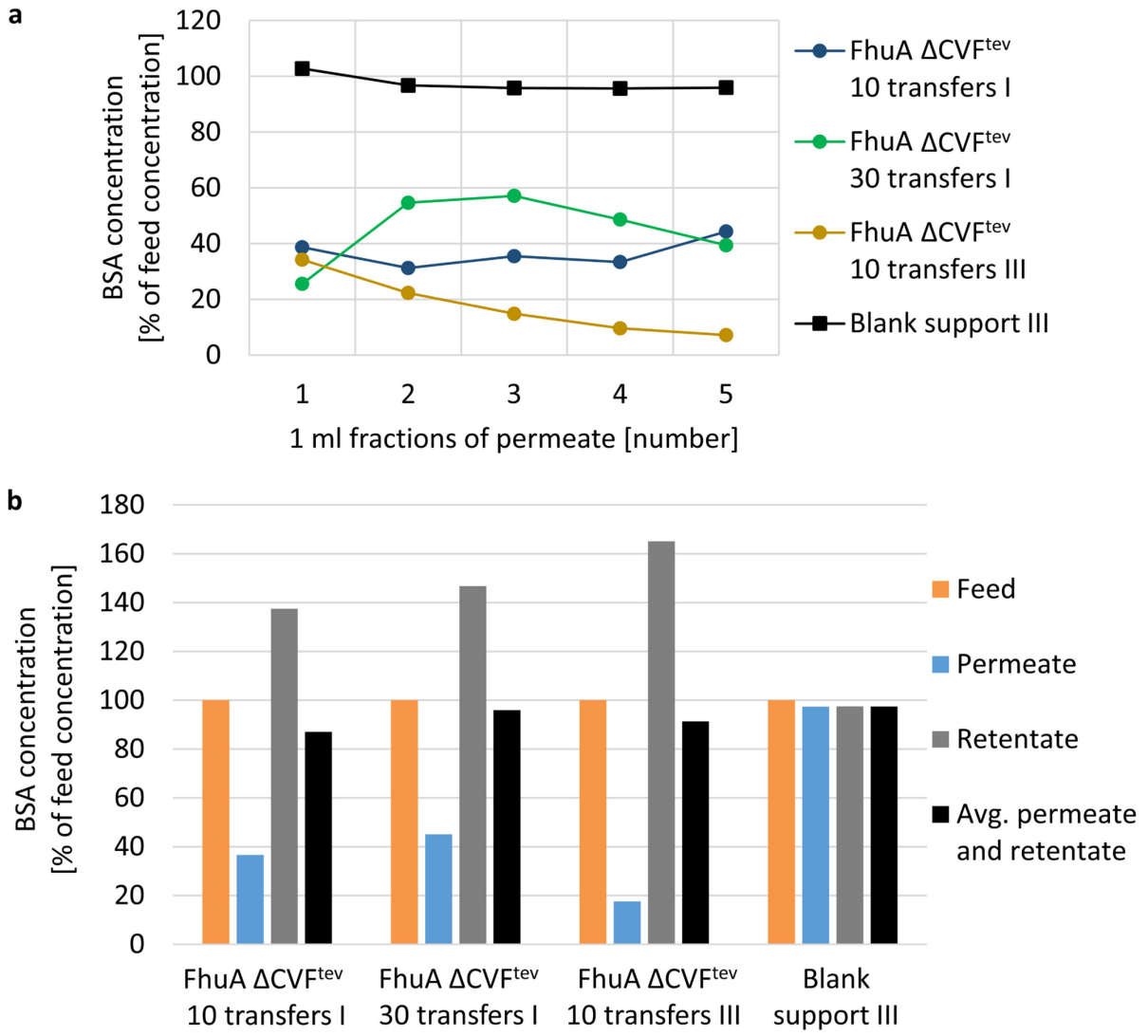

Figure 5.32: BSA rejection of ceramic membrane supports coated with FhuA membranes II. a, Diagram showing the BSA concentration in five 1 ml-permeate fractions collected after filtration through ceramic membrane supports coated with FhuA ΔCVF^{tev} membranes by performing 10 or 30 Langmuir-Schaefer transfers. Results shown here correspond to the three out of 11 membranes showing the highest BSA rejection. b, Bar chart comparing feed (10 ml), permeate (5 ml) and retentate (5 ml) concentrations with the average concentration of permeate and retentate, corresponding to the filtrations described in a.

5.8 Transfer of FhuA membrane preparation to TMV-derived particles

Engineering and extraction of TMV virus-like particles used in this work were done by Eva Schubert and others in the group of Prof. Wege at the University of Stuttgart.

TEM measurements were performed by Thomas Bick from the group of Prof. Petra Wendler at the University of Potsdam.

Up to this chapter, the preparation of ultrathin protein nanopore membranes at the air-water interface was investigated using the transmembrane protein FhuA as building block.

Furthermore, subsequent membrane characterization strongly suggested successful incorporation of functional and vertically aligned FhuA nanopores into the membrane. Ideally, the new membrane preparation approach could be used for fabrication of ultrathin membranes from different protein-based nanopores as well. This was exemplarily investigated using virus-like particles derived from tobacco mosaic virus (Chapter 3.1.2), and corresponding results are summarized in the present section. VLPs from TMV were kindly provided by the group of Prof. Christina Wege at the University of Stuttgart. It is pointed out that quite small amounts of VLPs were available from plant extraction, so that the results in this chapter may be seen as preliminary proof of principle study rather than a detailed examination as presented with FhuA.

VLPs from TMV were found a suited and interesting alternative to FhuA to demonstrate versatility of membrane preparation for two reasons: 1. TMV-derived VLPs were successfully incorporated as pores into membranes before and the corresponding publication[33] may serve as bench mark (Chapter 4). 2. TMV-derived VLPs are supramolecular structures and as such larger than FhuA molecules, the central pore being clearly visible in TEM when stained with uranyl acetate. The latter eases membrane characterization as compared to FhuA membranes and allows clear statements on the presence of nanopores.

TMV-derived VLPs can be prepared, depending on the length of the used RNA, in a wide range of particle lengths up to 300 nm of the native TMV. The assembly and orientation of particles with a very high aspect ratio (like native TMV) at the air-water interface of a Langmuir trough is unclear and could require detailed studies and rounds of optimization. Consequently, in the framework of the initial experiments for this thesis, rather small disc-shaped VLPs (therefore referred to as TMV discs from now on) were utilized. The TMV discs have an outer and inner diameter of 18 nm and 4 nm, respectively, and a height of 9.2 nm (as illustrated in **Figure 5.33**a),[31] and as such dimensions in the same order of magnitude as transmembrane proteins like the comprehensively investigated FhuA. Furthermore, the TMV discs applied here were assembled from 68 coat proteins, each presenting a lysine residue to the lateral surface[31] so that - analogous to FhuA - glutaraldehyde crosslinking was possible. Before membrane preparation was carried out, the quality of TMV disc samples was analyzed using dynamic light scattering (DLS) and TEM. DLS indicated a narrow particle size distribution around a hydrodynamic diameter of 22 nm, sufficiently resembling the real diameter of 18 nm to conclude TMV disc monomers and dimers were the dominating species (Figure 5.33b). This was confirmed by TEM that clearly showed a lot of intact TMV discs with visible pore structure (monomers and dimers) in different orientations as expected for TEM images of such

particles (Figure 5.33c). Additionally, some protein remnants not assembled as discs and randomly scattered across the grid were present. The latter was the case even though the discs were both, assembled at a shortfall ratio of coat proteins and RNA (so that all coat protein should have space along the RNA strands), and purified by size exclusion chromatography. Once assembled, TMV-derived virus-like particles are known to be considerably stable (Chapter 3.1.2) so that significant disintegration is unlikely. It is thus assumed that sample purification was not as effective as intended.

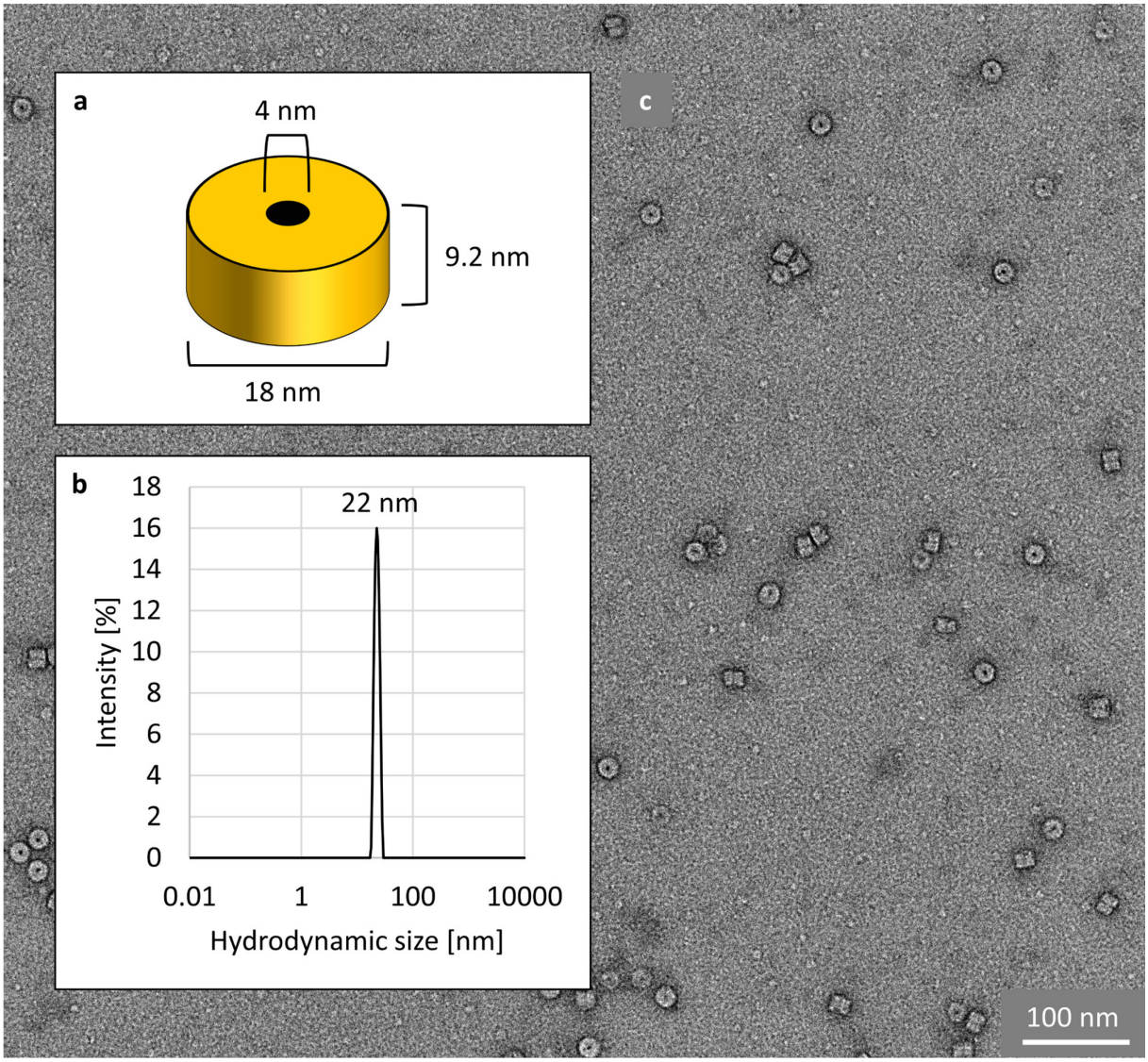

Figure 5.33: Quality assessment of TMV-derived particles used for membrane preparation as alternative to FhuA. a, Schematic illustration showing relevant dimensions of the TMV-derived particles used in this study (because of their shape also referred to as TMV discs). b, Particle hydrodynamic size distribution of a TMV disc sample measured by DLS. c, TEM image of a TMV disc sample stained with uranyl acetate.

To prepare TMV disc membranes (from now on TMV membranes), 0.16 nmol of TMV discs were spread to the air-water interface of the Langmuir trough. Theoretically, 0.16 nmol of uprightly oriented TMV discs (cross-section ~ 255 nm^2) occupy an area corresponding to the initial trough area of 241.5 cm^2 and since the adsorption behavior of TMV discs to the air-water interface was unknown, this was found a reasonable starting value. TMV disc adsorption was monitored as a function of surface pressure over time (**Figure 5.34**a(i)), showing an initial rise in surface pressure until asymptotically approaching an equilibrium around 10 mN m^{-1} after 8 hours. Upon reducing the trough area by barrier compression, the surface pressure increased almost linearly (Figure 5.34a(ii)), as similarly seen for FhuA (Chapter 5.3.2, Figure 5.7). No BAM was performed on TMV disc Langmuir films to determine a suited surface pressure to perform crosslinking, instead, the crosslinking pressure determined for FhuA membranes of 25 mN m^{-1} was taken on. Injection of glutaraldehyde into the buffer subphase was carried out reaching a final concentration of 0.5 vol% and is marked with an arrow at a trough area of 125 cm^2 in the compression curve (Figure 5.34a(ii)). The plateau in the compression curve indicates that keeping the surface pressure constant requires further reduction of the trough area. However, as also seen during preparation of FhuA membranes, the TMV membrane area stabilized shortly after the injection of glutaraldehyde and was 98 cm^2 after 8 hours.

Crosslinked TMV membranes were transferred to holey TEM grids, stained with uranyl acetate and investigated using TEM. Like FhuA membranes, TMV membranes freestandingly covered micron-sized holes in the TEM grid but ruptured shortly upon exposure to electron beams (Figure 5.34b). However, few TMV disc pores were visible in the membranes as emphasized in Figure 5.34b(ii). The surrounding membrane appeared very homogenous and is thus assumed to have either consisted out of stacked TMV discs (like coin rolls) lying horizontally in the interfacial plane or out of unassembled protein and RNA strands. When densely crosslinked with glutaraldehyde, both arrangements could result in membranes appearing homogenous in TEM measurements. It is further possible, that the visible TMV disc pores in Figure 5.34b belonged to TMV discs that were not incorporated in the membrane, but adsorbed on top of the homogenous membrane (either before Langmuir-Schaefer transfer, from the subphase, or upon drying of a subphase droplet after the transfer).

Accounting for the possibility that the homogenous parts of the membranes consisted out of unassembled proteins and RNA, the following considerations have been made: Based on the TEM image of the TMV disc sample (Figure 5.33c), a lower ratio of unassembled proteins and RNA to assembled TMV discs was expected than reflected by the TMV membrane in

Figure 5.34b. Thus, two scenarios could explain the assumed low amount of assembled TMV discs in the membrane: 1. Scenario: Unassembled protein and RNA strands preferentially adsorb to the air-water interface, as compared to properly assembled TMV discs. This scenario was already suggested in a literature report.[105] (Note: The estimation of interfacial area occupied by 0.16 nmol of TMV discs was based on assembled discs, while the same amount of disassembled discs could occupy a way larger area.) 2. Scenario: Assembled TMV discs first occupy the air-water interface but disassemble upon barrier compression when exposed to high surface pressures.

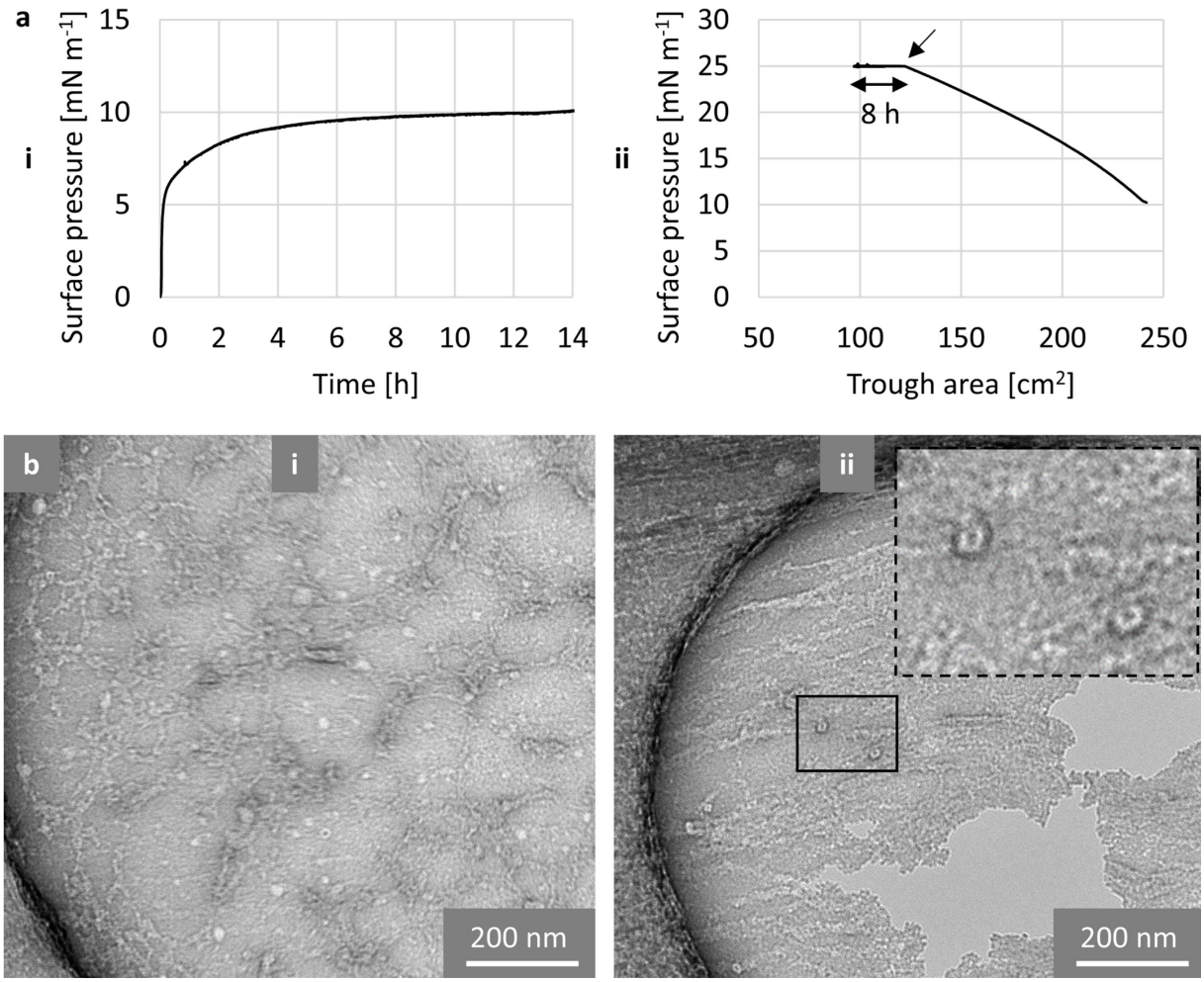

Figure 5.34: TMV membrane fabrication and transfer to microporous supports I. a, Set of Langmuir (i) adsorption and (ii) compression curves measured during membrane fabrication from 0.16 nmol TMV discs (pH 7.4, 200 µl, 1 mg ml^{-1}) spread on top of phosphate buffer. In a(ii), the injection of glutaraldehyde is marked with an arrow and crosslinking was performed at 25 mN m^{-1} for 8 h. b, TEM images of the TMV membrane (as prepared in a) on top of a holey carbon grid stained with UA. The TEM image in b(i) shows an intact, freestanding membrane shortly before rupturing. In b(ii), the TMV membrane is ruptured and some uprightly oriented TMV discs are clearly visible (in or on top of the membrane). The dashed box in the top right shows a magnification of the area marked with the continuous box in the image.

To test the second scenario, again, 0.16 nmol of TMV discs were spread to the air-water interface of the Langmuir trough. TMV disc adsorption was monitored overnight resulting in an equilibrium surface pressure of about 12.5 mN m^{-1}, slightly higher compared to the first experiment (Figure 5.34a). Then, without compressing the assembled TMV film beforehand, glutaraldehyde was injected into the buffer subphase reaching a final concentration of 0.5 vol%. Injection is visible as a peak in the corresponding surface pressure - time curve and once more crosslinking was allowed to proceed for 8 hours (**Figure 5.35**a). During the first 5 hours of crosslinking the surface pressure slightly increased from 12.5 mN m^{-1} to about 15 mN m^{-1}, indicating that the TMV disc film condensed, presumably due to the covalent bonds forming between the TMV discs. A TEM image of this TMV membrane covering a hole in a TEM grid is shown in Figure 5.35b.

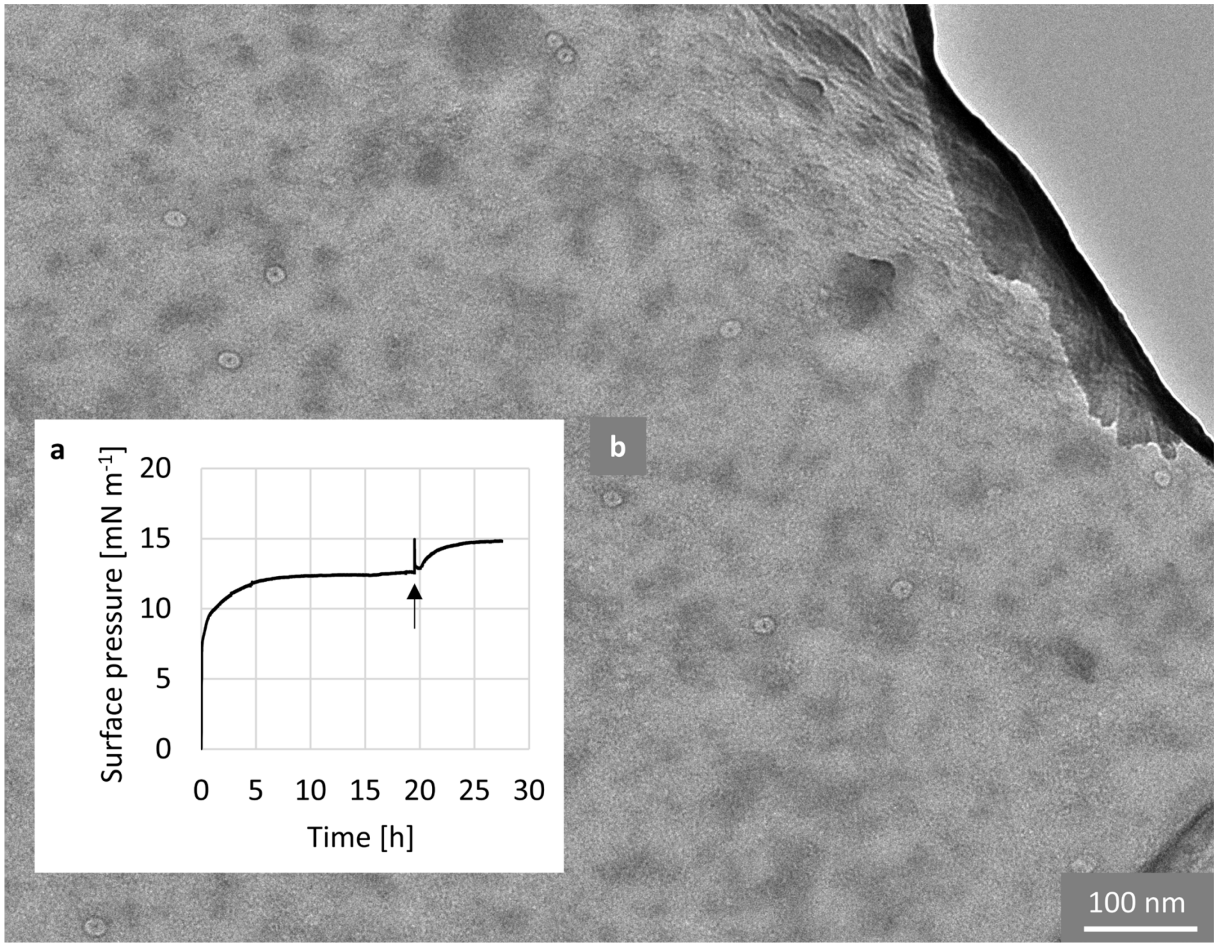

Figure 5.35: TMV disc membrane fabrication and transfer to microporous supports II. a, Langmuir curve measured during membrane fabrication from 0.16 nmol TMV discs (pH 7.4, 200 µl, 1 mg ml^{-1}) spread on top of phosphate buffer. The injection of glutaraldehyde is marked with an arrow and crosslinking was performed without barrier compression for 8 h. b, TEM images of the TMV membrane (as prepared in a) on top of a holey carbon grid stained with UA. The TMV membrane is ruptured and some uprightly oriented TMV discs are clearly visible as membrane pores.

The TEM image (Figure 5.35b) looks quite similar to the one of the TMV membrane prepared at a surface pressure of 25 mN m^{-1} (Figure 5.34b), with some distinct TMV pores aligned vertically in the otherwise homogenous membrane (that could consist out of unassembled coat protein and RNA). Because only single experiments were performed and only few TEM images acquired of each membrane, definitive statements on quantity of TMV disc pores in the membranes cannot be made. However, comparing the images in Figure 5.34b and Figure 5.35b, it appears that a little more TMV disc pores are present in the membrane prepared without barrier compression. This could be an indication that - to some extent - scenario 2 holds true, and barrier compression/high surface pressure causes TMV VLPs to disassemble. Nonetheless, wide parts of both membranes did not show the distinct TMV pores so that scenario 1 may also hold true (*Unassembled protein and RNA strands preferentially adsorb to the air-water interface, as compared to properly assembled TMV discs).* Also, the possibility of coin roll-like stacked TMV discs lying horizontally in the membrane plane mentioned above cannot be ruled out at this point. It is thus concluded that further investigations on TMV membrane formation are required to ascertain membrane composition and an optimal membrane formation strategy for VLPs. Useful measures contributing to a deeper understanding of TMV membrane formation following the proposed Langmuir-Schaefer approach could be: 1. Determining sample purity, in particular the ratio of unassembled CP to VLP, and interfacial activity (e.g., by tensiometry) of free CP and TMV particles of different length (from disc-shape up to native TMV of 300 nm length). 2. Improving assembly of VLP and/or sample purification. 3. Performing reference investigations, e.g., spreading of solely coat proteins to verify if the observed surface pressure differentiates and if homogenous parts of the membranes could indeed consist out of disassembled TMV discs. 4. Determining the orientation of TMV discs at the air-water interface for varying surface pressures and perform similar investigations for TMV particles of different length. SFG spectroscopy could be a powerful method here. Key questions are if TMV particles have a preferential orientation at the interface, if this orientation depends on the compression status and on the length of the VLPs. This could lead to the question if longer TMV particles can be aligned at the interface by increasing surface pressure and if a critical length of TMV particles can be determined to form membranes with upright oriented TMV pores by the presented Langmuir approach. 5. If needed, attempts could be made to controlling TMV particle orientation at the air-water interface by introducing amphiphilicity to the particles, e.g., by one-sided modification of the particles with hydrophobic molecules. These opportunities for improvement make further investigations on preparing TMV membranes using the established Langmuir protocol seem worthwhile.

5.9 Conclusion

Here, a new method for the fabrication of ultrathin, yet mechanically stable membranes incorporating the TP FhuA, which naturally forms a defined nanopore, was introduced. Due to their low thickness and the extremely high density of collectively aligned proteins inferred in this study, such membranes have very high water permeance compared to conventional nanofiltration membranes. Still, when transferred to scalable ceramic membrane supports, the new protein nanopore membranes significantly reject bovine serum albumin (BSA) molecules with a molecular size below 10 nm. Membranes made of two different FhuA variants mirrored the molecular properties of each variant, here demonstrated with respect to ion permeability. Given intensive research on imprinting functionalities to protein nanopores,[18,106–108] the membrane has potential to serve as a platform technology that allows tailoring membranes according to individual process requirements. Membrane fabrication uses the well-studied Langmuir technique and a common protein crosslinker, principally ensuring good scalability with view to future applications. At this point, two scale-up options seem worthwhile to be investigated: 1. Use of a larger Langmuir trough and automation of the Langmuir-Schaefer transfer, further using stiff membrane supports as done in this work. 2. Implementation of a roll-to-roll Langmuir-Blodgett method (Chapter 3.2) using flexible, polymeric membrane supports as introduced by Parchine et al. for the transfer of crystalline colloidal photonic Langmuir films to a flexible poly(ethylene terephthalate) support.[109] The main challenge of either option is to achieve homogenous and defect-free transfer of the ultrathin FhuA membranes to the support material. However, using flexible support materials, FhuA membrane stiffening upon drying has to be considered, which could result in post-transfer FhuA membrane rupture when the composite membrane is bent. The latter problem is likely to arise for other ultrathin and densely crosslinked protein nanopore membranes as well though.

At Fraunhofer IAP, the preparation of slightly thicker and therefore more robust protein nanopore membranes by alternately spraying protein and crosslinker solutions, and optionally a polymeric matrix material on top of membrane supports is planned. While the scalability of this fabrication process is out of question, experiments will have to demonstrate if it allows to prepare sufficiently thin and homogenous membranes with densely packed protein nanopores that still facilitate transport. Spray coating, however, is not expected to enable collective and upright alignment of the protein nanopores in the membranes as achieved by the Langmuir approach presented in this work.

5.10 Experimental

This section provides information on materials and methods used in the experiments described above.

5.10.1 Buffer

In this study, MPD buffer is defined as a buffer containing 7.5 mM sodium hydrogen phosphate (Na_2HPO_4), 2.5 mM sodium dihydrogen phosphate (NaH_2PO_4) and 50 mM 2-methyl-2,4-pentanediol (MPD). MPD is used as a stabilizing agent for FhuA variants in this study.[52,54] Phosphate buffer is defined as a buffer containing 7.5 mM sodium hydrogen phosphate (Na_2HPO_4) and 2.5 mM sodium dihydrogen phosphate (NaH_2PO_4). Buffers were made using Millipore pure water with a resistivity of 18.2 MΩcm.

5.10.2 FhuA refolding

Engineering and extraction of the FhuA variants used in this study were done by our collaboration partners; Dr. Daniel Sauer, Dr. Marco Grull, Dr. Mehdi Davari Dolatabadi and others in the group of Prof. Schwaneberg at the RWTH Aachen University.

Engineering, expression and extraction of the FhuA variants used in this study were performed according to previously published procedures.[50] Lyophilized powders of different FhuA variants were stored at -18 °C until used to prepare a refolded sample. Therefore, the lyophilized powder of the respective FhuA variant (containing approx. 66 wt% SDS) was dissolved in MPD buffer and passed through a sterile 0.2 µm PVDF filter (Thermo Fisher Scientific Inc., USA) in order to remove any larger aggregates or bacteria. Next, the FhuA concentration was determined by measuring the protein absorption at 280 nm using the UV-vis spectrophotometer SPECORD 210 (Analytik Jena AG, Germany). If needed, the FhuA solution was diluted to a concentration of 1 mg ml^{-1}. Controlled protein refolding was achieved by dialyzing the protein solution against MPD buffer (1:200) three times for 24 h at 4 °C using a dialysis membrane with a molecular weight cut-off (MWCO) of 12-14 kDa (Sigma Aldrich, USA). Before the use in any experiment, the FhuA concentration was adjusted by dilution in MPD buffer and the concentration determined by UV-vis spectroscopy.

5.10.3 SDS-PAGE

SDS-PAGE was performed with a 4-20% polyacrylamide gradient gel (Bio-Rad, USA), using the Mini-PROTEAN Tetra Cell (Bio-Rad, USA) for 1-D vertical gel electrophoresis and the standard protein ladder Roti®-Mark TRICOLOR XTRA (Carl Roth GmbH + Co. KG,

Germany). Protein samples were treated with a denaturing buffer and heated to 85 °C for 10 min prior to use. Bands were visualized using a standard Coomassie blue staining protocol.

5.10.4 CD spectroscopy

CD spectroscopy on FhuA samples was conducted by Maria Mathieu-Gaedke at the University of Potsdam.

CD spectroscopy was performed using a Jasco J-815 spectropolarimeter (JASCO Deutschland GmbH, Germany) featuring Peltier thermostat-controlled cell holders. CD spectra were recorded at 20 °C using 1.0 mm path length quartz cuvettes (Hellma, Germany) at a protein concentration of 0.125 – 0.25 mg ml^{-1}. Settings in all measurements were chosen as follows: Bandwidth of 1 nm, data pitch of 1 nm, scan speed of 50 nm min^{-1} and digital integration time of 4 s. Spectra shown in this thesis are the average of three measurements.

5.10.5 BAM

BAM measurements were performed together with Aleksei Chumakov in the lab of Prof. Svetlana Santer at the University of Potsdam.

BAM images were acquired using an Accurion nanofilm_ultrabam with a field of view of 800 x 430 µm and a lateral resolution down to 2 µm. BAM was performed on a Kibron MicroTrough XL equipped with two symmetrically movable barriers, a surface area of 232 cm^2 and a volume of 145 mL. Surface pressure was recorded using a small diameter (0.51 mm) special alloy wire attached to a microelectronic feedback system (dynamic range = 0 - 130 mN m^{-1}, resolution 10 µN m^{-1}). In a typical BAM experiment, 70 µl FhuA solution (FhuA in MPD buffer at a concentration of 12.6 µM) was spread to the clean air-water interface, the Langmuir trough filled with Millipore pure water. After 15 min of equilibration, the barriers of the Langmuir trough were set to motion at a speed of 1 mm min^{-1} to compress the adsorbed FhuA monolayer.

5.10.6 Langmuir trough and membrane formation

Langmuir experiments were performed on a KSV Nima minitrough system equipped with two symmetrically movable barriers, 273 cm^2 surface area and a volume of 176 ml. Barrier movement was controlled by a servo controlled DCmotor and surface pressure was recorded using a platinum Wilhelmy plate (Biolin Scientific, Sweden) attached to a microelectronic feedback system (dynamic range = 0 - 250 mN m^{-1}, resolution 4 µN m^{-1}). Membrane formation and transfer to support materials was performed as follows. First, the Langmuir trough was thoroughly cleaned with ethanol, rinsed with Millipore pure water, and filled with phosphate

buffer. Subsequently, the barriers of the Langmuir trough were fully closed, adsorbed particles were sucked away from the air-water interface and the phosphate buffer was refilled from behind the barriers. This procedure was repeated until the measured rise in surface pressure of the clean air-water interface upon full barrier compression was less than or equal to 0.05 mN m^{-1}. In a typical membrane fabrication experiment, 50 µl FhuA solution (FhuA in MPD buffer at a concentration of 6.3 µM) was spread to the clean air-water interface in 25 µl aliquots. After 2 hours of equilibration, the barriers of the Langmuir trough were set to motion at a speed of 1 mm min^{-1} to compress the adsorbed FhuA monolayer up to a surface pressure of 25 mN m^{-1}. While keeping the surface pressure constant, 1.76 ml glutaraldehyde solution (50 wt% in H_2O, Sigma Aldrich, USA) was injected to the phosphate buffer subphase from behind the Langmuir trough barriers. Crosslinking proceeded for at least 2 hours until the FhuA membrane was transferred to the respective substrate following the Langmuir-Schaefer method. Before drying in air, transferred FhuA membranes were washed in an MPD solution (5 vol% MPD in Millipore pure water) by dipping three times.

5.10.7 SFG spectroscopy

SFG measurements and analysis were carried out by Daizong Qi, Dr. Hao Lu and Dr. Konrad Meister from the group of Prof. Mischa Bonn at the Max Planck Institute for Polymer Research in Mainz.

A Langmuir trough was filled with 80 ml of the phosphate buffer applied for membrane fabrication dissolved in D_2O, before 6 nmol of the protein was carefully spread onto its surface. By precisely controlling the surface area using surface pressure as a feedback in real time, a surface pressure of 25 mN m^{-1} was achieved and retained in automatic compression mode (Kibron FilmwareX) throughout the experiment. The principles of the sum-frequency generation (SFG) technique are introduced in detail elsewhere.[93] Briefly, an infrared laser beam in resonance with a molecular vibration, in this case the O-H stretch vibration, is overlapped in space and time with a visible laser beam. At the interface, the sum-frequency light of the two incoming beams is generated. Due to SFG selection rules, the generation of sum-frequency signals is forbidden in centrosymmetric media. The appearance of an SFG signal thus means that the molecules are preferentially aligned, breaking centrosymmetry. The SFG signal is enhanced at resonance with the molecular vibration. In the used setup, the frequency range of interest was set mostly around the amide region, from which the secondary structure of the interfacial protein could be inferred. The measurements were taken both before and after 0.8 ml of the crosslinker (50 wt% glutaraldehyde solution) was added to the subphase.

As a useful complement, calculated spectra based on a referenced protein database (PDB) were also generated with a given angle of the protein's backbone to the surface normal, and a certain angular distribution, assumed to be Gaussian.

5.10.8 Substrates

QUANTIFOIL® Multi A TEM girds equipped with a holey carbon film and hole dimensions ranging from 1 µm to 8 µm (Figure 5.15, 5.16a) and QUANTIFOIL® R3/3 300-mesh holey carbon grids with 2 nm carbon support film (Figure 5.16b-d, 5.17) were purchased from Quantifoil Micro Tools GmbH, Germany. Silicon nitride membrane windows with a single hole of 1 µm (thickness of silicon nitride membrane 100 nm) or 5 µm/7µm (thickness of silicon nitride membrane 500 nm) diameter for ion conductivity and water permeation measurements, respectively, were purchased from Silson Ltd, UK. The silicon substrates (100) were purchased from Entegris Inc., USA. Sintered aluminum oxide microfiltration membranes with a pore size of about 70 nm were obtained from Fraunhofer IKTS, Germany. The surfaces of all supports were activated using air plasma treatment to increase the amount of active surface groups and improve membrane attachment during Langmuir-Schaefer transfer (TEM girds: 60 s, 300 W, 0.2 mbar; other supports: 300 s, 300 W, 0.2 mbar; PlasmaFlecto 10, plasma technology GmbH, Germany).

5.10.9 AFM

The AFM images were acquired in tapping mode with a Bruker Dimension Icon AFM equipped with OTESPA R3 tips ($k = 26$ N m^{-1}, $f_0 = 300$ kHz), when membranes were measured dry. PeakForce quantitative nanomechanical property mapping (PeakForce QNM) was performed in liquid using ScanAsyst Fluid tips ($k = 0.7$ N m^{-1}, $f_0 = 150$ kHz) with peak forces of 2 nN, 5 nN, 10 nN, and 20 nN. Nanoscope (Version 9.1) and Nanoscope Analysis (Version 1.9) software were used for measurements and image processing, respectively. The Young's moduli E (Pa) of FhuA membranes measured in PeakForce QNM (Figure 5.20) were estimated using a model deduced from point force elastic theory for homogenous membranes by Mueggenburg et al. as stated in Equation 4:[99–101]

$$E = \frac{3\,F_{point}\,R^2}{\pi\,h\,\delta^3} \tag{4}$$

where F_{point} is a point force applied to the center of the freestanding membrane (N), R is the radius of the hole covered by the membrane (m), h is the membrane thickness (m) and δ is the membrane deformation in the hole center (m). The Young's moduli of FhuA membranes were

calculated based on a membrane thickness of 5 nm (as measured by AFM and XRR in Chapter 5.4.1).

5.10.10 XRR and GISAXS

XRR and GISAXS experiments were performed at Synchrotron SOLEIL collaborating with Dr. Stephanie Taßler.

XRR and GISAXS experiments were performed at the SIRIUS beamline[110] of Synchrotron SOLEIL using X-rays with a wavelength of 1.54997 Å (8 keV). The software StochFit[95] was used for processing of XRR data as described in Chapter 5.4.1.2. To estimate the SLDs of FhuA membranes and the silicon substrate, the elemental composition and the density of the respective material were required. The density of the FhuA variants was estimated by relating the respective molecular volume to the molecular weight. To do so, the volume of FhuA was assumend as elliptical tube (height: 5 nm; outer diameters: 4.6 nm, 3.9 nm; inner diameters: 2.3 nm, 1.95 nm), fully hollow in case of FhuA A2a, and filled up to 2/3 in case of FhuA WT accounting for the cork domain. On this basis, StochFit calculated the following SLDs: FhuA WT 18.464 10^{-6}Å^{-2}, FhuA A2a 18.048 10^{-6}Å^{-2}, and silicon dioxide 22.453 10^{-6}Å^{-2}.

5.10.11 TEM

TEM measurements were performed by Thomas Bick from the group of Prof. Petra Wendler at the University of Potsdam.

TEM images were acquired with a Thermo Fisher Talos F200C microscope (USA) at 200 kV at 57kx or 150kx magnification using a 4k x 4k Ceta 16M CMOS camera and the image acquisition software Velox 2.14. Plunge freezing of freshly transferred membranes into liquid ethane was done using a Leica EM GP2 plunge freezer after 5 s dual blotting at 10 °C and 90% humidity.

5.10.12 HIM

HIM measurements were performed by Michael Westphal in the lab of Prof. Armin Gölzhäuser at the University of Bielefeld.

HIM images were acquired with a Carl Zeiss ORION Plus® helium ion microscope (Germany) either in the standard secondary electron detection mode (Figure 5.18e(i)) or by employing a scanning transmission ion microscopy detector (dark-field: Figure 5.18e(ii); bright-field: Figure 5.22a).[111]

5.10.13 ThioGlo1 labeling and fluorescence microscopy

A FhuA ΔCVF^{tev} monolayer membrane transferred to a silicon substrate was labeled with the thiol-reactive fluorescent dye ThioGlo1 according to a protocol established elsewhere.[28,50] Briefly, a 1.5 mM stock solution of ThioGlo1 in acetonitrile was prepared and diluted in phosphate buffer to a concentration of 15 µM. 15 ml of this solution were used to incubate the FhuA ΔCVF^{tev} membrane on top of the silicon substrate (2 cm^2) for 1 hour, protected from light. After incubation, samples were washed by dipping three times into fresh Millipore pure water, dried in air, and investigated using fluorescence microscopy. The fluorescence microscopy images were acquired with a Leica DMi8 inverted fluorescence microscope (Leica Microsystems GmbH, Germany). Images were processed using Leica's LAS X software (Version 2.0.0).

5.10.14 Water permeation experiments

Water permeation measurements were conducted under kind supervision of Raphael Dalpke and Dr. André Beyer in the lab of Prof. Armin Gölzhäuser at the University of Bielefeld.

Water permeation through FhuA WT membranes was studied with mass loss measurements.[102] Silicon nitride membrane windows with 5 µm-sized holes were used to prepare freestanding FhuA membranes. The FhuA membrane-coated chip was glued to a container cap, which in return was screwed on top of a container filled with 400 µl of Millipore pure water. The experiments started around 15 hours later to make sure that the relative humidity inside the container reaches 100% and a steady-state of the mass change was reached. To confirm the reliability of the setup, a control measurement was first done with different-sized open apertures, as published here.[14] The container was placed into an enclosed oven with a constant temperature (30 ± 0.1) °C, and the RH inside the oven was controlled around 13% ± 2% by saturated LiCl solution.[112] Due to the water vapor pressure difference inside and outside the container, water evaporates in the container and then permeates the FhuA membrane. The

mass loss of the container was measured after eight days by using a microbalance (Sartorius ME36S with a sensitivity of 1 µg). The water permeance *P* of the FhuA WT membrane was calculated by Equation 5:

$$P = \frac{\Delta m/M}{A\ t\ \Delta p} \tag{5}$$

where *Δm* is the mass change of the container (g), *M* is the molecular mass (g mol^{-1}), *A* is the membrane area (m^2), *t* is the time interval for an experiment (s), *Δp* is the vapor pressure difference (Pa). In this study, *Δp* was around 3700 Pa.

5.10.15 Ion conductivity measurements

Ion permeation measurements were carried out by Maxim Dirksen in the lab of Prof. Thomas Hellweg at the University of Bielefeld.

The ion conductivity measurements were performed using a specially designed microfluidic device made of two PMMA blocks. Each block contains a reservoir with a narrow channel for the electrolyte solution (the assembly of both reservoirs holds a volume of 250 µl). The end of each channel contains an embedded window in the size of the used silicon nitride membrane window to ensure precise placement of the sample. This device was already used to measure conductivity changes of thermoresponsive membranes and is well suited to detect small changes in resistance.[113,114] For preparation, both blocks were immersed into a phosphate buffer solution (10 mM NaCl, 10 mM sodium phosphate (NaPi), pH=7) to exclude bubble formation in the measuring channel while filling the reservoirs. The silicon nitride membrane window coated with the respective membrane and a PDMS seal were placed in the intended position and the two blocks were joined by screws. The electrical contact between the reservoirs was accomplished by two Ag/AgCl electrodes. In order to exclude external interferences, the measurements were performed in a Faraday cage at room temperature. For each sample, voltages in a range from ±1 mV to ± 20 mV were applied, and the current was measured with a time resolution of 1 kHz using an Axopatch 200B Amplifier (Molecular Devices, Biberach, Germany).

5.10.16 BSA rejection experiments

BSA rejection of FhuA membranes transferred to ceramic membrane supports (Fraunhofer IKTS, Germany) was measured using the set-up of a syringe pump (KDS 200 / 200P Legacy Syringe Pump, KD Scientific Inc., USA) described in Figure 5.28. FhuA membrane coated supports were placed into Swinnex filter holders (Merck Millipore, USA) and filtration of a BSA solution (~ 0.5 mg ml^{-1}) was performed at a flow rate of 0.1 ml min^{-1}. BSA concentration in feed, permeate and retentate was determined by measuring the protein absorption at 280 nm using the UV-vis spectrophotometer SPECORD 210 (Analytik Jena AG, Germany).

5.10.17 SEM

SEM measurements were performed by Minh Thu Tran at Fraunhofer IAP.

SEM images were acquired using a GeminiSEM 300 scanning electron microscope (Zeiss, Germany) at an acceleration voltage of 5 kV. Before imaging cross-sections, the samples were frozen and broken in liquid nitrogen, and sputtered with a thin layer of platinum to avoid charging during SEM analysis.

5.10.18 TMV discs and TMV membrane formation

Engineering and extraction of TMV virus-like particles used in this work were done by Eva Schubert and others in the group of Prof. Wege at the University of Stuttgart.

Engineering, expression and extraction of the TMV discs used in this study were performed according to previously published procedures.[31] TMV discs were provided as concentrated solutions (2-5 mg ml^{-1}) and diluted in phosphate buffer to a concentration of 2 mg ml^{-1} in advance of DLS measurements, which were performed using Malvern Zetasizer Nano ZS (UK) possessing a red 633 nm laser. Data processing was done using the Malvern Zetasizer Software (Version 7.11). TMV disc samples were further diluted in phosphate buffer to a concentration of 1 mg ml^{-1} and used for TMV membrane fabrication: Typically, 0.16 nmol of TMV discs were spread to the air-water interface of the Langmuir trough (when uprightly oriented, 0.16 nmol of TMV discs occupy an area corresponding to the initial trough area of 241.5 cm^2). Analogous to FhuA membrane stabilization, TMV membranes were crosslinked by injecting 1.76 ml glutaraldehyde solution (50 wt% in H_2O, Sigma Aldrich, USA) to the phosphate buffer subphase from behind the Langmuir trough barriers.

6 Summary

Filtration through membranes with nanopores is typically associated with high transmembrane pressures and high energy consumption. This problem can be addressed by reducing the respective membrane thickness, but forming ultrathin membranes with uniform nanopores represents a technical challenge. In this light, the present thesis describes a simple procedure to prepare ultrathin membranes from protein nanopores, since such building blocks of biological origin naturally show a high degree of uniformity. Moreover, given intensive research on engineering functionalities into protein nanopores, the new approach of membrane fabrication has potential to serve as a platform technology allowing to prepare membranes tailored to individual process requirements.

Membranes and membrane processes applied today are versatile and possess great technical, economic and societal value. The general goals of a *good* membrane process (high flux, low transmembrane pressure and desired selectivity) are interdependent, and possibilities to further optimize conventionally fabricated membranes, especially those with pores in the lower nanometer range, are limited. To enable more energy-efficient filtration processes with enhanced selectivity, new, ultrathin membrane concepts featuring defined and vertically aligned (nano-)pores are needed. Biological membranes incorporating transmembrane proteins as natural nanopores have served as a model for designing such membranes for many years. Previously reported strategies aiming to design biohybrid membranes featuring protein nanopores can be assigned into four general categories as follows: I. Dense, but random crosslinking of globular proteins (that do not form a nanopore) on top of porous support membranes. Transport in such membranes occurs through the interstitial space (pores) between the crosslinked proteins. II. Insertion of pore-forming transmembrane proteins into lipid bilayer or amphiphilic block copolymer membranes based on hydrophobic interactions, mimicking the incorporation of transmembrane proteins in biological membranes. III. Synthesis of so-called protein-polymer conjugates (that are proteins with laterally attached polymer chains), interfacial assembly and subsequent UV-crosslinking of the polymer chains. IV. Direct crosslinking of interfacially assembled protein nanopore monolayers.
However, the concepts reported so far involve rather cumbersome procedures, motivating the development of a simple fabrication approach for protein nanopore membranes in the presented doctoral project.

Two types of nanopores of biological origin were exemplarily studied for membrane preparation in this thesis, the transmembrane protein ferric hydroxamate uptake protein

component A (FhuA) and virus-like particles derived from tobacco mosaic virus (TMV). Both can be biotechnologically engineered (e.g., to present lysines at their lateral surface that allow for chemical modification) and isolated from bacteria cultures and plants, respectively. FhuA is one of the largest β-barrel transmembrane proteins found in nature and its open-channel variant constitutes a pore of about 2-3 nm in diameter. TMV particles have a central pore with a diameter of approximately 4 nm and can be prepared at variable lengths of up to 300 nm. In the framework of this project, quite short TMV particles with a length of only 9.2 nm were used.

Fabrication of ultrathin protein nanopore membranes presented in this work relies on the Langmuir technique that allows for the preparation and investigation of planar films of amphiphiles assembled at the liquid-gas interface. The newly proposed Langmuir approach for membrane preparation can be assigned into strategy category IV of the penultimate paragraph, and was mostly developed and demonstrated using the transmembrane protein FhuA or its open-pore variant. To form a membrane, protein nanopores were assembled at the air-water interface of a Langmuir trough, compressed to a surface pressure of 25 mN m^{-1} and then crosslinked by glutaraldehyde injected into the buffer subphase. Crosslinked films were transferred to dense or porous support materials following the Langmuir-Schaefer method (horizontal dipping of support materials to the crosslinked membrane) leading to either mono- or multilayer membranes after repeated transfer.

As a basis for membrane preparation, experiments assessing the quality of the membrane building material FhuA were conducted, covering sodium dodecyl sulfate polyacrylamide gel electrophoresis (SDS-PAGE), circular dichroism (CD) spectroscopy and transmission electron microscopy (TEM). Such experiments indicated sufficient purity and proper protein folding of the FhuA samples, even though some protein aggregates were visible in TEM images. Brewster-angle microscopy (BAM) was used to evaluate FhuA film homogeneity at different compression states at the air-water interface of the Langmuir trough. At surface pressures of 30 mN m^{-1} and higher, unfavorable cracks in the FhuA film were visible, which is why a surface pressure of 25 mN m^{-1} was chosen for membrane stabilization using glutaraldehyde. At this surface pressure, sum-frequency generation (SFG) spectroscopy indicated collective and upright orientation of FhuA molecules at the air-water interface, and no alteration upon glutaraldehyde crosslinking. Next, crosslinked FhuA membranes transferred to either dense or holey/porous substrates were investigated. Atomic force microscopy (AFM) and X-ray reflectivity (XRR) measurements on FhuA mono- and multilayer membranes proved that single

FhuA membrane sheets are molecular monolayers with a thickness of only 5 nm, and that those monolayer sheets may be effectively layered to form thicker membranes by repeated Langmuir-Schaefer transfer. Moreover, experiments involving CD spectroscopy and fluorescence microscopy suggested proper protein structure also in transferred and dried FhuA membranes. Freestanding membranes covering holes up to 7 µm in diameter were visualized by AFM, helium ion microscopy (HIM), and TEM. AFM PeakForce quantitative nanomechanical property mapping (PeakForce QNM) demonstrated remarkable mechanical stability and even elastic properties of freestanding monolayer membranes, which - when covering a hole with a diameter of 7 µm and loaded with the maximum force of 10 nN - stretched up to 250 nm. Furthermore, water permeation experiments showed FhuA multilayer membranes (2-5 layers) to exhibit excellent water permeance of average 3.87 x 10^{-4} mol Pa^{-1} m^{-2} s^{-1}, two orders of magnitude superior to comparable, industrially applied membranes. Ion conductivity measurements demonstrated that membranes made from almost closed FhuA pores were about 30% less conductive than those made from open FhuA pores, indicating tailorability of the membranes based on the chosen building blocks. Finally, FhuA membranes were transferred to scalable, ceramic membrane supports, and the resulting composite membranes showed significant rejection (up to 80%) towards bovine serum albumin (BSA) molecules with a molecular size below 10 nm.

At the end, transferability of membrane preparation investigated using FhuA throughout this work to TMV-derived virus-like particles was discussed on basis of a proof-of-principle study. TEM images of TMV membranes prepared analogously to FhuA membranes clearly showed few TMV pores, though less than expected, and it was thus concluded that further experiments are required to ascertain membrane composition and an optimal membrane formation strategy for virus-like particles.

In conclusion, a generally successful implementation of the Langmuir approach for preparing membranes incorporating the naturally pore-forming transmembrane protein FhuA could be demonstrated in this thesis. This new strategy of membrane preparation has potential to constitute a platform technology to form ultrathin and tailored protein nanopore membranes. Next steps could be the development of an improved, possibly automated transfer of FhuA membranes to scalable membrane supports and further experiments verifying the different rejection properties expected for FhuA membranes with “closed” vs. “open” pores towards small molecules.

7 Zusammenfassung

Filtration durch Membranen mit Nanoporen ist typischerweise mit hohen Transmembrandrücken und hohem Energieverbrauch verbunden. Dieses Problem kann durch eine Verringerung der Membrandicke reduziert werden, jedoch stellt die Fertigung ultradünner Membranen mit einheitlichen Nanoporen eine technische Herausforderung dar. Vor diesem Hintergrund beschreibt die vorliegende Doktorarbeit ein einfaches Verfahren zur Herstellung ultradünner Membranen aus Protein-Nanoporen. Solche Bausteine biologischen Ursprungs weisen natürlicherweise ein hohes Maß an Einheitlichkeit auf. Angesichts intensiver Forschung, um Protein-Nanoporen mit maßgeschneiderten Funktionalitäten zu generieren, könnte der neue Ansatz zur Membranfertigung als Plattformtechnologie dienen, um auf individuelle Prozessanforderungen zugeschnittene Membranen herzustellen.

Heute eingesetzte Membranen und Membranverfahren sind vielseitig und stellen einen hohen technischen, wirtschaftlichen und gesellschaftlichen Wert dar. Die generellen Ziele eines *guten* Membranprozesses (hoher Fluss, niedriger Transmembrandruck und gewünschte Selektivität) beeinflussen sich wechselseitig und die Möglichkeiten zur weiteren Optimierung konventionell hergestellter Membranen, insbesondere solcher mit Poren im unteren Nanometerbereich, sind begrenzt. Um dennoch energieeffiziente Filtrationsprozesse mit hoher Selektivität zu gestalten, werden neue, ultradünne Membrankonzepte mit definierten und vertikal ausgerichteten (Nano-)Poren benötigt. Biologische Membranen, die Transmembranproteine als natürliche Nanoporen enthalten, dienen seit vielen Jahren als Modell für das Design solcher Membranen. Bisher beschriebene Strategien zum Design von Biohybridmembranen mit Protein-Nanoporen können wie folgt in vier Kategorien eingeteilt werden: I. Dichte, aber ungeordnete Vernetzung von globulären Proteinen (die keine Nanopore bilden) auf porösen Trägermembranen. Der Transport in solchen Membranen erfolgt durch die Poren zwischen den vernetzten Proteinen. II. Einfügen von porenbildenden Transmembranproteinen in Lipid-Doppelschicht- oder amphiphile Blockcopolymer-Membranen, basierend auf hydrophoben Wechselwirkungen nach dem Vorbild des natürlichen Einbaus von Transmembranproteinen in biologische Membranen. III. Synthese sogenannter Protein-Polymer-Konjugate (Proteine mit seitlich angebundenen Polymerketten), anschließende Grenzflächenassemblierung der Konjugate und UV-Vernetzung der Polymerketten. IV. Direkte Vernetzung von an Grenzflächen assemblierten Monolagen aus Protein-Nanoporen.

Die bisher publizierten Konzepte beinhalten jedoch eher umständliche Verfahrensschritte, woraus sich die Motivation zur Entwicklung eines einfachen Herstellungsverfahrens für Protein-Nanoporen-Membranen im vorliegenden Promotionsprojekt ergibt.

In dieser Arbeit wurden beispielhaft zwei Arten von Nanoporen biologischen Ursprungs für die Membranherstellung untersucht, das Transmembranprotein *ferric hydroxamate uptake protein component A* (FhuA) und auf dem Tabakmosaikvirus (TMV) basierende, virusähnliche Partikel. Beide können biotechnologisch verändert (z. B. um Lysine an ihrer lateralen Oberfläche zu präsentieren, die eine chemische Modifikation ermöglichen) und aus Bakterienkulturen bzw. Pflanzen isoliert werden. FhuA ist eines der größten in der Natur vorkommenden β-Fass-Transmembranproteine, und seine biotechnologisch modifizierte Variante mit offenem Kanal bildet eine Pore mit einem Durchmesser von etwa 2-3 nm. TMV-Partikel hingegen haben eine zentrale Pore mit einem Durchmesser von ca. 4 nm und können in variablen Längen von bis zu 300 nm hergestellt werden. Im Rahmen dieses Projektes wurden vergleichsweise kurze TMV-Partikel mit einer Länge von nur 9,2 nm verwendet.

Der in dieser Arbeit vorgestellte Ansatz zur Herstellung von ultradünnen Protein-Nanoporen-Membranen basiert auf der Langmuir-Technik, die schon lange zur Präparation und Untersuchung von planaren Filmen amphiphiler Moleküle an der Flüssig-Gas-Grenzfläche verwendet wird. Der verfolgte Langmuir-Ansatz zur Membranfertigung ist der Strategiekategorie IV des vorletzten Absatzes zuzuordnen und wurde am Beispiel des Transmembranproteins FhuA oder seiner offenporigen Variante demonstriert und entwickelt. Um eine Membran zu bilden, wurden Protein-Nanoporen an der Wasser-Luft-Grenzfläche eines Langmuir-Trogs assembliert, bis zu einem Oberflächendruck von 25 mN m^{-1} komprimiert und dann durch in die Puffer-Subphase injiziertes Glutaraldehyd vernetzt. Vernetzte Membranen wurden mittels der Langmuir-Schaefer-Methode (horizontales Absenken von Trägermaterialien auf die vernetzte Membran) als Mono- oder Multilagen auf dichte oder poröse Trägermaterialien übertragen.

Als Grundlage für die Membranherstellung wurden zunächst folgende Experimente zur Charakterisierung des Membranbausteins FhuA durchgeführt: Natriumdodecylsulfat-Polyacrylamid-Gelelektrophorese (SDS-PAGE), Circulardichroismus (CD)-Spektroskopie und Transmissionselektronenmikroskopie (TEM). Diese Experimente zeigten eine ausreichende Reinheit und korrekte Proteinfaltung der FhuA-Proben, wobei in TEM-Aufnahmen einige Proteinaggregate sichtbar waren. Um die Beschaffenheit von FhuA-Filmen an der Wasser-Luft-Grenzfläche des Langmuir-Trogs für verschiedene Kompressionsstadien zu vergleichen, wurde

Brewster-Winkel-Mikroskopie (BAM) verwendet. Dabei waren für Oberflächendrücke ab etwa 30 mN m^{-1} Bruchstellen in den FhuA-Filmen sichtbar, weshalb FhuA-Membranen nach dieser Analyse bei einem etwas niedrigeren Oberflächendruck von 25 mN m^{-1} durch Glutaraldehyd stabilisiert wurden. Mittels Summenfrequenzerzeugung (SFG)-Spektroskopie wurde bei diesem Oberflächendruck eine kollektive und aufrechte Ausrichtung der FhuA-Moleküle an der Wasser-Luft-Grenzfläche und keine Veränderung durch die Vernetzung mit Glutaraldehyd nachgewiesen. Als nächstes wurden vernetzte FhuA-Membranen untersucht, die entweder auf dichte oder löchrige/poröse Substrate übertragen wurden. Rasterkraftmikroskopie (AFM) und Röntgenreflektometrie (XRR) an FhuA-Mono- und Multilagen-Membranen zeigten, dass einzelne FhuA-Membranen molekulare Monolagen mit einer Dicke von nur 5 nm sind und dass diese Monolagen durch wiederholten Langmuir-Schaefer-Transfer effektiv zu dickeren Membranen geschichtet werden können. Darüber hinaus wiesen Experimente mit CD-Spektroskopie und Fluoreszenzmikroskopie auch in übertragenen und getrockneten FhuA-Membranen auf eine richtige Proteinstruktur hin. Freistehende Membranen, die sogar Löcher mit einem Durchmesser von bis zu 7 µm überspannen, wurden durch AFM, Heliumionenmikroskopie (HIM) und TEM visualisiert. *AFM PeakForce quantitative nanomechanical property mapping* (PeakForce QNM) demonstrierte eine bemerkenswerte mechanische Stabilität und elastische Eigenschaften von freistehenden Monolagen-Membranen, die bis zu 250 nm ausgelenkt werden konnten (wenn sie ein Loch mit einem Durchmesser von 7 µm überspannten und mit der maximalen Kraft von 10 nN belastet wurden). In anschließenden Wasserpermeations-Messungen zeigten FhuA-Multilagenmembranen (2-5 Schichten) eine ausgezeichnete Wasserpermeanz von durchschnittlich 3.87 x 10^{-4} mol Pa^{-1} m^{-2} s^{-1}, zwei Größenordnungen besser als vergleichbare, industriell eingesetzte Membranen. In Ionenleitfähigkeitsmessungen waren Membranen mit fast geschlossenen FhuA-Poren etwa 30% weniger leitfähig als solche mit offenen FhuA-Poren, was auf eine Anpassungsfähigkeit der Membranen entsprechend der gewählten Bausteine schließen lässt. Schließlich wurden FhuA-Membranen auf skalierbare, keramische Membranträger übertragen, wobei die resultierenden Kompositmembranen einen deutlichen Rückhalt (von bis zu 80%) gegenüber Rinderserumalbumin-Molekülen (BSA) mit einer Größe unter 10 nm zeigten.

Abschließend wurde die Übertragbarkeit der in dieser Arbeit mit FhuA untersuchten Membranherstellung auf virusähnliche TMV-Partikel anhand einer Machbarkeitsstudie diskutiert. TEM-Aufnahmen von TMV-Membranen, die analog zu FhuA-Membranen

hergestellt wurden, zeigten jedoch weniger TMV-Poren als erwartet. Somit wurde geschlussfolgert, dass weitere Experimente erforderlich sind, um die Membranherstellung für virusähnliche Partikel zu optimieren.

Zusammenfassend konnte die Umsetzung des neuen Langmuir-Ansatzes zur Herstellung von Membranen anhand des porenbildenden Transmembranproteins FhuA in dieser Arbeit erfolgreich demonstriert werden. Diese Strategie der Membranfertigung hat das Potenzial, eine Plattformtechnologie zur Herstellung ultradünner und maßgeschneiderter Protein-Nanoporen-Membranen zu bilden. Nächste Schritte könnten die Entwicklung eines verbesserten, möglicherweise automatisierten Transfers von FhuA-Membranen auf skalierbare Trägermembranen und weitere Experimente hinsichtlich der zu erwartenden, unterschiedlichen Rückhalteeigenschaften von FhuA-Membranen mit „geschlossenen“ und „offenen“ Poren gegenüber kleinen Molekülen sein.

8 References

[1] Y. Wang, B. Seo, B. Wang, N. Zamel, K. Jiao, X. C. Adroher, *Energy and AI* **2020**, *1*, 100014.

[2] X. Yu, L. An, J. Yang, S.-T. Tu, J. Yan, *J. Membr. Sci.* **2015**, *496*, 1.

[3] G. Zhang, L. Li, Y. Huang, A. Hozumi, T. Sonoda, Z. Su, *RSC Adv.* **2018**, *8*, 5306.

[4] X. Lu, M. Elimelech, *Chem. Soc. Rev.* **2021**, *50*, 6290.

[5] M. Qasim, M. Badrelzaman, N. N. Darwish, N. A. Darwish, N. Hilal, *Desalination* **2019**, *459*, 59.

[6] C. Ronco, W. R. Clark, *Nat. Rev. Nephrol.* **2018**, *14*, 394.

[7] R. Xie, L.-Y. Chu, J.-G. Deng, *Chem. Soc. Rev.* **2008**, *37*, 1243.

[8] H. B. Park, J. Kamcev, L. M. Robeson, M. Elimelech, B. D. Freeman, *Science* **2017**, *356*, eaab0530.

[9] R. W. Baker, *Membrane technology and applications*, Wiley, Chichester, U.K. **2012**.

[10] M. Radjabian, V. Abetz, *Prog. Polym. Sci.* **2020**, *102*, 101219.

[11] Y.-M. Tu, W. Song, T. Ren, Y.-X. Shen, R. Chowdhury, P. Rajapaksha, T. E. Culp, L. Samineni, C. Lang, A. Thokkadam, D. Carson, Y. Dai, A. Mukthar, M. Zhang, A. Parshin, J. N. Sloand, S. H. Medina, M. Grzelakowski, D. Bhattacharya, W. A. Phillip, E. D. Gomez, R. J. Hickey, Y. Wei, M. Kumar, *Nat. Mater.* **2020**, *19*, 347.

[12] K. Celebi, J. Buchheim, R. M. Wyss, A. Droudian, P. Gasser, I. Shorubalko, J.-I. Kye, C. Lee, H. G. Park, *Science* **2014**, *344*, 289.

[13] F. Fornasiero, H. G. Park, J. K. Holt, M. Stadermann, C. P. Grigoropoulos, A. Noy, O. Bakajin, *Proc. Natl. Acad. Sci. USA* **2008**, *105*, 17250.

[14] Y. Yang, P. Dementyev, N. Biere, D. Emmrich, P. Stohmann, R. Korzetz, X. Zhang, A. Beyer, S. Koch, D. Anselmetti, A. Gölzhäuser, *ACS Nano* **2018**, *12*, 4695.

[15] Y. Yang, R. Hillmann, Y. Qi, R. Korzetz, N. Biere, D. Emmrich, M. Westphal, B. Büker, A. Hütten, A. Beyer, D. Anselmetti, A. Gölzhäuser, *Adv. Mater.* **2020**, *32*, e1907850.

[16] Z. Zhang, M. M. Rahman, C. Abetz, A.-L. Höhme, E. Sperling, V. Abetz, *Adv. Mater.* **2020**, *32*, e1907014.

[17] H. Ryu, A. Fuwad, S. Yoon, H. Jang, J. C. Lee, S. M. Kim, T.-J. Jeon, *Int. J. Mol. Sci.* **2019**, *20,* 1437.

[18] A. A. Vorobieva, P. White, B. Liang, J. E. Horne, A. K. Bera, C. M. Chow, S. Gerben, S. Marx, A. Kang, A. Q. Stiving, S. R. Harvey, D. C. Marx, G. N. Khan, K. G. Fleming, V. H. Wysocki, D. J. Brockwell, L. K. Tamm, S. E. Radford, D. Baker, *Science* **2021**, *371,* eabc8182.

[19] T. Mirzaei Garakani, D. F. Sauer, M. A. S. Mertens, J. Lazar, J. Gehrmann, M. Arlt, J. Schiffels, U. Schnakenberg, J. Okuda, U. Schwaneberg, *ACS Catal.* **2020**, *10*, 10946.

[20] H. Killmann, R. Benz, V. Braun, *EMBO J.* **1993**, *12*, 3007.

[21] D. Wong, T.-J. Jeon, J. Schmidt, *Nanotechnology* **2006**, *17*, 3710.

[22] C. Edlinger, T. Einfalt, M. Spulber, A. Car, W. Meier, C. G. Palivan, *Nano Lett.* **2017**, *17*, 5790.

[23] P. S. Zhong, T.-S. Chung, K. Jeyaseelan, A. Armugam, *J. Membr. Sci.* **2012**, *407-408*, 27.

[24] M. Kumar, J. E. O. Habel, Y.-X. Shen, W. P. Meier, T. Walz, *J. Am. Chem. Soc.* **2012**, *134*, 18631.

[25] M. Kumar, M. Grzelakowski, J. Zilles, M. Clark, W. Meier, *Proc. Natl. Acad. Sci. USA* **2007**, *104*, 20719.

[26] S. S. Klara, P. O. Saboe, I. T. Sines, M. Babaei, P.-L. Chiu, R. DeZorzi, K. Dayal, T. Walz, M. Kumar, M. S. Mauter, *J. Am. Chem. Soc.* **2016**, *138*, 28.

[27] H. Wang, T.-S. Chung, Y. W. Tong, K. Jeyaseelan, A. Armugam, Z. Chen, M. Hong, W. Meier, *Small* **2012**, *8*, 1185-90, 1125.

[28] T. Mirzaei Garakani, Z. Liu, U. Glebe, J. Gehrmann, J. Lazar, M. A. S. Mertens, M. Möller, N. Hamzelui, L. Zhu, U. Schnakenberg, A. Böker, U. Schwaneberg, *ACS Appl. Mater. Interfaces* **2019**, *11*, 29276.

[29] P. H.H. Duong, T.-S. Chung, K. Jeyaseelan, A. Armugam, Z. Chen, J. Yang, M. Hong, *J. Membr. Sci.* **2012**, *409-410*, 34.

[30] Y. Li, S. Qi, M. Tian, W. Widjajanti, R. Wang, *Desalination* **2019**, *467*, 103.

[31] K. Altintoprak, A. Seidenstücker, P. Krolla-Sidenstein, A. Plettl, H. Jeske, H. Gliemann, C. Wege, *Bioinspired, Biomimetic and Nanobiomater.* **2017**, *6*, 208.

[32] K. Altintoprak, F. Farajollahi, A. Seidenstücker, T. Ullrich, N. L. Wenz, P. Krolla, A. Plettl, P. Ziemann, O. Marti, P. Walther, D. Exner, R. Schwaiger, H. Gliemann, C. Wege, *Bioinspired, Biomimetic and Nanobiomater.* **2019**, *8*, 47.

[33] S. Zhang, J. Zhang, W. Fang, Y. Zhang, Q. Wang, J. Jin, *Nano Lett.* **2018**, *18*, 6563.

[34] N. C. Mougin, P. van Rijn, H. Park, A. H. E. Müller, A. Böker, *Adv. Funct. Mater.* **2011**, *21*, 2470.

[35] P. van Rijn, N. C. Mougin, D. Franke, H. Park, A. Böker, *Chem. Commun.* **2011**, *47*, 8376.

[36] P. van Rijn, N. C. Mougin, A. Böker, *Polymer* **2012**, *53*, 6045.

[37] P. van Rijn, H. Park, K. Özlem Nazli, N. C. Mougin, A. Böker, *Langmuir* **2013**, *29*, 276.

[38] P. van Rijn, M. Tutus, C. Kathrein, N. C. Mougin, H. Park, C. Hein, M. P. Schürings, A. Böker, *Adv. Funct. Mater.* **2014**, *24*, 6762.

[39] H. Charan, J. Kinzel, U. Glebe, D. Anand, T. M. Garakani, L. Zhu, M. Bocola, U. Schwaneberg, A. Böker, *Biomaterials* **2016**, *107*, 115.

[40] H. Charan, U. Glebe, D. Anand, J. Kinzel, L. Zhu, M. Bocola, T. M. Garakani, U. Schwaneberg, A. Böker, *Soft Matter* **2017**, *13*, 2866.

[41] K. P. Locher, B. Rees, R. Koebnik, A. Mitschler, L. Moulinier, J. P. Rosenbusch, D. Moras, *Cell* **1998**, *95*, 771.

[42] A. D. Ferguson, E. Hofmann, J. W. Coulton, K. Diederichs, W. Welte, *Science* **1998**, *282*, 2215.

[43] T. Surrey, F. Jähnig, *J. Biol. Chem.* **1995**, *270*, 28199.

[44] H. Charan, *Self-assembled transmembrane protein polymer conjugates for the generation of nano thin membranes and micro compartments*, doctoral thesis, Potsdam **2017**.

[45] C.-I. Branden, J. Tooze, *Introduction to protein structure*, Garland Pub, New York **1999**.

[46] R. Koebnik, K. P. Locher, P. van Gelder, *Mol. Microbiol.* **2000**, *37*, 239.

[47] U. T. Bornscheuer, M. Höhne (Eds.), *Protein engineering: Methods and protocols*, Humana Press, New York, NY **2018**.

[48] R. Verma, U. Schwaneberg, D. Roccatano, *Comput. Struct. Biotechnol. J.* **2012**, *2*, e201209008.

[49] H. J. Gross, C. Köhrer, U. L. RajBhandary, *Protein Engineering*, Springer, Berlin, Heidelberg **2009**.

[50] F. Philippart, M. Arlt, S. Gotzen, S.-J. Tenne, M. Bocola, H.-H. Chen, L. Zhu, U. Schwaneberg, J. Okuda, *Chemistry* **2013**, *19*, 13865.

[51] T. Dworeck, A.-K. Petri, N. Muhammad, M. Fioroni, U. Schwaneberg, *Protein Expr. Purif.* **2011**, *77*, 75.

[52] C. Michaux, N. C. Pomroy, G. G. Privé, *J. Mol. Biol.* **2008**, *375*, 1477.

[53] G. Roussel, E. A. Perpète, A. Matagne, E. Tinti, C. Michaux, *Biotechnol. Bioeng.* **2013**, *110*, 417.

[54] J. Kinzel, D. F. Sauer, M. Bocola, M. Arlt, T. Mirzaei Garakani, A. Thiel, K. Beckerle, T. Polen, J. Okuda, U. Schwaneberg, *Beilstein J. Org. Chem.* **2017**, *13*, 1498.

[55] M.H.V. van Regenmortel, in *Encyclopedia of virology* (Eds.: B. W. J. Mahy, M. H. V. van Regenmortel), Elsevier. Amsterdam **2008**, p. 54.

[56] P. J. Butler, *Philos. Trans. R. Soc. Lond., B, Biol. Sci.* **1999**, *354*, 537.

[57] L. W. Janson, M. E. Tischler, *The big picture: Medical biochemistry*, McGraw-Hill Medical, New York **2012**.

[58] X. Z. Fan, E. Pomerantseva, M. Gnerlich, A. Brown, K. Gerasopoulos, M. McCarthy, J. Culver, R. Ghodssi, *J. Vac. Sci. Technol. A: Vac. Surf. Films* **2013**, *31*, 50815.

[59] H. Grünewald, *Angew. Chem.* **1968**, *80*, 52.

[60] I. Langmuir, K. B. Blodgett, *Kolloid-Zeitschrift* **1935**, *73*, 257.

[61] R. Y.N. Gengler, *A modified Langmuir Schaefer method for the creation of functional thin films,* doctoral thesis, Groningen **2010**.

[62] R. J. Needs, M. Mansfield, *J. Phys. Condens. Matter* **1989**, *1*, 7555.

[63] B. E. Rapp, in *Microfluidics: Modelling, Mechanics and Mathematics*, Elsevier **2017**, p. 453.

[64] I. Langmuir, V. J. Schaefer, *J. Am. Chem. Soc.* **1938**, *60*, 1351.

[65] G. Gonzalez, F. MacRitchie, *J. Colloid Interface Sci.* **1970**, *32*, 55.

[66] D. J. Adams, M. T. A. Evans, J. R. Mitchell, M. C. Phillips, P. M. Rees, *J. Polym. Sci., Part C: Polym. Symp.* **1971**, *34*, 167.

[67] I. Migneault, C. Dartiguenave, M. J. Bertrand, K. C. Waldron, *Biotechniques* **2004**, *37*, 790-6, 798-802.

[68] G. T. Hermanson, in *Bioconjugate Techniques*, Elsevier **2013**, p. 275.

[69] G. T. Hermanson, in *Bioconjugate Techniques*, Elsevier **2013**, p. 589.

[70] R. Fernandez-Lafuente, C. M. Rosell, V. Rodriguez, J. M. Guisan, *Enzyme Microb. Technol.* **1995**, *17*, 517.

[71] O. Barbosa, C. Ortiz, Á. Berenguer-Murcia, R. Torres, R. C. Rodrigues, R. Fernandez-Lafuente, *RSC Adv.* **2014**, *4*, 1583.

[72] A. A. Stonehill, S. Krop, P. M. Borick, ***Am***. *J. Health-Syst. Pharm.* **1963**, *20*, 458.

[73] T. Takigawa, Y. Endo, *J. Occup. Health* **2006**, *48*, 75.

[74] D. Chakraborty, A. H. Quadery, M. A. K. Azad, *Bangladesh J. Sci. Ind. Res.* **2009**, *43*, 553.

[75] X. Peng, J. Jin, E. M. Ericsson, I. Ichinose, *J. Am. Chem. Soc.* **2007**, *129*, 8625.

[76] X. Peng, J. Jin, Y. Nakamura, T. Ohno, I. Ichinose, *Nat. Nanotechnol.* **2009**, *4*, 353.

[77] J. Zhao, Y. Zhang, Y. Su, J. Liu, X. Zhao, J. Peng, Z. Jiang, *J. Membr. Sci.* **2013**, *445*, 1.

[78] L. Wu, U. Glebe, A. Böker, *Polym. Chem.* **2015**, *6*, 5143.

[79] A. Böker, P. van Rijn (Eds.), *Bio-Synthetic Hybrid Materials and Bionanoparticles*, Royal Society of Chemistry, Cambridge **2015**.

[80] M. Mathieu-Gaedke, *Grafting-to and grafting-from proteins – synthesis and characterization of protein-polymer conjugates on the way to biohybrid membrane materials,* doctoral thesis, Potsdam **2021**.

[81] D. R. Walt, V. I. Agayn, *TRAC* **1994**, *13*, 425.

[82] Z. Liu, I. Ghai, M. Winterhalter, U. Schwaneberg, *ACS Sens.* **2017**, *2*, 1619.

[83] M. Krewinkel, T. Dworeck, M. Fioroni, *J. Nanobiotechnology* **2011**, *9*, 33.

[84] J. M. Manns, *Curr. Protoc. Microbiol.* **2011**, *22*.

[85] S. M. Kelly, N. C. Price, *CPPS* **2000**, *1*, 349.

[86] S. Brahms, J. Brahms, *J. Mol. Biol.* **1980**, *138*, 149.

[87] S. de Carlo, J. R. Harris, *Micron* **2011**, *42*, 117.

[88] C. Breyton, A. Flayhan, F. Gabel, M. Lethier, G. Durand, P. Boulanger, M. Chami, C. Ebel, *J. Biol. Chem.* **2013**, *288*, 30763.

[89] K. Mladenova, S. D. Petrova, T. D. Andreeva, V. Moskova-Doumanova, T. Topouzova-Hristova, Y. Kalvachev, K. Balashev, S. S. Bhattacharya, C. Chakarova, Z. Lalchev, J. A. Doumanov, *Colloids Surf., B* **2017**, *149*, 226.

[90] T. D. Andreeva, S. D. Petrova, K. Mladenova, V. Moskova-Doumanova, T. Topouzova-Hristova, Y. Petseva, N. Mladenov, K. Balashev, Z. Lalchev, J. A. Doumanov, *Colloids Surf., B* **2018**, *161*, 192.

[91] D. Hoenig, D. Moebius, *J. Phys. Chem.* **1991**, *95*, 4590.

[92] Y. Li, M. Shrestha, M. Luo, I. Sit, M. Song, V. H. Grassian, W. Xiong, *Langmuir* **2019**, *35*, 13815.

[93] S. Hosseinpour, S. J. Roeters, M. Bonn, W. Peukert, S. Woutersen, T. Weidner, *Chem. Rev.* **2020**, *120*, 3420.

[94] S. J. Roeters, C. N. van Dijk, A. Torres-Knoop, E. H. G. Backus, R. K. Campen, M. Bonn, S. Woutersen, *J. Phys. Chem. A* **2013**, *117*, 6311.

[95] S. M. Danauskas, D. Li, M. Meron, B. Lin, K. Y. C. Lee, *J. Appl. Crystallogr.* **2008**, *41*, 1187.

[96] M. Schalke, M. Lösche, *Adv. Colloid Interface Sci.* **2000**, *88*, 243.

[97] W. C. Johnson, *Annu. Rev. Biophys. Biophys. Chem.* **1988**, *17*, 145.

[98] B. Pittenger, N. Erina, C. Su, in *Nanomechanical analysis of high performance materials*, Vol. 203 (Ed.: A. Tiwari), Springer. Dordrecht **2014**, p. 31.

[99] K. E. Mueggenburg, X.-M. Lin, R. H. Goldsmith, H. M. Jaeger, *Nat. Mater.* **2007**, *6*, 656.

[100] U. Komaragiri, M. R. Begley, J. G. Simmonds, *J. Appl. Mech.* **2005**, *72*, 203.

[101] K.-T. Wan, S. Guo, D. A. Dillard, *Thin Solid Films* **2003**, *425*, 150.

[102] ASTM E96/E96m-16, Standard Test Methods for Water Vapor Transmission of Materials, ASTM International, West Conshohocken, PA **2016**.

[103] J. D. Faraldo-Gómez, G. R. Smith, M. S.P. Sansom, *Biophys. J.* **2003**, *85*, 1406.

[104] D. Some, H. Amartely, A. Tsadok, M. Lebendiker, *J. Visualized Exp.* **2019**.

[105] Z. Wang, S. Gao, X. Liu, Y. Tian, M. Wu, Z. Niu, *ACS Appl. Mater. Interfaces* **2017**, *9*, 27383.

[106] D. Anand, G. V. Dhoke, J. Gehrmann, T. M. Garakani, M. D. Davari, M. Bocola, L. Zhu, U. Schwaneberg, *Chem. Commun.* **2019**, *55*, 5431.

[107] X. Guan, L.-Q. Gu, S. Cheley, O. Braha, H. Bayley, *ChemBioChem* **2005**, *6*, 1875.

[108] F. Haque, J. Lunn, H. Fang, D. Smithrud, P. Guo, *ACS Nano* **2012**, *6*, 3251.

[109] M. Parchine, J. McGrath, M. Bardosova, M. E. Pemble, *Langmuir* **2016**, *32*, 5862.

[110] G. Ciatto, M. H. Chu, P. Fontaine, N. Aubert, H. Renevier, J. L. Deschanvres, *Thin Solid Films* **2016**, *617*, 48.

[111] D. Emmrich, A. Wolff, N. Meyerbröker, J. K. N. Lindner, A. Beyer, A. Gölzhäuser, *Beilstein J. Nanotechnol.* **2021**, *12*, 222.

[112] L. Greenspan, *J. Res. Natl. Bur. Stand., Sec. A* **1977**, *81A*, 89.

[113] J. Bookhold, M. Dirksen, L. Wiehemeier, S. Knust, D. Anselmetti, F. Paneff, X. Zhang, A. Gölzhäuser, T. Kottke, T. Hellweg, *Soft Matter* **2021**, *17*, 2205.

[114] M. Dirksen, T. Brändel, S. Großkopf, S. Knust, J. Bookhold, D. Anselmetti, T. Hellweg, *RSC Adv.* **2021**, *11*, 22014.

[115] K. P. Locher, B. Rees, R. Koebnik, A. Mitschler, L. Moulinier, J. P. Rosenbusch, D. Moras, FHUA FROM E. COLI **1999**; PDB Entry - 1BY3; DOI: 10.2210/pdb1by3/pdb.

9 Appendix

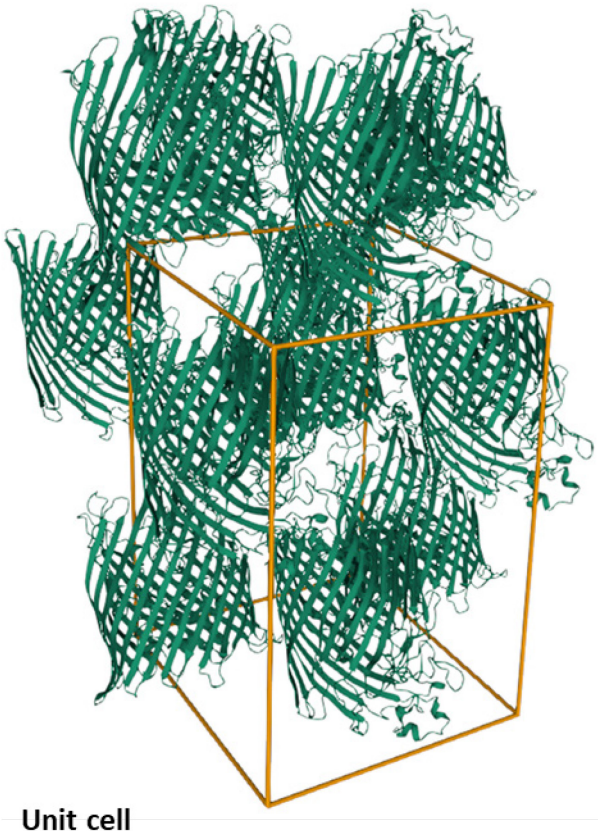

Unit cell

Length (nm)	Angle (°)
a = 132.9	α = 90
b = 89.9	ß = 95.2
c = 90	γ = 90

Estimation of the molecular area of an upright orientated FhuA molecule when densly packed in a crystal (1BY3):

→ 2 FhuA molecules/ base area b x c

→ 40.5 nm^2/ FhuA molecule

0.32 nmol FhuA were used for membrane preparation:

→ interfacial area occupied by FhuA calculated based on estimation above: ~ 78 cm^2

Trough area (interfacial area) of the Langmuir trough at the beginning of membrane preparation: 241.5cm^2

→ adsorbed FhuA film rather consists of one than multiple molecular layers

Figure S1: Interfacial area occupied by upright oriented FhuA molecules. Estimation is based on crystal structure 1BY3[41] and suggests that the FhuA film spread during membrane preparation is a molecular monolayer. The image was generated using the corresponding protein data bank entry.[115]

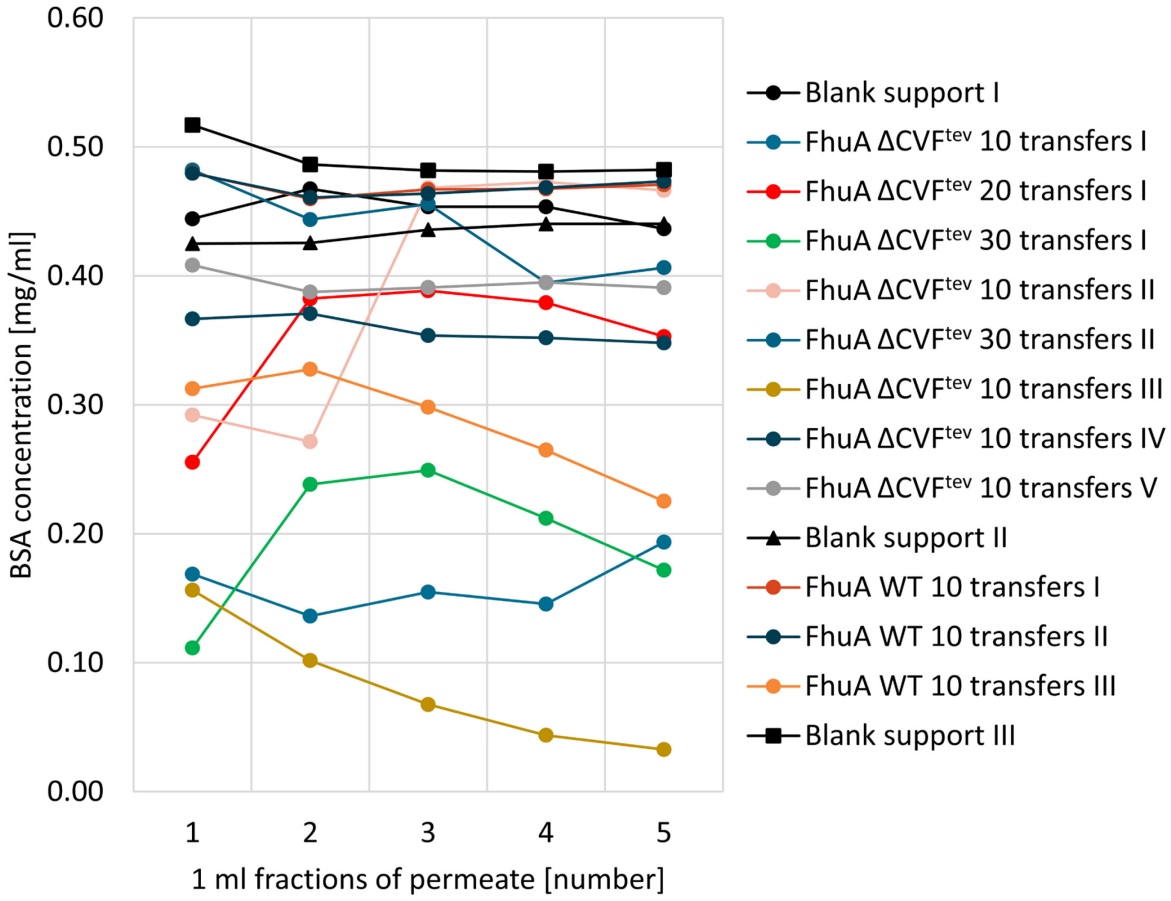

Figure S2: BSA rejection of ceramic membrane supports, blank or coated with FhuA membranes. Diagram showing the BSA concentration in five 1 ml-permeate fractions collected after filtration through ceramic membrane supports, either blank or coated with FhuA WT or FhuA ΔCVF^{tev} membranes by performing 10, 20 or 30 Langmuir-Schaefer transfers. The broad distribution of the graphs indicates low reproducibility.